Morphological analysis of the dendritic tree and the expression and localization of actin-modulating protein synaptopodin in hippocampal granule cells of TNF-α KO mice

Smilović, Dinko

Doctoral thesis / Disertacija

2021

Degree Grantor / Ustanova koja je dodijelila akademski / stručni stupanj: **University of Zagreb, School of Medicine / Sveučilište u Zagrebu, Medicinski fakultet**

Permanent link / Trajna poveznica: https://urn.nsk.hr/urn:nbn:hr:105:524607

UNIVERSITY OF ZAGREB

SCHOOL OF MEDICINE

Dinko Smilović

Morphological analysis of the dendritic tree and the expression and localization of actin-modulating protein synaptopodin in hippocampal granule cells of TNF-α KO mice

DISSERTATION

Zagreb, 2021.

UNIVERSITY OF ZAGREB
SCHOOL OF MEDICINE

Dinko Smilović

Morphological analysis of the dendritic tree and the expression and localization of actin-modulating protein synaptopodin in hippocampal granule cells of TNF-α KO mice

DISSERTATION

Zagreb, 2021.

This dissertation was made at the Laboratory for confocal microscopy, Croatian Institute for Brain Research, University of Zagreb School of Medicine, and at the Clinical Neuroanatomy laboratory, Goethe University Frankfurt am Main, University Hospital.

This work was supported by the billateral Croatian-German project (Ministry of Science and Education of the Republic of Croatia and Deutsche Akademische Austauschdiesnst (MZOŠ-DAAD), Deutsche Forschungsgemeinschaft (DFG CRC 1080), the Scientific Centre of Excellence for Basic, Clinical and Translation Neuroscience (project "Experimental and clinical research of hypoxic-ischemic damage in perinatal and adult brain"; GA KK01.1.1.01.007 funded by the European Union through the European Regional Development Fund)

Mentors: Mario Vukšić, MD, PhD
Professor of Neuroscience,
University of Zagreb, School of Medicine

Thomas Deller, MD
Professor of Anatomy
Institute for Clinical Neuroanatomy
Goethe University Frankfurt am Main, NeuroScience Center

CHAPTERS

LIST OF SYMBOLS AND ABBREVIATIONS:

CA	Cornu ammonis
CNS	Central nervous system
DG	Dentate gyrus
DIV	Days *in vitro*
EC	Entorhinal cortex
ECL	Entorhinal cortex lesion
GC	Granule cell
GCL	Granule cell layer
GFP	Green fluorescent protein
HF	Hippocampal fissure
HPF	Hippocampal formation
IML	Inner molecular layer
KO	Knockout mice
mEPSC	Miniature excitatory post-synaptic current
MML	Middle molecular layer
OML	Outer molecular layer
OTC	Organotypic hippocampal cultures
PSD	Post-synaptic density
SA	Spine apparatus
SER	Smooth endoplasmic reticulum
SP	Synaptopodin
TNF-α	Tumor necrosis factor – alpha
TNF-KO	Mice lacking the tumor necrosis factor – alpha gene
WT	Wildtype mice

1. INTRODUCTION AND BACKGROUND

The morphology of neurons as a discipline exists since the seminal works of Ramon J Cajal (1). More than a century ago, he had the intuition to know just how important this discipline will be for understanding the inner workings of the brain. This is best captured by his quote: „The future will prove the great physiological role played by the spines“ (1904). As we looked into the secrets that these structures contain, so has our methodology improved. Neuromorphology as a discipline investigates what rules, conclusions and new insights might be gained from studying the shape, form and structure of the cells in the central nervous system (2).

The hippocampal formation (HPF) is a structure located deep in the temporal lobe and has a clearly defined three-layered architecture. Its function is primarily that of learning, memory, particularly spatial memory that enables navigation through space. It consists of four parts to enable its function: The entorhinal cortex (EC), dentate gyrus (DG), Cornu Ammonis areas 1-3 (CA1, CA2, CA3) and subiculum (SA). The DG is the main afferent structure of the hippocampus, receiving a vast network of afferents from the entorhinal cortex (EC) through the perforant path (3). In the dentate gyrus, the granule cells (GC) receive this input and any disruptions in the network, either by extrinsic factors or by genetic modifications, will present with changes in the morphology of GCs (4).

In this regard, dendrites, as the part of the neuron that receives excitatory input, are well studied. Dendrites are extensions of the cell body that branch in a specific manner and transfer molecules from and back to the soma. They also allow the transfer of currents towards the soma and axon hillock. Their branched structure is indicative of the extent of innervation the cell is receiving, and any changes in the length of its arbor or its complexity is suggestive of significant changes in the neurons receptive profile (5). On these structures we find dendritic spines, small extensions emanating laterally from the dendrite. They serve as post-synaptic sites where most excitatory, glutamatergic synapses are made. These are very dynamic structures, with most spines in adult animals being transient, while a very select few remain stable for extended periods of time. Their structure changes with regards to their function, with small spines having less excitatory function compared to their larger counterparts (6). It is therefore possible to infer certain functional properties of affected neurons through the investigations into the shape and size of its dendritic tree and its spines.

Tumor necrosis factor–alpha (TNF–α) is a cytokine that is active in the immune response. While its function in the context of the immune system has been thoroughly studied, it has also been shown that it has a prominent role in the central nervous system (CNS). The seminal work of Beattie and Stellwagen has shown that TNF–α controls synaptic strength by influencing the surface expression of AMPA receptors (7). Throughout the last 20 years, it has been shown that TNF–α has multiple roles in synaptic plasticity, and that its function can be both detrimental and homeostatic for the function of neurons (8). With this in mind, we aimed to illuminate its influence in the context of *in vitro* and *ex vivo* experiments.

Synaptopodin (SP) is an actin-associated protein that has a critical function in a subset of dendritic spines. There it interacts with a specialized structure called the spine apparatus (SA), which is a form of a smooth endoplasmic reticulum (SER), allowing it to influence the dynamics of calcium concentrations inside the dendritic spines (9). This protein is also important in synaptic plasticity, and recent investigations have shown it to influence dendritic spine stability (10). The functions of SP and TNF–α are connected, and this doctoral work has aimed to bring further information concerning their interactions.

1.1. The hippocampal formation and the dentate gyrus of the rodent brain

The hippocampus has been one of the most intensely studied regions of the brain. This is partially due to the structure having a clear, relatively simple organization of its cell layers coupled with a highly defined anatomy of its many inputs, many of which come from a single source. These inputs, unlike most of the other cortical areas, are predominantly unidirectional, which allows the study and manipulations of upstream targets with high precision. The hippocampal formation consists of the following structures: the *entorhinal cortex, dentate gyrus, cornu ammonis* and the *subiculum*. Unlike other parts of the cerebral cortex which have a clearly defined six-layered organization, the structure of the entorhinal cortex is considered to be transitional (11). It is further divided into the medial entorhinal cortex (MEC) and lateral entorhinal cortex (LEC). This is a functional division, not a layered one. The function of the MEC is to enable the representation of intrinsically generated signals for perceived and planned movements in stable, already familiar contexts. The function of the LEC is to provide a mechanism for the understanding of new information in novel environments (12). The principal neurons of the EC are pyramidal cells and stellate cells located in layers III and II (13) which use glutamate as an excitatory neurotransmitter. The dentate gyrus is comprised of three layers, the *molecular layer*, *granule cell layer* and the *polymorphic layer*. In the rodent brain, it is one of the rare brain structures known to have a significant rate of adult neurogenesis (14). The granule cell layer houses the principal neurons of the DG, the granule cells. Their dendritic trees are located in the molecular layer, where they receive inputs from the EC. The cornu ammonis area of the hippocampus is further divided into areas CA1, CA2 and CA3. These areas also have a clearly defined layered structure consisting of the *stratum oriens*, *stratum pyramidale*, *stratum radiatum* and *stratum lacunosum-moleculare*.

The principal neurons of the CA area are pyramidal cells located in the *stratum pyramidale*. The subiculum area is comprised of the parasubiculum, presubiculum, postsubiculum (15). It is the main output area of the hippocampus, sending projections towards the entorhinal cortex and multiple different areas of the brain, including the nucleus accumbens, septal nuclei, prefrontal cortex, hypothalamus, mammillary nuclei and the amygdala. The organisation of axonal projections of the hippocampal formation starts at the entorhinal cortex. The EC receives inputs from all parts of the neocortex and then relays that information to the dentate gyrus through the cells in its superficial layers. The DG receives its dominant input from the entorhinal cortex layer II neurons via the perforant pathway (16). The projections from the

MEC terminate onto the proximal dendritic area of the molecular layer (medial perforant pathway (MPP)) while the projections of the LEC end on the distal dendritic area (lateral perforant path (LPP)) (17). The principal cells of the dentate gyrus, the granule cells, that receive the perforant pathway give rise to axons that, again unidirectionally, project to the pyramidal cells of the CA3 field of the hippocampus. This pathway is known as mossy fibers. The pyrammidal cells of the CA3 area project to the CA1 hippocampal field through the Schaffer collaterals pathway. The perforant pathway, mossy fibers and Shaffer collaterals together form what is called the trisynaptic pathway/loop (18). From the CA1 pyramidal cells, the axons leave either for the subiculum, and then for the EC, or directly back towards the entorhinal cortex. Through these connections the CA1 area and the subiculum close the hippocampal loop, ending their projections in the deep layers of the EC (19). Although this simplified view of the anatomy of the hippocampal formation leaves out a myriad of different cell types and regulatory and specific innervations, it still serves to show that this unidirectional characteristic is somewhat unique in the central nervous system, which has allowed researchers to investigate specificaly defined monosynaptic circuits with a clear understanding of the presynaptic and postsynaptic cellular targets. The anatomical localization of the rodent hippocampus starts at the midline of the brain near the septal nuclei, which marks its rostrodorsal border, and extends laterally in the caudoventral direction over and behind the talamus, ending in the deep temporal lobe. This gives it the appearance of a C-shaped structure. The entorhinal cortex, the structure that provides major inputs towards the hippocampus, is located caudoventrally, and unlike the HP, is located on the surface exterior of the rodent brain. (20).

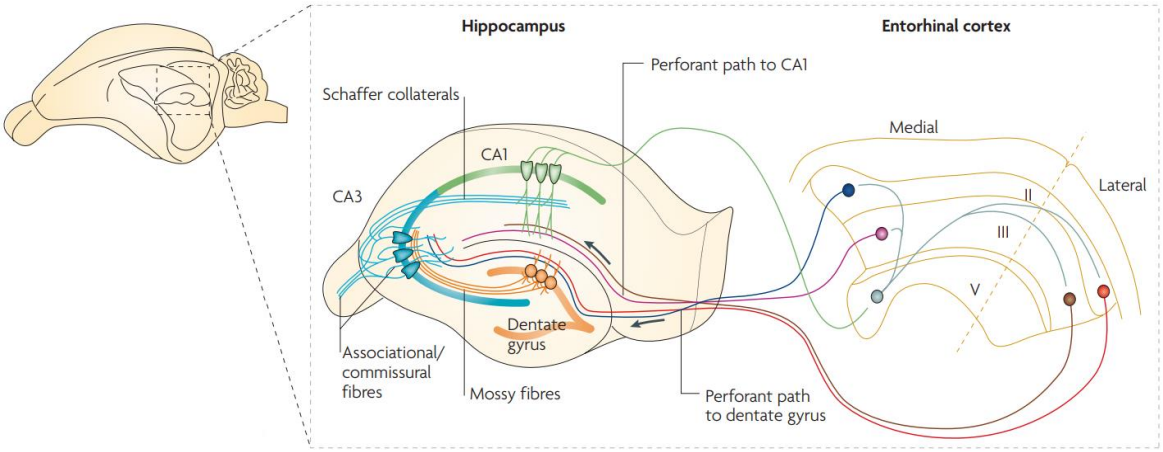

Figure 1. Basic anatomy of the hippocampus. The wiring diagram of the hippocampus is traditionally presented as a trisynaptic loop. Information arrives in the dentate gyrus through the axons of the perforant path. They make excitatory synaptic contact with the dendrites located in the molecular layer belonging to the granule cells, where the lateral entorhinal cortex innervates the outer molecular layer while the medial entorhinal cortex innervates the middle molecular layer. Axons of granule cells innervate the proximal apical dendrites of the CA3 pyramidal cells through the mossy fibers pathway. The circle is further propagated through the Schaffer collaterals pathway, connecting the CA3 with the CA1 pyramidal cells. It is important to note that CA1 pyramidal cells also project to contralateral CA3 and CA1 pyramidal cells through commissural connections. CA3 pyramidal cells are also innervated by a direct projection from layer II cells of the entorhinal cortex, while CA1 pyramidal cells are innervated by layer III cells of the entorhinal cortex. The axons of CA1 pyramidal cells then return to the entorhinal cortex and project to layer V cells. The hippocampus is also home to a wealth of different inhibitory and regulatory neurons not shown in the figure. Taken from (21) with adaptations.

1.1.1. Anatomical description and projections of the dentate gyrus

Similar to other parts of the hippocampus, the DG consists of three layers. The understanding of the aforementioned three-layered architecture is crucial in understanding any changes in the system. They are from outer in: the molecular layer (ML), which further is divided into the outer molecular layer (OML), middle molecular layer (MML) and inner molecular layer (IML); the granule cell layer (GCL) and the hilus (HL). The molecular layer is a relatively cell-free layer closest to the hippocampal fissure and it contains the dendritic trees of granule cells, fibers of local inhibitory neurons, and the fibers of the perforant path from stellate cells of the layer II of the EC (22). However, there is a difference between the fibers originating from the medial compared to lateral parts of the EC. Hjort-Simonsen and Jeune (23) have reported that fibers originating in the LEC terminate in the OML while fibers originating in the MEC terminate in the MML. Besides the granule cells, which will be explained in detail in the next chapter, there is a multitude of cells in the DG and their cell bodies are located in the GCL or in the HL. Radial glial cells are located both in the HL and the GCL. They are GFAP positive, and it is believed that they provide the scaffolding needed for the apical dendrite of the newborn GCs to grow into the molecular layer (24). Basket cells are also located in the HL and GCL and are either GABA or parvalbumin positive (25). They form symmetric synapses with the somata and dendrites of granule cells located in the IML, and they receive afferents from the granule cells, commissural axons of the contralateral DG and perforant path. These connections suggest that they work as a feed-forward inhibitory circuit for granule cells (26). Mossy cells are numerous neurons that populate the HL area. Their proximal dendrites contain complex dendritic spines, called thorny excrescences, while the rest of their dendritic tree has typical spines. The predominant afferent projection comes from mossy fibers of GCs, while the axons of mossy cells contain glutamate, and terminate on the GABAergic interneurons of the hilar region and on dendrites of GCs in the IML. Therefore, the hypothesis is that mossy cells provide excitatory feedback to granule cells and activate local inhibitory elements playing a crucial role in lamellar organization of the hippocampal formation (27). Fusiform cells are located in the HL area, and they are further divided into spiny and aspiny forms. They receive axons from the granule cells and send projections towards the OML, making symmetric synapses on the dendrites of the GCs. They are predominantly GABAergic neurons (28). The chandelier cells are inhibitory interneurons with a unique set of features: their axons form highly-organized rows of boutons and they send their inhibitory projections exclusively on axon initial segments. They are located in the GCL, and more rarely in the HL. They densely

innervate the GCs, while their dendrites extend radially all the way to the HF. This allows them to provide a spatially based inhibition of granule cells (29). Taking all of these cell types into account, their cumulative function is to provide support and provide a selective inhibition/excitation pattern to the granule cells of the DG, thereby allowing a higher degree of accuracy and information content to this principal cell.

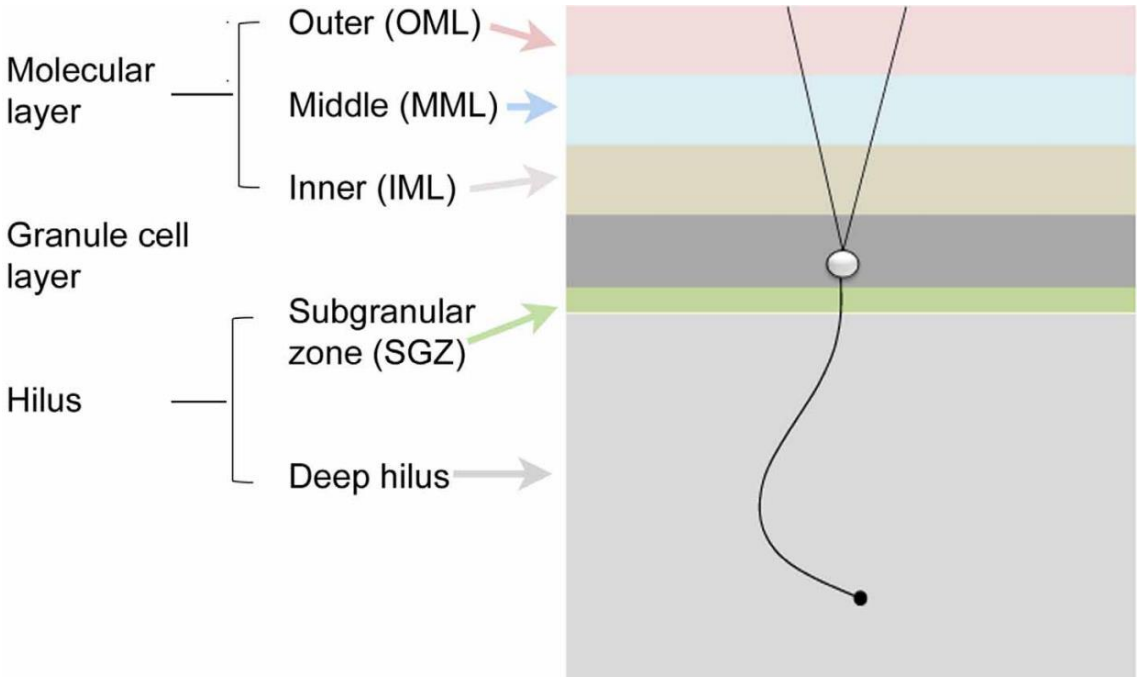

Figure 2. The layers of the dentate gyrus. The illustration shows the laminar organization of the DG, with a single granule cell. The dendritic tree of the granule cell extends towards all parts of the molecular layer, while the axon extends into the opposite direction, called the mossy fiber. The molecular layer is divided into three zones of approximately the same width: the outer molecular layer (light red), middle molecular layer (light blue) and the inner molecular layer (light brown). The granule cell layer (dark gray) contains multiple levels of very densely organized granule cell bodies. The subgranular zone (light green) contains a multitude of hilar neurons described in the text above. The deep hilus is the area that ends at the border of the CA3 area (light gray). Taken from (30) with adaptations.

1.1.2. Dentate gyrus granule cells

The most numerous and crucial cell type of the dentate gyrus is the granule cell. The cells are densely packed in the GCL with little to none glial sheath between them, and the thickness of the GCL is large enough for around 7-8 cell nuclei (31). They are also the only cells to have axons that leave the DG, and they innervate the CA3 field of the hippocampus, as a part of the trisynaptic circuit. The axons of neurons located in layer II of the entorhinal cortex end strictly in the OML and MML of the dentate gyrus, on dendritic spines of granule cells (23). Here they form asymmetrical synapses that account for nearly 85% of total synaptic connections in the DG (32). Glutamatergic input to the IML comes from the axons of mossy cell axons of the commissural/associational collaterals (33). Their dendritic tree is shaped in a cone with the direction towards the hippocampal fissure through the ML, with the distal dendrite tips ending at the fissure (34). The dendrites contain more dendritic spines in the MML and OML due to the perforant path innervation, with around 25% of dendritic spines being located in the IML, 42% of spines in the MML and 33% of spines located in the OML (35).

The perforant path lesion has been used as a brain injury model of denervation since it interrupts the main input to the granule cells of the dentate gyrus (4). Due to the highly stable and laminated structure of these cells, it allows precise tracking of changes in dendritic and spine morphology. Likewise, since the site of the lesion is distant from the dentate gyrus, local inflammatory or degenerative effects in the entorhinal cortex do not influence the post-lesion circuit reorganization in the dentate gyrus (36). Following entorhinal denervation in mice *in vivo*, it has been shown that dendrites react with a loss of predominantly distal dendritic segments (with a reduction of total dendritic length of ~50%) and with a reduction of spine density to ~65% of original values. Dendritic spines recover quite fast, with densities reaching original values in 30 days, while dendrites partially recover to ~70% of initial length after six months. However, this partial recuperation is due to the extension of existing dendrites, as opposed to the formation of new branches (37). After the denervation, there is an expansion of the non-denervated IML that is due to the ingrowth of commissural fibers in order to counteract the heavy loss of afferents (38–41), while inhibitory projections remain stable and relatively unchanged. In fact, even with pharmacological inhibition of excitatory neurotransmission, there is no down-scaling of GABAergic synapses on granule cells after ECL (42). Granule cells are also unique with regards to their ability to withstand pathological conditions such as stress, anoxia, transient cerebral ischemia as compared to CA1 pyramidal neurons (43). It is important

to note that mammalian dentate gyrus granule cells have the ability to proliferate throughout the adult life of the animal (14). The morphology of these cells stays distinct from developmentally born granule cells and they are prone to alterations in their dendritic arbors while maturating (44). The role of adult-born neurons is believed to be novel memory encoding and distinct pattern separation (45).

1.2. Dendrites and dendritic spines

Dendrites are branched extensions of a neuron that propagate electrochemical signals from other neurons via synapses. The morphology of dendrites, such as total length, number of branches, and arborization is highly correlated with neuronal function (46). While highly mobile during development, they retain a modest form of plasticity in adulthood. Dendritic spines are the primary recipients of synaptic inputs and are the smallest multifunctional integrative unit of the nervous system (47). This is in large part due to their ability to detect the temporal coincidence of pre and postsynaptic activity, the coupling of synaptic activity and local, isolated calcium release from their compartments and multiple mechanisms of change in response to this activity (2). After undergoing a period of maturation, every fully formed spine has an excitatory synapse, while many contain both excitatory and inhibitory synapses (48). They emerge from dendritic shafts, and contain a spine neck, the narrow substructure connecting and isolating the structure from the dendrite, and a spine head, the structure that is part of the synapse, specifically the postsynaptic terminal. Their length from the dendrite to the synaptic surface is from 0.5 – 3 μm, while the head is roughly spherical with a diameter between 0.5 – 1.5 μm. The density of spines is between 1-10 spines per micrometer of dendritic length, meaning that some neurons contain thousands of spines (49).

Electron microscopical studies have shown that not all spines have a synaptic contact and that those that lack a synapse (~4%) have a distinct morphology, being very slender, elongated, small and without a clearly defined head (50). These thin, long protrusions without a clear head are called filopodia. It is believed that they are transient structures in the formation of adult stable spines. A significant number of spines also contain the smooth endoplasmic reticulum (SER), mostly involved with intracellular trafficking and calcium storage and dynamics. The SER is usually organized in the form of a spine apparatus (SA), with stacked dense plates and SER cisternae between them (51). Dendritic spines are structures that do not contain any microtubules, rather relying on actin for stability and formation. Due to the predominantly filamentous actin-based structural composition, they are quite plastic structures. The dominant function of dendritic spines is to compartmentalize the transmission of information through the synapse to a single point and to reduce the diffusion of postsynaptic molecules (52).

1.2.1. Morphology and function of dendrites

The shape and volume of the dendritic arbor of neural cells determine the maximum amount and localization of synaptic contacts it can make with efferent structures (53). During development, dendrites are highly plastic structures, dynamically extending and retracting individual branches during maturation (54). It is in development that dendrite structure and synapse formation mechanics are unequivocally connected, where their emergence promotes dendritic stabilization (55). The developmental patterning of dendrites conditions the function of the future, mature neuron. In this regard, the most important parameters to study are dendrite shape with its branching patterns, dendritic arbor size, the localization of dendrites to specific innervation sites and the subdivision of dendrites into electrically isolated compartments (56).

More than 20 years ago, classical experiments demonstrated a correlation between the dendritic arborization within the Wernicke's area related to language and the amount of education of an individual (57). However, successive experiments found that dendrites in adult subjects are very stable, and this is due to the precisely controlled turnover of cytoskeletal elements, in particular of microtubules (58). Besides microtubules, a myriad of F-actin based structures has been discovered inside dendritic shafts that contribute to its structure, such as actin patches, longitudinal fibers and rings (59). Although dendritic spine turnover rate was found to be drastically changed in loss of function experiments, such as focal lesions of the retina (60) and removal of vibrissal input to the barrel cortex of the rat (61), there were no significant changes to the arborization of dendrites in these animals. This post-developmental stability in dendrites is largely due to a packed network of microtubules, also serving as a highway for anterograde and retrograde transport of structural proteins and organelles (62,63).

1.2.2. Morphology and function of dendritic spines

Dendritic spines are tiny actin-rich protrusions that emerge from dendrites and are postsynaptic sites of excitatory synapses (48). Although small, changes in size and morphology of spines have been shown to have functional differences at the level of the synapse (64–68), and this has been confirmed in *in vivo* experiments as well (69). For example, experiments showed that the size of spine remodeling correlates with improved learning and that novel sensory experiences lead to spine formation. A small fraction of new spines, induced by novel experiences, can be preserved throughout the entire life of the animal (70). This outgrowth and subsequent enlargement of nascent spines is very closely connected to the formation of new excitatory synapses (71). The actin network of the spines is highly dynamic, with changes in the amount of F-actin propagating alterations in spine size and subsequently, synaptic efficacy (72,73).

AMPA and NMDA receptors located on the post-synaptic density are the primary culprits responsible for synaptic transmission and plasticity. AMPA receptors bind glutamate and allow sodium and potassium to pass inside the dendritic spine, thereby depolarising the spine (74). In a study by Matsuzaki et al., (75) the researchers showed that the amount of functional AMPA receptors is correlated with spine geometry and volume. In this regard, AMPA receptor activation serves to maintain the shape and activity of spines. They couple the release of glutamate from the presynapse to the depolarization of the postsynapse, and their activation is sufficient to maintain the structure and function of dendritic spines (76). NMDA receptors also bind glutamate, but this is not enough for the opening of the ion channel. Due to a magnesium or zinc ion lodged in the ion channel it is also voltage dependent. Once the dendritic spine is sufficiently depolarised through the activation of AMPA receptors, these ions are dislodged and the channel is then opened. Unlike the majority of AMPA receptors, NMDA receptors are also permeable to calcium (77). This influx of calcium is a critical component of enabling synaptic plasticity, allowing the spine to either grow, expressing more AMPA receptors, or to shrink, expressing less AMPA receptors on its postsynaptic density (78,79). The process of lasting strengthening of synapses is called long-term potentiation (LTP) while lasting weakening of synapses is called long-term depression (LTD) (80). Frequent activity of synapses, caused by high-frequency LTP inducing stimulation protocols, promotes actin polymerization inside the spine, thereby enlarging it (81), and this increases the number of AMPA receptors on the postsynaptic density (82). Likewise, long-term depression (LTD)

inducing stimulation protocols result in actin loss and dendritic spine shrinkage (83), with endocytosis of AMPA receptors at the postsynapse (84).

Although the primary effector on the postsynaptic membrane is the axon end segment with the release of neurotransmitters, there is also an another important participant in the activity of synapses. Glial cells, most commonly astrocytes, play an active role in the integration of synaptic information by the release of gliotransmitters and selective uptake of neurotransmitters in the synaptic cleft. This has caused the acknowledgement that the synapse is composed of three parts: the presynaptic membrane, postsynaptic membrane and surrounding glia; the tripartite synapse (85). Astrocytes produce transient changes in their intracellular calcium concentrations through the release of calcium from the endoplasmic reticulum (86), and they use this mechanism to detect neurotransmitters in the synaptic cleft, causing a release of their gliotransmitters or neurotransmitters to change the electrophysiological excitability of neurons (87). These changes in calcium concentrations due to neurotransmitter stimulation are not linear, providing indirect proof of synaptic information processing by astrocytes (88). The exocytosis of glutamate from astrocytes has been shown to enhance synaptic strength at excitatory synapses between the perforant path and granule cells. This mechanism is activated by neuronal activity-dependent stimulation of purinergic P2Y1 receptors on astrocytes during normal functioning of these synapses (89). It is important to note that this pathway is mediated, in part, by TNF-α (90).

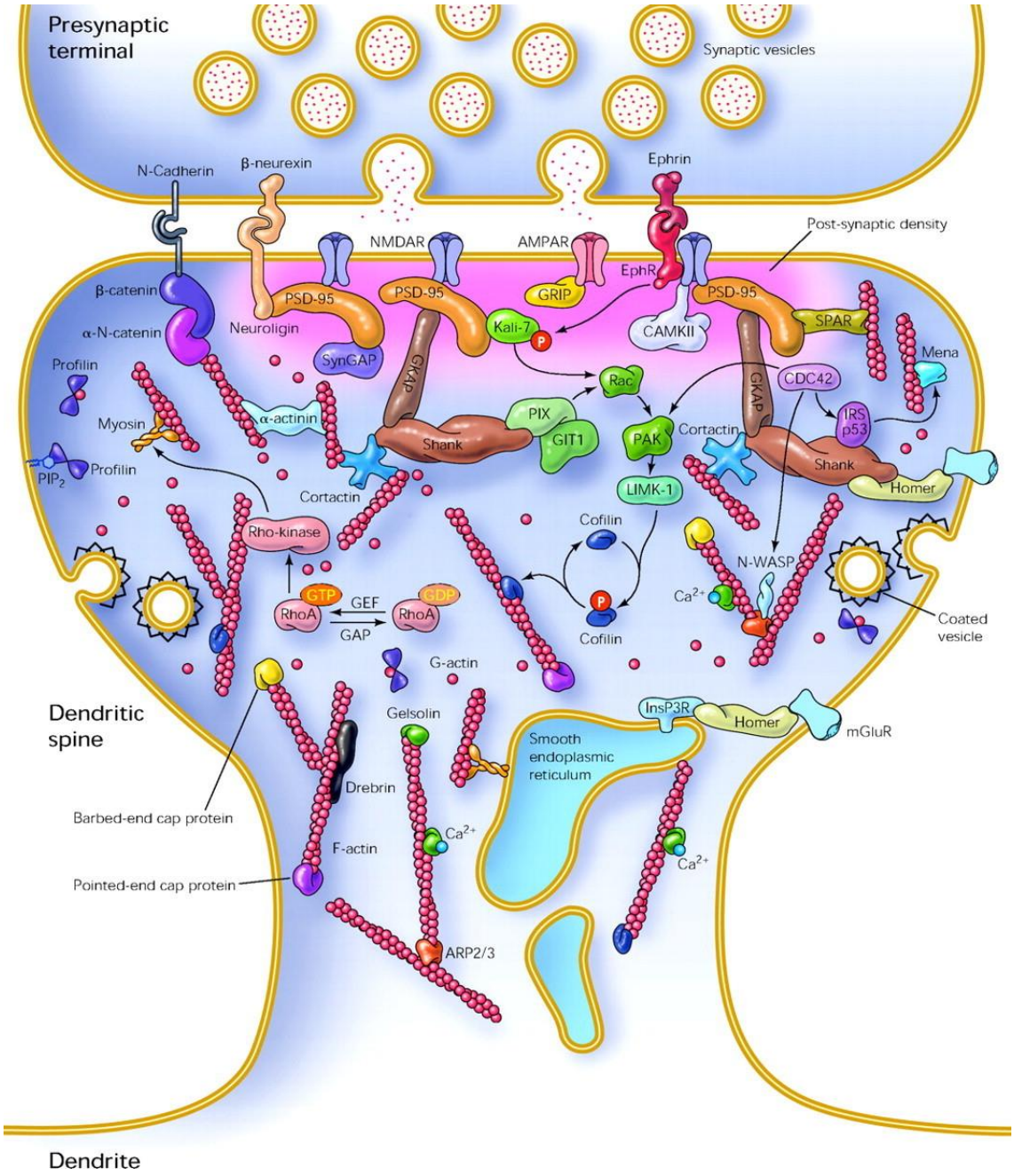

Figure 3. The molecular composition of a dendritic spine. Spines protrude from the dendrite where they form synapses with the presynaptic terminals of axons. At the post-synaptic density, AMPA and NMDA subtypes of glutamate receptors bind the excitatory neurotransmitter glutamate, which is released from synaptic vesicles from the presynapse. On the membrane, outside of the areas of the post-synaptic density, are G protein-coupled glutamate receptors and endocytic zones for recycling of membrane proteins. AMPA and NMDA receptors bind to scaffolding molecules such as PSD-95, which recruit multiple signaling complexes such as regulators of RhoGTPases and protein kinases. Actin filaments provide the main structural basis for spine shape. Through this network of protein interactions, actin filaments link up with

Eph receptors, cadherins and neuroligins to regulate spine development and plasticity-related changes in morphology. Profilin, debrin, cofilin, amongst others, control the extent and rate of actin polymerization, and they are in turn regulated by signaling cascades through the engagement of the transmembrane receptors. Taken from (91) with adjustments.

1.2.3. Homeostatic mechanisms of spines

Hebbian plasticity, which is associated with baseline mechanisms of learning and memory is derived from Hebb's rule, which is summarized as „Neurons wire together if they fire together" (92). We have already mentioned classical Hebbian mechanisms, such as LTP and LTD. Homeostatic plasticity refers to the ability of neurons to change their excitability (specifically in their dendritic arbors) in regard to long-term changes in network activity (93). In order to do that, homeostatic plasticity requires protein synthesis, which happens on a scale of hours or days, and it controls crucial physiological parameters like the number and strength of synaptic inputs to neurons and changes in the levels of intrinsic excitability of post-synaptic compartments (94). Therefore, it can be said that this form of plasticity stabilizes the activity of adult, stable neurons around a clearly defined value (95). In this regard several mechanisms have been found to follow these rules: the activity-dependent regulation of intrinsic firing (96), synaptic scaling (97), the balancing of excitation and inhibition within neural networks (98) and homeostatic regulation of intrinsic excitability (99).

Synaptic scaling is a key homeostatic mechanism that allows the neuron to change the strengths of all of its spines equally in response to a prominent change in activity levels. Although it was believed that this happens on a cell-wide level (100), recent work has shown that synaptic scaling is branch-specific, and is correlated with the degree of recent local spine loss within the branch (101). Experiments that selectively block postsynaptic firing, usually through the aplication of tetradotoxin, have shown that the scaling up of synaptic strengths leads to an accumulation of AMPA-type glutamate receptors that contain the GluA2 subunit (102). In this regard, it has been found that BDNF (103), the immediate early gene Arc (104), the immune molecule MHC1 (105), the scaffold proteins PSD-95 and PSD-93 (106) and importantly, TNF-α, contribute to synaptic scaling (107,108).

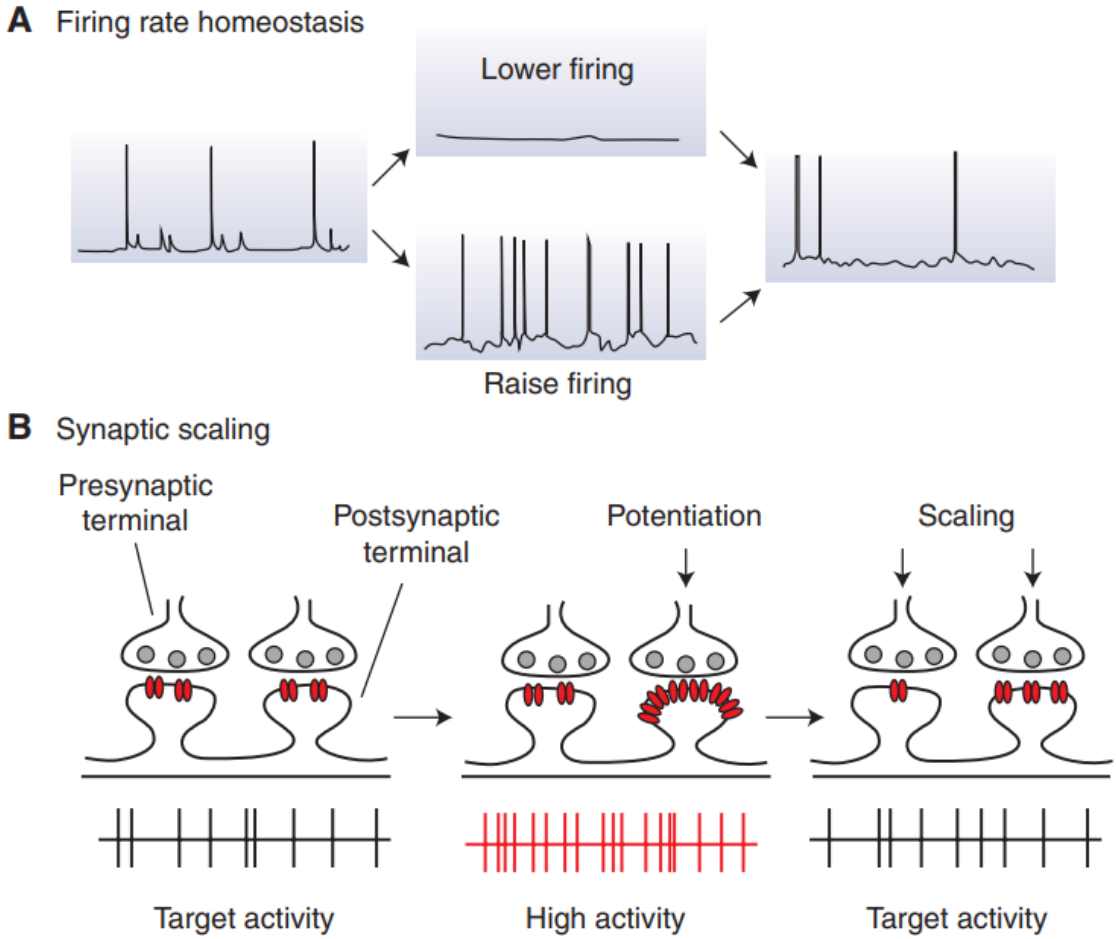

Figure 4. Homeostasis of neuronal firing through the mechanism of homeostatic plasticity. (A) Dissociated neocortical networks show that a reduction or increase in the frequency of action potential generation results in the homeostatic regulation of intrinsic properties so that the initial, stable firing rates are restored. **(B)** Here shown is an increase of activity and subsequent LTP induction at the right dendritic spine, which then triggers synaptic scaling, producing a proportional reduction in strength of all synapses by the same amount in order to return the firing rate to baseline levels. Since this mechanism scales synaptic strength proportionally, the relative difference in synaptic strength is maintained. Taken from (95) with adjustments.

1.2.4. Dendritic spines and brain pathology

A wealth of literature exists connecting different diseases to dendritic spine morphology alterations and loss of dendrite arbor complexity. In Alzheimer's disease, the most common dementia in humans, extensive spine loss and atrophy of dendritic trees is seen (109). The loss of spines is very strongly correlated with disease intensity, specifically with memory impairment in patients (110,111). Down syndrome, the genetic disease caused by trisomy of the chromosome 21, is the most common cause of mental retardation. At birth, patients have a reduced brain size, and this is in part due to reductions of dendritic branching, average dendritic length and spine density (112). The pathological changes in neuronal morphology in children with Down syndrome start developing after 2.5 months of postnatal age (113). Major depressive disorder, which affects ~17% of the population of the world, has also been shown to affect synapse function. Pathological examinations of brain tissue in patients showed anatomical abnormalities in the prefrontal and limbic cortical structures (114). This was followed by the identification of reduced dendritic tree sizes of neurons in those areas (115). In a landmark study by Kang et al. (2012), they showed that patients suffering from major depressive syndrome have a decreased expression of synaptic function-related genes and a corresponding reduction in the number of synapses (116). In autism spectrum disorders, conversely, it was found that patients suffering from this disease have an enlargement of the hippocampus and amygdala (117). Comparative studies also found that patients with autism spectrum disorders have an increase in dendritic spine densities of cortical pyramidal neurons in frontal, temporal and parietal lobes (118). Fragile X syndrome, an inherited neurodevelopmental disease that is the most common single gene cause of autism, also includes a myriad of spine and dendrite alterations. Specifically, there is a higher density of dendritic spines in the cingulate and temporal cerebral cortex, and the spines were more often thin and tortuous (119,120). In schizophrenia, the cause of the reduction of cerebral cortex volume was a mystery since there was no loss of neurons or axons in the brains of patients (121). This was later attributed to the reduction of dendritic arbor size and dendritic spine density of patients (122). Chronic stress is marked by a consistent elevation of the levels of glucocorticoids in the blood. It has been found that glucocorticoids can induce atrophy of dendritic arbors due to glutamate excitotoxicity. This again results in reduced apical dendrite branching, total dendritic lengths and dendritic spine densities (123). Stroke is one of the leading causes of death and disability. Although the primary affected area experiences extreme neuronal loss, the

surrounding area and any connected structures are also highly affected by it. The advent of *in-vivo* imaging allowed us to track changes to different parts of the brain that were previously though to be unaffected by the stroke. In mice, stroke causes degradation of dendrite stability, particularly in the first 2 weeks. Apical dendrites of pyramidal neurons in the somatosensory cortex had intense periods of growth and retraction. However, the net length of arbors remained unchanged as dendritic extensions away from the stroke counteracted the retraction near it (124). Therefore, major pathological events in the brain can cause stable dendrites to exhibit highly plastic behavior.

1.3. Tumor necrosis factor–α

TNF–α is a pro-inflammatory cytokine active in the innate immune response. It exists in two forms, as a transmembrane protein (mTNF) and, more abundantly as a soluble protein (sTNF). Its activity is vital in host defense and inflammatory responses while also causing cell death and degeneration in high enough concentrations. This activity is achieved through the influence of 2 receptors: TNF-receptor 1 (TNF-R1) and TNF-receptor 2 (TNF-R2) (125). In the central nervous system, it is an important regulatory cytokine that has both homeostatic and pathophysiological roles that are concentration dependent (8). Its beneficial roles include synapse formation and regulation, neurogenesis, regeneration of glial cells, promoting excitation and Hebb's plasticity (126).

By contrast, elevated levels of TNF–α are involved in a number of pathologies. It is involved in closed brain injury, where a study has shown that inhibition of TNF–α with pharmacological agents facilitates recovery of motor function and lessens the extent of the developing edema (127). Animal experiments showed that overexpression of TNF–α increases the severity of autoimmune encephalomyelitis, causing chronic microglial activity and demyelination (128). It is also involved in dopaminergic neurotoxicity with regards to Parkinson's disease (129) and amyloid beta generation in Alzheimer's disease (130). The pathological role of TNF–α has been investigated in human patients as well. Specifically, it has been found to be relevant in multiple sclerosis (131), HIV encephalopathy (132), bacterial meningitis (133), cerebral stroke (134) and head injury (135). The multitude of beneficial and pathological effects of TNF–α are shown in Figure 5.

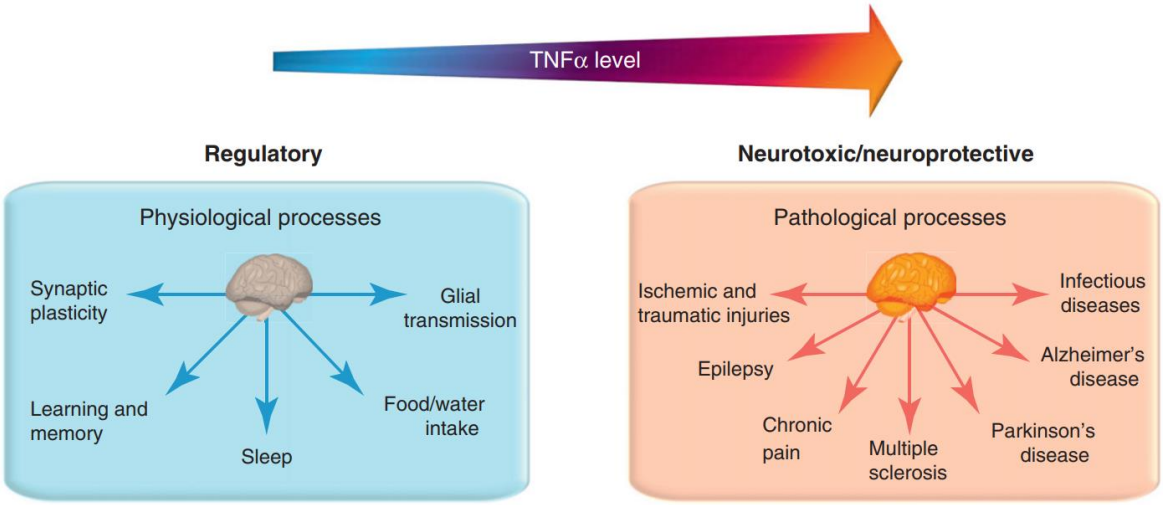

Figure 5. Physiological and pathological processes of TNF–α according to its levels in the CNS. In the healthy brain, constitutive, low levels of TNF–α exert a permissive and regulatory function on several physiological processes, such as learning and memory, food and water intake, sleep, synaptic plasticity and astrocyte-induced synaptic strengthening through its control of glial transmission. Although the concentrations of TNF–α are low, small, locally isolated changes in its levels introduce highly functionally-related changes. Pathologically elevated levels of TNF–α are seen in a number of brain pathologies, where depending on the mechanism of the disease and the activation of different TNF–α receptors, it produces either beneficial or detrimental effects and its role in disease pathology has not been elucidated yet. Taken from (136) with adjustments.

1.3.1. Biochemistry of TNF-α and its receptors

TNF–α is a part of the TNF ligand family, sharing it with LT-α, LT-β and LIGHT. These proteins form trimers, organizing as homotrimers (except for LT-β) (125). First formed as a 26 kDa transmembrane protein (mTNF) which acts by cell-to-cell contact, it is then proteolytically cleaved to the soluble, 17 kDa sized cytokine (sTNF) that is constitutively more active. Both the mTNF and sTNF are active as ligands. mTNF mediates a subset of protective, beneficial effects while lacking the systemic inflammatory effects of sTNF (137). They bind to TNF-R1 and TNF-R2 with different affinities, with sTNF activating primarily TNF-R1 and mTNF activating TNF-R2 but also TNF-R1, although in a much lesser extent compared to sTNF (138). TNF-R1 is ubiquitously expressed on all cells , and its activation leads to multiple, highly complex signaling pathways. Firstly, it recruits TNFR1-associated death domain protein (TRADD), which can have two paradoxically different outcomes: either cell survival or cell death. Cell death is achieved by recruitment of Fas-associated death domain protein (FADD) and caspase 8 to TRADD through the homotypic death domain interactions (139). Cell survival is achieved through pro-inflammatory signaling through the transcription factors NF- kB and AP-1. NF-kB then induces transcription of genes for the production of cytokines, chemokines, and factors against apoptosis (140). Apoptosis, in particular, is achieved through the activation of TNF-R1 by sTNF (141).

In the human body, TNF–α is primarily produced by macrophages (142). Unlike TNF-R1, TNF-R2 is expressed only on immune cells, endothelial cells and a couple of neuronal/glial cell types. TNF-R2 achieves is effects by activation of TRAF2, and downstream, NF-kB and PKB/AKT pathways (143). TNF–α, while in its membrane form (mTNF), besides being a ligand, can also act as a receptor. This inverted way of functioning is called reverse signaling. Through this effect, mTNF can be stimulated by TNF-R2 expressing cells or by anti-TNF antibodies, further complicating the already convoluted landscape of possible interactions (144). This suggests that TNF-R2 plays a specialized, homeostatic role in the brain (145). TNF–α can cross the blood-brain barrier, however this is not the primary source of the protein in the brain. It is produced by some types of neurons (146), microglia with regards to noxious stimuli (147) and, being its biggest source of production in the CNS, astrocytes (148).

In a number of experimental studies, strong activation of only TNF-R1 (due to TNF-R2 being genetically silenced or removed) has caused neuronal damage and pathological circuit

alterations, while activation of only TNF-R2 was found to be protective for the environment of the CNS (136). TNF-R1-KO mice were found to have a higher threshold of seizure resistance in the hippocampus while TNF-R2-KO mice had a lower threshold, being more susceptible to convulsions (149). A similarly designed study found that TNF-R1-KO animals were protected against the development of experimental autoimmune encephalomyelitis, which is used as an animal model of multiple sclerosis. TNF-R2-KO mice actually developed a more severe form of the encephalomyelitis, with the onset happening on a faster time-scale (150). Studies done in cell cultures show that elevated concentrations of TNF–α cause a pronounced apoptosis of hippocampal neurons. This effect is mediated by TNF-R1 (as it was abolished in a loss-of-function experiment, genetically removing the TNF-R1 from the animal), and is prevented by TNF-R2 (due to the effect being amplified in TNF-R2-KO animals) (151).

1.3.2. TNF-α in synaptic transmission

At the start of the 21'st century, multiple groups started investigating the role of TNF-α in synaptic communication and plasticity. One of the first discoveries was that the continual presence of low levels of TNF-α is required for the preservation of synaptic strength. This is due to TNF-α promoting AMPA receptor surface expression at the post-synaptic density of excitatory synapses (7). Further investigation showed that the AMPA receptor clustering is mediated by TNF-R1, because genetic deletion of TNF-R1, but not TNF-R2, decreases AMPA surface expression even with short or long term exposure to TNF-α. In contrast, in TNF-R2-KO animals, TNF-α application promotes AMPA receptor trafficking to the synapse and increases miniature excitatory postsynaptic currents frequency (152). This effect is not indiscriminate, as only GluA2-lacking AMPA receptors join the synapse under TNF-α stimulation, and are then slowly replaced as the synapse stays stable (153). Besides acting on AMPA, TNF-α is responsible for the endocytosis of $GABA_A$ receptors, consequently decreasing inhibitory synaptic strength (154,155).

Experiments done on acute brain slices showed a tightly regulated concentration-based dichotomy of effects on the ability of neurons to express LTP. Application of low concentrations of TNF-α enhanced synaptic plasticity by making it easier to induce LTP, while high concentrations had the opposite effect, impairing synaptic plasticity. This mechanism is dependent on intracellular calcium stores and synaptopodin (8). Synaptic scaling, the negative feedback process of changing all synaptic strengths by a set multiplier thereby preserving the relative differences in synaptic strengths (156), is very closely mediated by TNF-α (107). It does not act as an instructive signal for the initiation of scaling, but is critical in maintaining synapses in a plastic state that would allow them to express synaptic scaling once the mechanism is initiated (108).

Denervation experiments done on organotypical entorhino-hippocampal cultures *in vitro* show that the compensatory increase (synaptic upscaling) of the remaining dendritic spines is due to elevated TNF-α levels, and that astrocytes are the primary source of the molecule in this regard (157). For this effect, it seems that both TNF-R1 and TNF-R2 play an important role (158).

Besides its effects on TNF-R1 and TNF-R2, TNF-α is also critically important in gliotransmission. Astrocytes detect activity at the synapse through purinergic P2Y1 receptors and in response induce calcium dependent glutamate release locally (89). This can then in turn

enhance synaptic transmission by providing an external source of glutamate, besides the vesicles of the presynaptic terminal. It is important to note that in TNF-KO or TNF-R1-KO animals, this mechanism was blocked (90). The glutamatergic gliotransmission causes a presynaptic NMDA receptor-dependent synaptic potentiation. While TNF-KO preparations had similar calcium elevations in astrocytes due to P2Y1 receptor activation, the release of glutamate was severely slowed down due to altered vesicle docking, and was rescued by external application of TNF-α. In this regard, TNF-α is also a permissive factor for gliotransmission (159).

Behavioral analysis of genetically modified mice lacking TNF-α (TNF-KO), TNF-R1 (TNF-R1-KO) or TNF-R2 (TNF-R2-KO) showed multiple deficits. In a study by Baune et al., they investigated learning and retention, spatial learning, cognitive flexibility and learning effectiveness in these mice mutants. All mice were successful in exploration and learning processes, while they differed in specific cognition-like tests. TNF-KO mice performed significantly worse than wildtype (WT), TNF-R1-KO and TNF-R2-KO mice in the novel object test. They also performed worse in spatial learning and learning effectiveness compared to WT mice. This shows that the absence of TNF-α is essential for normal cognitive functioning, while knockout of either receptor can be somewhat compensated by the other one (160).

1.4. Synaptopodin

Synaptopodin (SP) is an actin-associated protein that is located on renal podocytes and in a subpopulation of dendritic spines in the CNS (161). In the brain, its function is closely tied to the SA, an organelle located at the base of a spine head (162–164). The SA is comprised of stacked endoplasmic reticulum plates which allow it to interact with and alter the dynamics of calcium transients inside the dendritic spine (165). It has been found that SP is a critical component of the SA due to it being essential for its formation (9). A modeling study has shown that the organization of dendritic spines with flattened and small heads would lead to a very small or absent SA (and its function as the smooth endoplasmic reticulum) which would ensure rapid signal propagation towards the dendritic shaft. On the other hand, the growth of a bigger and spheroidal-shaped spine head and thereby a bigger endoplasmic reticulum would ensure that calcium, as a vital second messenger, stays active for a long time in the dendritic spine, promoting synaptic plasticity (166).

SP was also found to associate with both F-actin and alpha-actinin, positioning the protein as a possible intermediary between the release of intracellular calcium from the SA and the dynamics of actin with regards to spine morphology and motility (167,168). This was later confirmed by Vlachos et al., where they showed that SP-positive spines have a higher degree of plasticity directly mediated by the activation of intraspinal calcium stores (169). It was recently found that SP interacts with actin-based motor proteins myosin V and VI, and through this connection it can directly influence actin dynamics inside the spine (170). SP mediated release of calcium from the SA could be mediated by the store-operated calcium entry channel Orail1. Orail1 is activated by the STIM1, the intracellular sensor of calcium levels. The high degree of colocalization of both Orail1 and STIM1 with SP indicates their close association (171).

1.4.1. Biochemistry of synaptopodin

SP is a proline-rich actin-associated protein. In the kidney, it is located in differentiated podocytes, where it is part of the contractile apparatus in the foot processes (172), while in the brain it is found near the postsynaptic density, and its expression is also tied to differentiated neurons (161). It exists in two variants, a shorter, 100 kDa isoform, in telencephalic neurons and a longer, 110 kDa isoform, in renal podocytes (161,173). It is has a high content of proline, making it very susceptible to proteolytic degradation and gives it linearity in shape (161). SP interacts with RhoA, an important small GTPase protein associated with cytoskeleton regulation. Specifically, SP acts as a competitive inhibitor of Smurf1-mediated ubiquitination of RhoA, regulating its signaling during the formation and reorganization of the actin cytoskeleton (174,175). In the development of the rat hippocampus, SP mRNA expression is first found only in CA3 pyramidal neurons at birth. This is changed at postnatal day 6, where SP mRNA can also be found in CA1 pyramidal neurons and granule cells. This expression gradually rises until postnatal day 12, where the adult pattern is reached (176). In the adult dentate gyrus, SP is located predominantly inside dendritic spines (>95%), with the biggest density of SP located in spines located on the outer molecular layer (177). SP is formed inside dendritic spines, as there is no evidence of active microtubule-based transport of SP from the soma of the neuron (170). On a genetic level, the combination of heterozygosity of SP and Cd2ap enhances susceptibility to general glomerular damage and the onset of focal segmental glomerulosclerosis in humans (178).

1.4.2. Synaptopodin in synaptic transmission

Ryanodine receptors are large ion channels responsible for the release of calcium from the endoplasmic reticulum. In dendritic spines the primary ligand for the opening of their channels is calcium that entered at the postsynaptic density through open NMDA receptors (179). In a study by Korkotian and Segal, the authors found that the presence of SP in dendritic spines significantly slows down the decay time of the calcium transient, thereby ensuring its pivotal role as a second messenger (165). Through this effect, ryanodine receptors facilitate the expression of LTP. Loss-of-function experiments linked SP with this effect, where SP mediates the effects of ryanodine on LTP (165,180). This effect is also seen in the developing hippocampus, where the researchers were unable to elicit protein kinase A-dependent LTP in SP-deficient mice (181). SP-deficient mice have an impairment of theta-burst stimulation based LTP with an additional effect of reduced paired-pulse inhibition showcasing local network inhibition deficits (182).

After the induction of synaptic strengthening, such as with the activation of synaptic NMDA receptors, the overexpression of SP did not induce a significantly higher enlargement of dendritic spine volumes compared to controls. Instead, it ensured that the increase was persistent over a longer period of time (183). In our previous work, the role of SP was further elucidated, proving that SP is crucial for dendritic spine stability. In this regard, spines that contain SP follow a much slower two-stage exponential decay, surviving for a longer period of time (10). In the context of ECL-induced plasticity, the densities of SP and the SA follow the reduction in dendritic spine densities in the OML and MML (184).

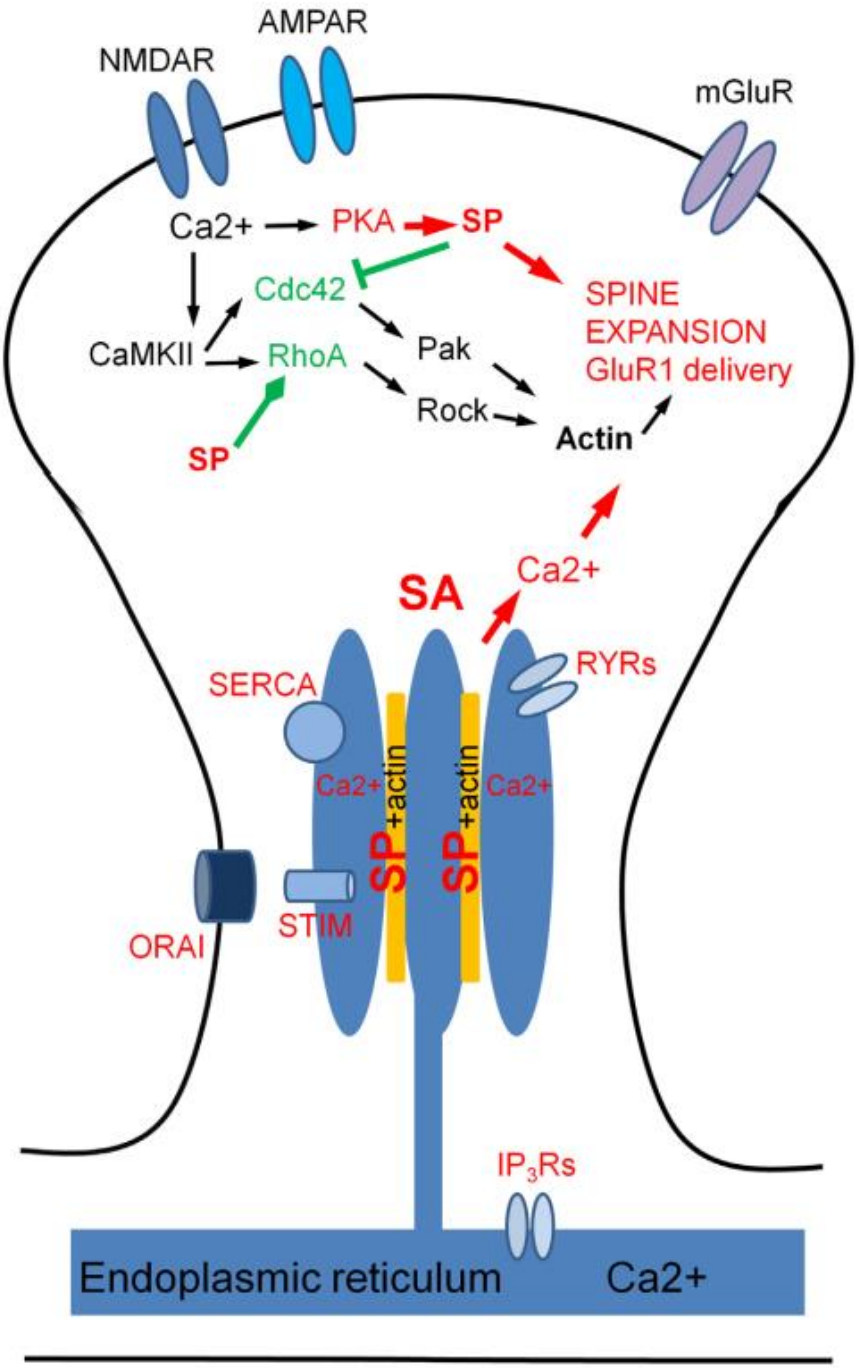

Figure 6. Signaling pathways of SP associated with LTP in the dendritic spine. SP is necessary for the formation of the SA, the local calcium store. Through its connection with the SA, it modulates calcium transients inside the spine. SP also stabilizes F-actin in spines, via the cAMP-PKA signaling pathway. Another possible mode of influencing actin dynamics is through its effects on RhoA and Cdc42 GTPases. Experimentally observed SP effects in neuronal spines (*red arrows*). Hypothetical SP interactions based on experiments in podocytes (*green arrows*). Taken from (185) with adjustments.

2. HYPOTHESIS

Gyrus dentatus granule cells in mice that do not express TNF-α have smaller spine sizes and synaptopodin cluster levels when compared to wildtype controls.

3. AIMS AND PURPOSE OF THE RESEARCH

3.1. General aim

The aim of this research is to investigate the influence of TNF-α on neuronal morphology in mice, with a special emphasis on the study of dendritic spine density and shape.

3.2. Specific aims

3.2.1. Investigate the morphology of granule cells dendritic tree in wildtype mice and TNF-α knockout mice.

3.2.2. Investigate the shape of granule cell dendritic spines in wildtype mice and TNF-α knockout mice.

3.2.3. Investigate the granule cell dendritic spine density in wildtype mice and TNF-α knockout mice.

3.2.4. Investigate the influence of synaptopodin presence in spines to the size of those spines in wildtype mice and TNF-α knockout mice.

3.2.5. Investigate the correlation of synaptopodin presence in spines to morphology in wildtype mice and TNF-α knockout mice.

4. MATERIALS AND METHODS

Throughout this doctorate thesis, the hypothesis was tested on organotypic slice cultures (OTC) prepared from Thy1-eGFP newborn (P=0) mice line lacking TNF-α (TNF-KO) and *ex vivo* mouse brain slices from mice lines lacking TNF-α (TNF-KO), TNF-R1 (TNF-R1-KO), TNF-R2 (TNF-R2-KO) and a mice line lacking both TNF-R1 and R2 (TNF-R1+2-DKO). We used an entorhinal cortex lesion model for the slice cultures and intracellular filling of fluorescent dyes with immunofluorescence staining for mouse slices, imaging was done with confocal microscopy, and the dendritic arbors and dendritic spines of granule cells in the hippocampus were manually analyzed in ImageJ/Fiji (186).

4.1. Animals

We have used a Thy1-eGFP mouse line (C57BL/6J Jackson Laboratory, Bar Harbor, Maine, RRID: IMSR_JAX:007788) and a Thy1-eGFP mouse line lacking TNF-α (TNF-KO) for the preparation of organotypic entorhinohippocampal tissue cultures (OTCs). Thy1-eGFP-TNF-KO mice were obtained by crossbreeding Thy1-eGFP transgenic mice with TNF-deficient mice (TNF-KO, C57BL/6J Jackson Laboratory, Bar Harbor, Maine, RRID: IMSR_JAX:003008), so that neurons in the culture would be fluorescently labeled, while devoid of endogenous TNF-α. For the *ex vivo* analysis of granule cell spines in fixed hippocampal slices, we used adult male mice (12-26 weeks) lacking TNF-α (TNF-KO, C57BL/6J background (187)), TNF-Receptor 1 (TNF-R1-KO, C56BL/6J background (137)), TNF-Receptor 2 (TNF-R2-KO, C56BL/6J background (137)), TNF-Receptor 1 and 2 (TNF-R1+2-DKO, C56BL/6J background (137)) and wildtype mice (WT, C57BL/6J background). Only male mice were used because the density of spines and synapses varies with the estrus cycle in female mice dependent on local estrogen concentrations (188). Adult mice used for fixed brain slices were housed and bred at MfD Diagnostics GmbH, Wendelsheim, and after delivery to the NeuroScience Center, Goethe University, were kept in an in-house scantainer for a minimum of 24 h to reduce stress and facilitate adaptation to the new environment. Mice used for organotypic tissue cultures were housed and bred at the animal facility of Goethe University Hospital Frankfurt. All animals were maintained on a 12 h light/dark cycle with food and water available *ad libitum*. Experimental procedures and animal care were performed in accordance with the German animal welfare legislation, Croatian animal welfare legislation and approved by the ethical committee of the University of Zagreb, School of Medicine, and by the animal

welfare officer of Goethe University Frankfurt, Faculty of Medicine. Every effort was made to minimize the distress and pain of animals.

4.2. Perfusion and slice preparation

Animals were killed with an overdose of intraperitoneal Pentobarbital sodium solution (65 mg/kg) and subsequently intracardially perfused (0.1 M Phosphate Buffer Saline (PBS) containing 4% paraformaldehyde (PFA)) using the following protocol (189) with modifications:

- Preparing the apparatus
    - Warm perfusion buffer to air temperature
    - Place outlet valve in a beaker filled with PBS
    - Fill a container attached to 50cm above the operational area with PBS and attach to fixative tubing, then do the same with a second container filled with PFA
    - Clear the lines until all air bubbles are eliminated
    - Close the outlet port with the needle end and enable the flow from the buffer valve
- Perfusion surgery
    - After the animal has reached a surgical plane of anesthesia, place it in the operating area. Test depth of anesthesia using the toe pinch-response method.
    - Make a 5 cm lateral incision through the abdominal wall just beneath the rib cage.
    - Make a small incision in the diaphragm using curved scissors, continue to expose the pleural cavity.
    - Carefully cut through the rib cage up to the collarbone in the anterio-axillar line in both sides.
    - Lifting the sternum, trim any tissue connecting it to the heart, then immobilize the sternum to the right collarbone so that the left ventricle is more exposed.
    - Using a 24-gauge needle connected to the outlet port, enter the left ventricle and pass it 0.5cm inside.
    - Make an incision to the animal's right atrium using iris scissors, taking care not to damage the aorta or pulmonary blood vessels.

- Perfusion
    - Open the outlet port and allow the flow of the buffer. Keep the flow of the buffer until the liver color changes to from red to white and the liquid exiting the right atrium is clear.
    - Switch the buffer valve to the fixative valve and perfuse for 4 minutes. Note the signs of a good perfusion (twitching of arms and legs, flexion of the tail).
    - Close the outlet port and remove the needle.
- Dissection
    - Remove the head using a pair of scissors.
    - Make a midline incision along the integument from the neck to the nose and expose the skull.
    - Place the sharp end of iris scissors into the foramen magnum and make an incision 0.5 cm deep at the midline, then make incisions laterally 2.5 cm deep following the line connecting the foramen magnum and ears.
    - Using the sharp end of iris scissors, make a hole between the olfactory bulbs of the skull.
    - Make incisions laterally 2.5 cm deep following the line connecting the hole to the ears, then make a incision in the middline from the hole caudally, taking extreme care that the blunt end is ventrally placed and that you do not touch the brain tissue.
    - Using rongeur forceps peel the dorsal surface of the skull away from the brain.
    - Using a spatula, sever the olfactory bulbs and nervous connections along the ventral surface of the brain.
    - Remove the brain and place it in a vial filled with PFA so that the brain is fully submerged.

Tail biopsies were obtained after death to re-confirm the genotype. Brains were taken out with care after perfusion, post-fixed overnight (18 h, 4% PFA in 0.1 M PBS, 4° C) and washed three times in ice-cold 0.1 M PBS. Afterwards, mouse brains were sectioned in 250 µm thick coronal slices on a vibratome (Leica VT 1000 S) and slices containing the dorsal hippocampus were stored at 4° C until use.

4.3. Organotypic slice culture preparation and transection of entorhinal afferents

Organotypic entorhino-hippocampal tissue cultures 300 µm thick were prepared from postnatal 4-5 days old Thy1-eGFP and Thy1-eGFP-TNF-KO mice as previously described (190), and as shown in the schematic (Fig. 7).

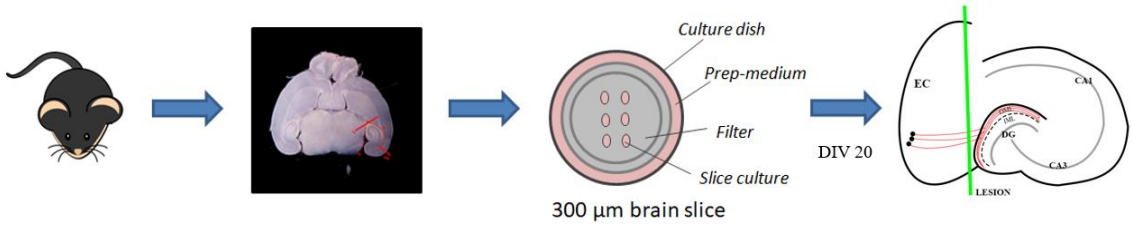

Figure 7. Schematic showing the preparation of mouse entorhino-hippocampal slice cultures followed by an entorhinal cortex lesion. 300 µm thick organotypic slice cultures were prepared from P4-5 mice pups and placed on filter membranes. After maturation, a subset of OTCs were transected of entorhinal afferents. DG: Dentate gyrus; CA3: Cornu ammonis area 3; CA1: Cornu ammonis area 1; EC: Entorhinal cortex; OML: Outer molecular layer; IML: Inner molecular layer.

Culture incubation medium contained 42% MEM, 25% Basal Medium Eagle, 25% heat-inactivated normal horse serum, 25 mM HEPES, 0.15% sodium bicarbonate, 0.65% glucose, 0.1 mg/ml streptomycin, 100 U/ml penicillin, 2 mM glutamax, adjusted to pH 7.30. The cultivation medium was refreshed every 2 to 3 days. All tissue cultures were allowed to mature *in vitro* for 20 days (DIV 20) in a humidified incubator (5% CO2, at 35° C). A subset of tissue cultures was completely transected from the rhinal fissure to the hippocampal fissure using a sterile scalpel blade after imaging the dentate gyrus granule cells at DIV 20. The entorhinal cortex was removed from the culture dish to ensure permanent separation from the hippocampus (Fig. 8A.)

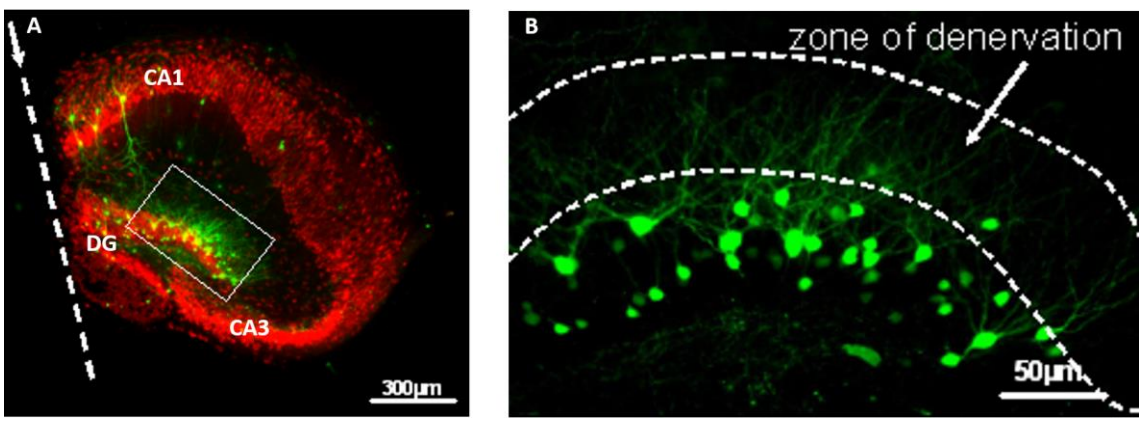

Figure 8. Thy1-eGFP expressing granule cells in the hippocampal dentate gyrus after transection of afferent fibers. (A) Horizontal section showing the pattern of GFP-expressing neurons *(green)* in the hippocampus, counterstained for NeuN *(red)*. OTCs show the classical anatomical organization of the hippocampus, with the site of the lesion shown *(dotted line)*. **(B)** GFP expression is sufficient for detailed analysis of dendritic arbors, with the zone of denervation presented *(between dotted lines)*. DG: Dentate gyrus; CA3: Cornu ammonis area 3; CA1: Cornu ammonis area 1.

Both control cultures from Thy1-eGFP and Thy1-eGFP-TNF-KO mice and transected cultures from Thy1-eGFP and Thy1-eGFP-TNF-KO mice were returned to the incubator and were kept for 14 days. Afterward, the previously imaged granule cells in all described cultures were found and reimaged at DIV34.

4.4. Intracellular filling of fluorescent dyes

Intracellular injections of granule cells in fixed hippocampal slices were performed as previously described (191,192) with the following modifications: Hippocampal slices were placed in a custom-built, transparent, and grounded recording chamber filled with ice-cold 0.1M PBS. The chamber was attached to an epifluorescent microscope (Olympus BX51WI; 10x objective LMPlanFLN10x, NA 0.25, WD 21 mm) mounted on a x-y anti-vibration table (Science Products, VT-1 xy Microscope Translator). Sharp quartz-glass microelectrodes. Sharp quartz-glass microelectrodes (Sutter Instruments, QF100-70-10, with filament) were pulled using a P-2000 laser puller (Sutter Instruments). Microelectrodes were tip-loaded with 0.75 mM Alexa 568–Hydrazide (Invitrogen) in HPLC-grade water (VWR Chemicals, HiPerSolCHROMANORM) and subsequently back-filled with 0.1 M LiCl in HPLC-grade water. Microelectrodes were attached to an electrophoretic setup via a silver wire and 500 MΩ resistance. The tip of the microelectrode was navigated into the granule cell layer of the hippocampus under visual control under the microscope using a micromanipulator (Märzhäuser Wetzlar, Manipulator DC-3K). A square-wave voltage (1mV, 1 Hz) was applied using a voltage generator (Gwinstek SFG-2102). Granule cells were filled under visual control for 10 min. If the fluorescent dye reached the tips of the dendrites in the outer molecular layer of the dentate gyrus, the filling was considered successful (Fig. 9A). Injected sections were fixed (4% PFA in PBS, overnight, 4° C, in darkness) and subsequently washed in 0.1 M PBS.

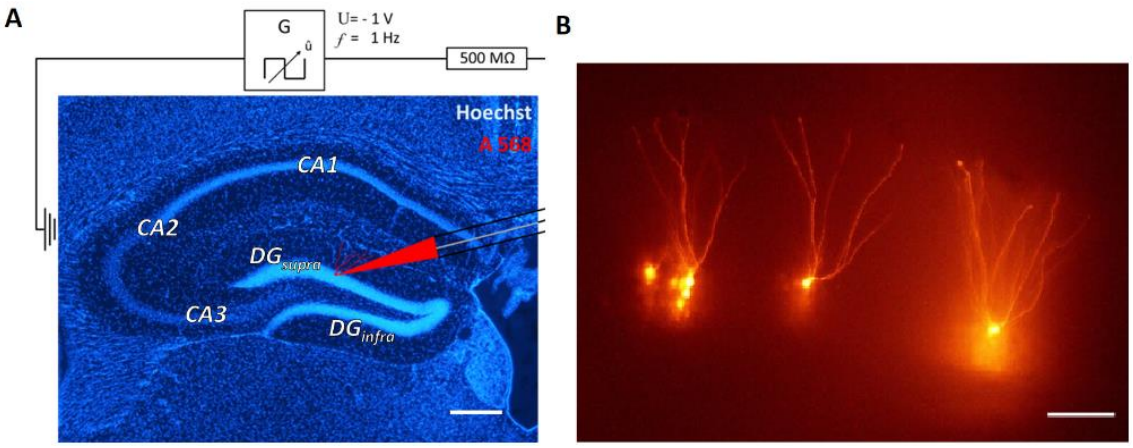

Figure 9. Intracellular injections of fluorescent dyes. **(A)** Schematic representation of intracellular filling of dentate gyrus granule cells in a coronal 250 µm section of the hippocampal formation in mice. The cells are impaled by a quartz glass electrode loaded with 1 mM Alexa Fluor 568 dye and filled for 10 minutes. DG_{supra}: Suprapyramidal blade of the dentate gyrus. DG_{infra}: Infrapyramidal blade of the dentate gyrus. CA1, CA2, CA3: Cornu ammonis areas 1, 2 and 3. Scale bar = 500 µm. **(B)** An overview image taken on the filling setup (10x magnification). Shown are fully filled granule cells in the suprapyramidal blade of the dentate gyrus layer. Scale bar = 100 µm.

4.5. Immunohistochemistry

Filled and fixed injected sections 250 µm thick were embedded in 5% agar and resliced to smaller sections of 40 µm thickness on a vibratome (Leica VT 1000 S). The following protocol was used for staining of slices for synaptopodin:

- Wash free-floating sections 3 times for 5 minutes in 50 mM Tris buffered saline (TBS) containing 0.1% Triton X-100.
- Incubate in a blocking buffer (0.5% Triton X-100, 5% bovine serum albumin (BSA)) for 30 minutes at room temperature (RT).
- Incubate with primary antibody (anti-synaptopodin, guinea pig polyclonal (SP, Synaptic Systems, RRID: AB_10549419), dilution 1:2000, dissolved in TBS containing 0.5% Triton X-100, 1% BSA) for 3 days at RT on a shaker (180 spins/min).
- Wash 3 times for 5 minutes in 50 mM TBS containing 0.1% Triton X-100.

- Incubate with secondary antibody (donkey anti-guinea pig Alexa Fluor 488 (Dianova), dilution 1:2000, dissolved in TBS containing 0.5% Triton X-100, 1% BSA) for 4 hours at RT.
- Wash 3 times for 5 minutes in 50 mM TBS.
- Mount the slices in DAKO fluorescence mounting medium (Dako North America Inc.).

4.6. Imaging

Live imaging of eGFP labeled neurons (Thy1-eGFP) was done using an upright Zeiss LSM Pascal confocal microscope, equipped with a 40x water immersion objective (Plan-Apochromat, NA 1.0, Zeiss). The membrane insert with the 20 days old OTCs (DIV20) was placed in a dish containing warm imaging buffer (129 mM NaCl, 4 mM KCl, 1 mM MgCl2, 2 mM CaCCl2, 4.2 mM glucose, 10 mM HEPES buffer solution, 0.1 mM Trolox, 0.1 mg/ml streptomycin, 100 U/ml penicillin), and pH was buffered to 7.4. Complete granule cells with all dendrites visible were imaged (20-40 images per z-stack, 0.5 µm z-axis step size) at a resolution of 1024 x 1024 pixels, i.e. 0.32 µm x 0.32 µm in the focal plane (Fig. 10A). The positions of identified and imaged granule cells were noted. After a subset of slices were transected from afferents, the same granule cells were imaged in transected and non-transected cultures at DIV34; 14 days after the first imaging session (Fig. 10B). Imaging time was minimized to reduce the risk of phototoxic damage.

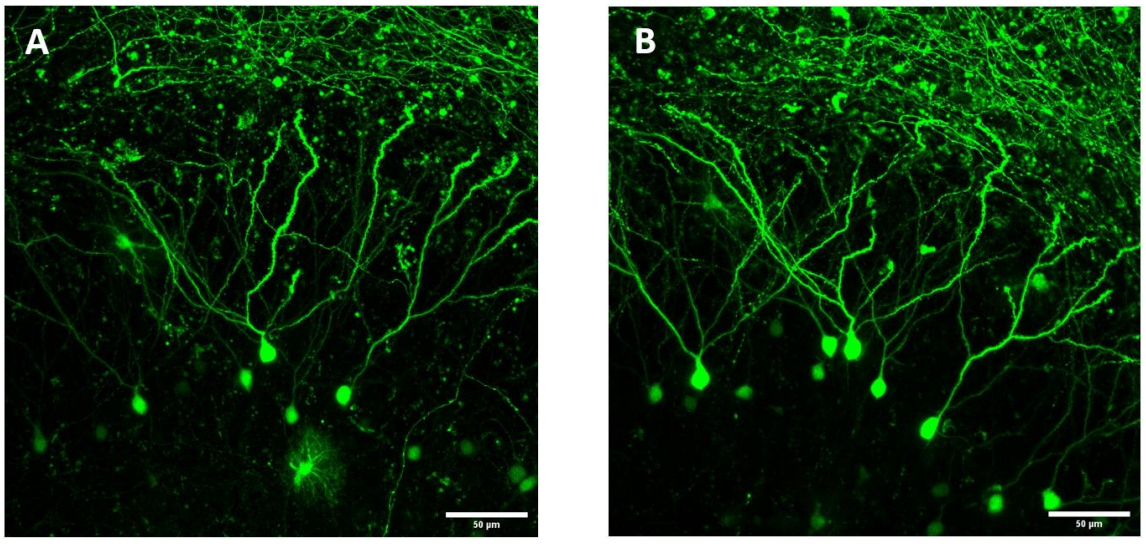

Figure 10. Max z-projections of confocally imaged z-stacks in OTCs. eGFP tagged dentate gyrus granule cells *(green)* were imaged at DIV 20 **(A)**, and then were identified at DIV 34 **(B)**, and imaged again to allow the analysis of changes in dendritic arbors after entorhinal cortex transection. Images were taken with an upright Zeiss LSM Pascal confocal microscope, 40x water immersion objective lens.

Confocal imaging of dendritic spines in fixed dendritic segments from identified, Alexa 568–labeled dentate gyrus granule cells (Fig. 11A) in the outer molecular layer (OML) of the suprapyramidal blade was done with an upright Olympus FV1000 microscope and a 60x oil-immersion objective (UPlanSApo, NA 1.35, Olympus). 3D image z-stacks of dendritic segments (~40 µm length, 30-90 images per z-stack, 0.15 µm z-axis step size) were taken using FV10-ASW software with 5x scan zoom at a resolution of 1024 x 1024 pixels, i.e. 0.04 µm x 0.04 µm in the focal plane. Crossing dendritic segments or branch points were avoided to facilitate spine attribution to a given segment. Imaging parameters were set as to capture the dendritic segment as bright as possible, while not oversaturating any dendritic spines. This was needed due to the uneven strength of signal from cells due to the limitations of the intracellular filling method. Imaging of synaptopodin was done by having all imaging parameters the same across all images (Fig. 11B). The images obtained were deconvolved with Huygens Professional Version 17.10 (Scientific Volume Imaging, The Netherlands).

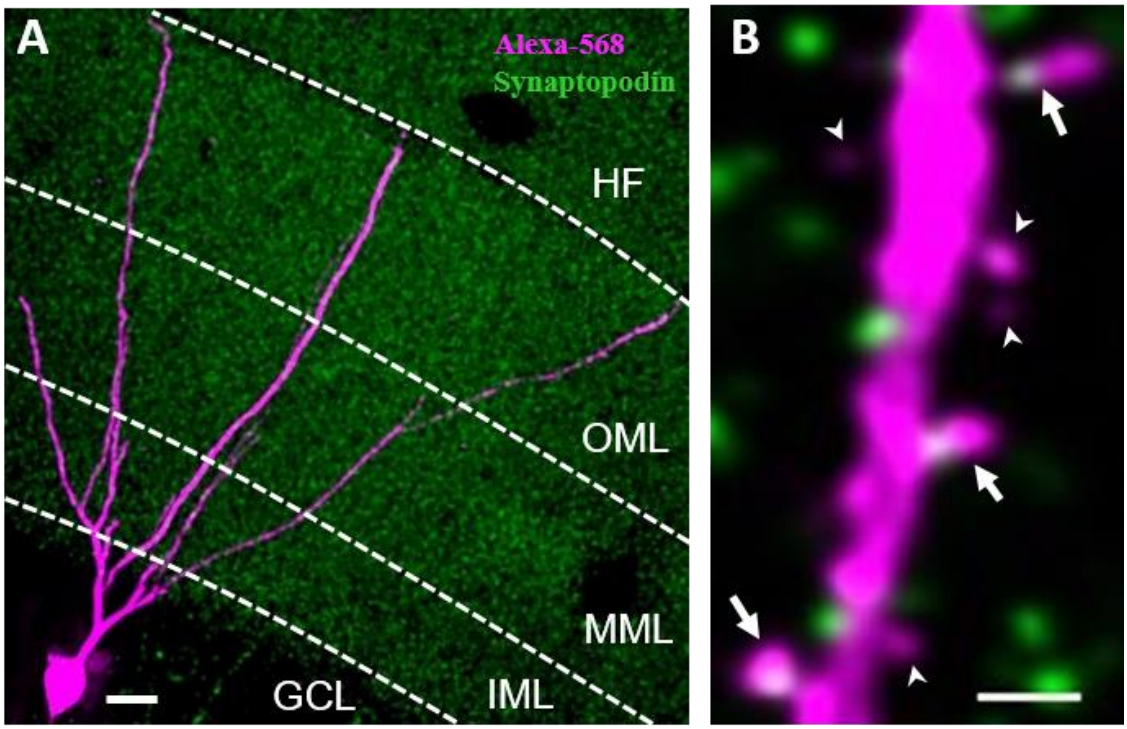

Figure 11. Intracellularly filled granule cell and its dendrite, immunostained for synaptopodin. (A) Dentate gyrus granule cell located in the suprapyramidal blade is shown with its dendrites reaching the hippocampal fissure *(purple)*. Only segments located in the outer molecular layer (OML) were used for analysis. Synaptopodin (SP) clusters are predominantly located in the molecular layer *(green)* MML: middle molecular layer; IML: inner molecular layer; GCL: granule cell layer; HF: hippocampal fissure. Scale bar 20 µm. **(B)** Dendritic segment of a filled cell in the OML shown at a higher magnification. Arrows point to SP clusters in SP-positive (SP+) spines; Arrowheads mark SP- negative (SP-) spines. Scale bar = 1 µm.

4.7. Analysis of dendritic arbors

Dendrites of identified dentate gyrus granule cells imaged in OTCs at DIV20 and DIV34 were manually traced using the Simple Neurite Tracer plugin for ImageJ/Fiji (NIH, Bethesda, MD,USA) (193). After identifying the cell body, each primary dendrite was traced and branching points were noted until it terminated. Images of pairs of cells imaged at DIV20 and DIV34 were analyzed by the experimenter who was blinded to the genotype of the animal and to the experimental procedure (with or without the entorhinal cortex transection) (Fig. 12A, B).

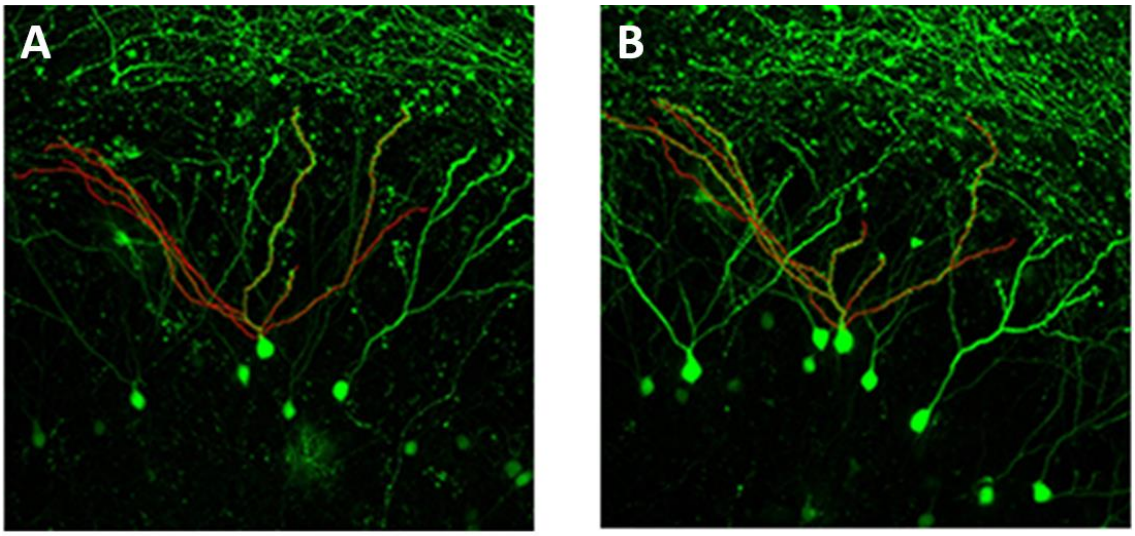

Figure 12. Representative image of max z-projections showing individually traced eGFP-expressing granule cells *(green)*. The tracing *(red)* was done manually in single z-slices of imaged z-stacks, and pairs of cells were analyzed at DIV 20 (A) and DIV 34 (B). Images were taken with an upright Zeiss LSM Pascal confocal microscope, 40x water immersion objective lens.

The Simple Neurite Tracer plugin allowed for detailed analysis of total dendritic lengths, total dendritic lengths per branching order of dendrites, total number of dendrites, average dendritic length and Sholl analysis (194). A total of 6 neurons, 1 neuron per mouse (imaged at DIV20 and DIV34) were analyzed for each group and experimental condition (Thy1-eGFP non-transected: n = 6; Thy1-eGFP transected: n = 6; Thy1-eGFP-TNF-KO non-transected: n = 6; Thy1-eGFP-TNF-KO transected: n = 6).

4.8. Analysis of dendritic spines

Image processing and data analysis were manually performed using Fiji version 1.52h (186) with spine analysis adapted from published criteria (195). All measurements were made blind to the genotype of the animals. Dendritic spines of all shapes were assessed manually on z-stacks of dendritic segments in the OML. Only protrusions emanating laterally in the x-y directions, not above or below the dendrite, and exceeding the dendrite for at least 5 pixels (0.2 µm) were included for analysis (10,195,196). The length of each segment was determined (Fig. 13A).

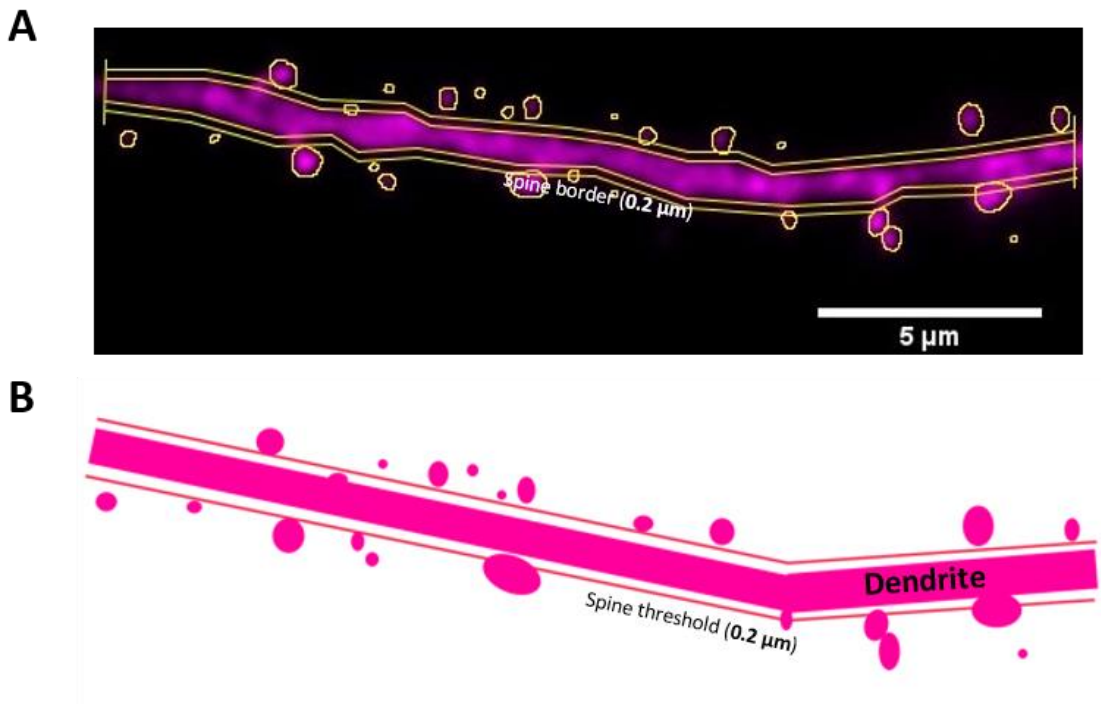

Figure 13. Manual analysis of dendritic spine head sizes and dendritic length. **(A)** A max-z projection of an analyzed segment. The outer borders of the segment represent the application of the Holtmaat criteria. ROI's of identified spines are shown. 60x magnification, 5x digital zoom, scale bar = 5 µm. **(B)** A schematic showcasing the method to reliably count and quantify dendritic spines in confocal image-stacks. A spine threshold of 0.2 µm was applied in maximum z-projection and used as an inclusion criterion. All counting and quantification of spine sizes were performed manually in single x-y images while scrolling through the z-stack, permitting a detailed quantification of 3-dimensional dendritic spines.

For spine head area and SP cluster area measurements, the largest maximum cross-sectional area of the spine head or SP cluster in one of the x-y planes within the z-stack was manually measured using a predefined gray-value as a cut-off for the border of the spine head or SP cluster (Fig. 14A). A spine was considered SP+ if the SP cluster overlapped with the spine head, neck, and/or base in both the x-z and y-z directions when scrolling through the z-stacks (Fig. 14B). The subcellular location of SP clusters in the spine head, spine neck, spine base, or dendritic segment was noted. SP clusters were considered within the spine head, if most (> 80%) of the SP-cluster was located within the identified area of the spine head. SP-clusters were considered within the spine neck, if most (> 80%) of the cluster was located outside the dendritic shaft border, between the identified area of the spine head and the shaft, where a fluorescently filled, visible, spine neck was marked. SP clusters were considered associated with the spine base, if they were found within 0.2µm of the intersection between the dendritic spine and the dendritic shaft border. SP clusters were considered inside dendritic shafts if they did not meet any of the aforementioned criteria but were still localized within the investigated dendritic segment.

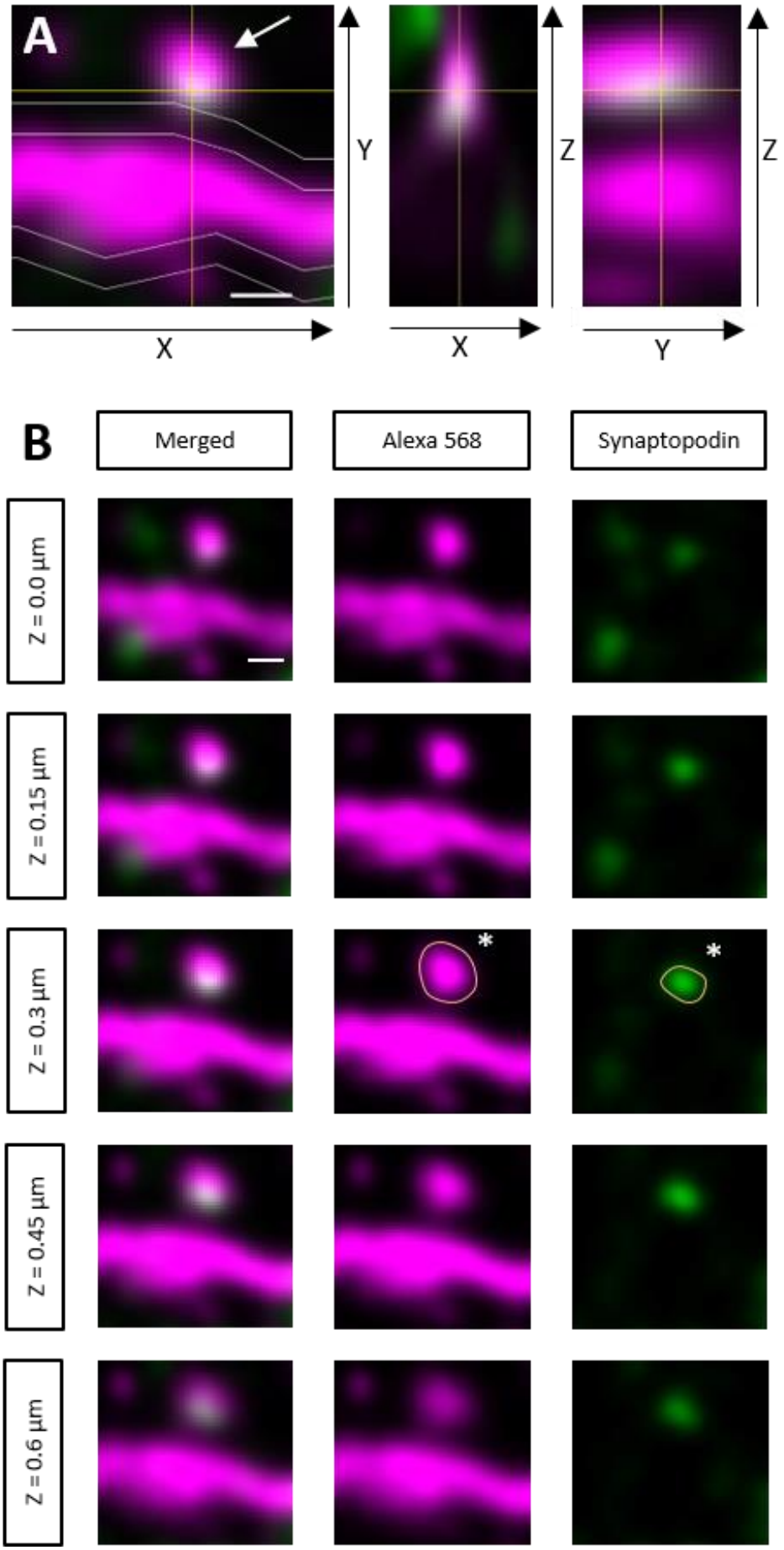
A
Y
Z
Z
X
X
Y
B
Merged
Alexa 568
Synaptopodin
Z = 0.0 µm
Z = 0.15 µm
Z = 0.3 µm
Z = 0.45 µm
Z = 0.6 µm
*
*

Figure 14. Quantification of dendritic spine head size and synaptopodin (SP) cluster size. **(A)** Only spines with heads protruding at least 0.2 µm from the parent dendrite (parallel white lines) were analyzed. Spines colocalizing with an SP cluster in the x-y, x-z, y-z directions when scrolling through the z-stack were considered to be Sp+ (arrow). Scale bar = 0.5 µm. **(B)** Spine head size and SP cluster size were defined as the largest x-y crossectional area obtained in a z-stack. X-y image containing the largest area of spine head (middle column, orange outline of spine head, asterisk) is highlighted. Scale bar = 0.5 µm.

4.9. Statistics

Statistical tests and n-values are indicated in figure captions. Statistical comparisons were performed using the paired t-test (when comparing the difference between two variables for the same subject, in this case comparing variables of dendritic trees of neurons at DIV20 and DIV34), Mann-Whitney U-test (when comparing two independent groups), Kolmogorov-Smirnov test (when comparing cumulative distributions of two independent groups), Wilcoxon signed-rank test (when comparing two paired groups), Kruskal-Wallis test (when comparing more than two independent groups) and correlation analysis (comparing all linked values in a single genotype). Sholl analysis data were compared using two-way repeated measures ANOVA with days in vitro (DIV) as the between group factor and distance from soma in 20 µm increments as the repeated-measure factor. Bonferroni multiple comparison test was used to compare means of a defined distance to the soma between DIV 20 and DIV 34 granule cells. Since dendritic spine sizes do not follow a normal distribution, but a log-normal distribution (197), all statistical tests concerning spine sizes were done with non-parametric tests. All statistical tests were performed using GraphPad Prism 7. If p values were less than 0.05, the null hypothesis was rejected. Statistical values were expressed as mean ± standard error of the mean (SEM) unless otherwise stated. *$p < 0.05$, **$p < 0.01$, ***$p < 0.001$.

5. RESULTS

5.1. Analysis of dendritic trees of granule cells in organotypic hippocampal cultures after ECL *in vitro*

The perforant path projection is the main excitatory input to the dentate gyrus of the hippocampus (32,36,198–200). Ample studies have shown that deafferentiation of granule cells by entorhinal cortex lesion leads to a reduction in dendritic arbor sizes early on after lesion, promotes contrallateral axonal sprouting and causes neuronal death (4,37,201–203). In our study, we hypothesized that the granule cells in TNF-KO OTCs would exhibit different morphological parameters as a response to an ECL when compared to wildtypes. Therefore, we prepared OTCs at postnatal day 4-5 (P4-5), let them maturate until DIV20 and then performed an ECL on a subset of DIV 20 cultures and analyzed dendritic arbor and length parameters of granule cells at DIV 20 and at DIV 34. In total, we had four groups, WT controls (without transection of the entorhinal cortex), WT ECL, TNF-KO controls and TNF-KO ECL, with all groups analyzed at DIV20 and DIV 34.

5.1.1. Dendritic remodeling after entorhinal denervation is partially independent of TNF-α expression

We used a Thy1-eGFP mouse model as controls (WT-CT) and a Thy1-eGFP-TNF-KO mouse mutant model (TNF-CT) to investigate how the lack of TNF influences normal dendritic maturation in organotipical hippocampo-entorhinal cultures *in vitro*. This was combined with an ECL in wildtypes (WT-ECL) and mutants (TNF-ECL) to see how these cells react to deafferentiation. After manually analyzing the dendritic arbors of neurons that were fully imaged at DIV20 and subsequently at DIV34, we compared how total dendritic lengths changed in regards to being deafferentiated in the wildtype and mutant groups. As expected, there were no significant differences between DIV20 and DIV34 for both the WT-CT (n.s. $p = 0.156$) and TNF-CT (n.s. $p = 0.438$) groups, and there was a pronounced, significant reduction in both WT-ECL (~18% reduction; $*p = 0.031$) and TNF-ECL (~14% reduction; $*p = 0.031$) groups (Fig. 15A, Wilcoxon matched-pairs signed rank test). We then compared the change in dendritic length between DIV20 and DIV34 and subsequently compared the results between groups (Fig. 15B). The reduction of total dendritic length was most pronounced in WT-ECL group, followed by the TNF-ECL group and this change was highly significant compared to the relatively preserved dendrites of the control groups ($**p = 0.004$, Kruskal-Wallis test). The

first differences between the deafferentiated groups became visible after analyzing the total number of dendrites. There was a ~22% reduction in the WT-ECL group (*p = 0.031), while surprisingly the TNF-ECL group did not show any significant reductions (n.s. p = 0.500). Both control groups were also unchanged in this parameter (Fig. 15C; n.s., Wilcoxon matched-pairs signed rank test). Comparing the change of dendritic length between groups showed that this reduction in WT-ECL mice was significantly different from all other groups (Fig. 15D; *p = 0.029, Kruskal-Wallis test). Average length of individual dendrites was highly variable between different cells, and there were no differences inside groups (Fig. 15E; n.s., Wilcoxon matched-pairs signed rank test). This was also reflected when comparing between different groups, where the change in average dendritic length stayed similar in all groups (Fig. 15F; n.s. Kruskal-Wallis test). As there was a discrepancy between the WT-ECL and TNF-ECL group in the reduction of the total number of dendrites, we decided to analyze dendritic complexity using Sholl analysis.

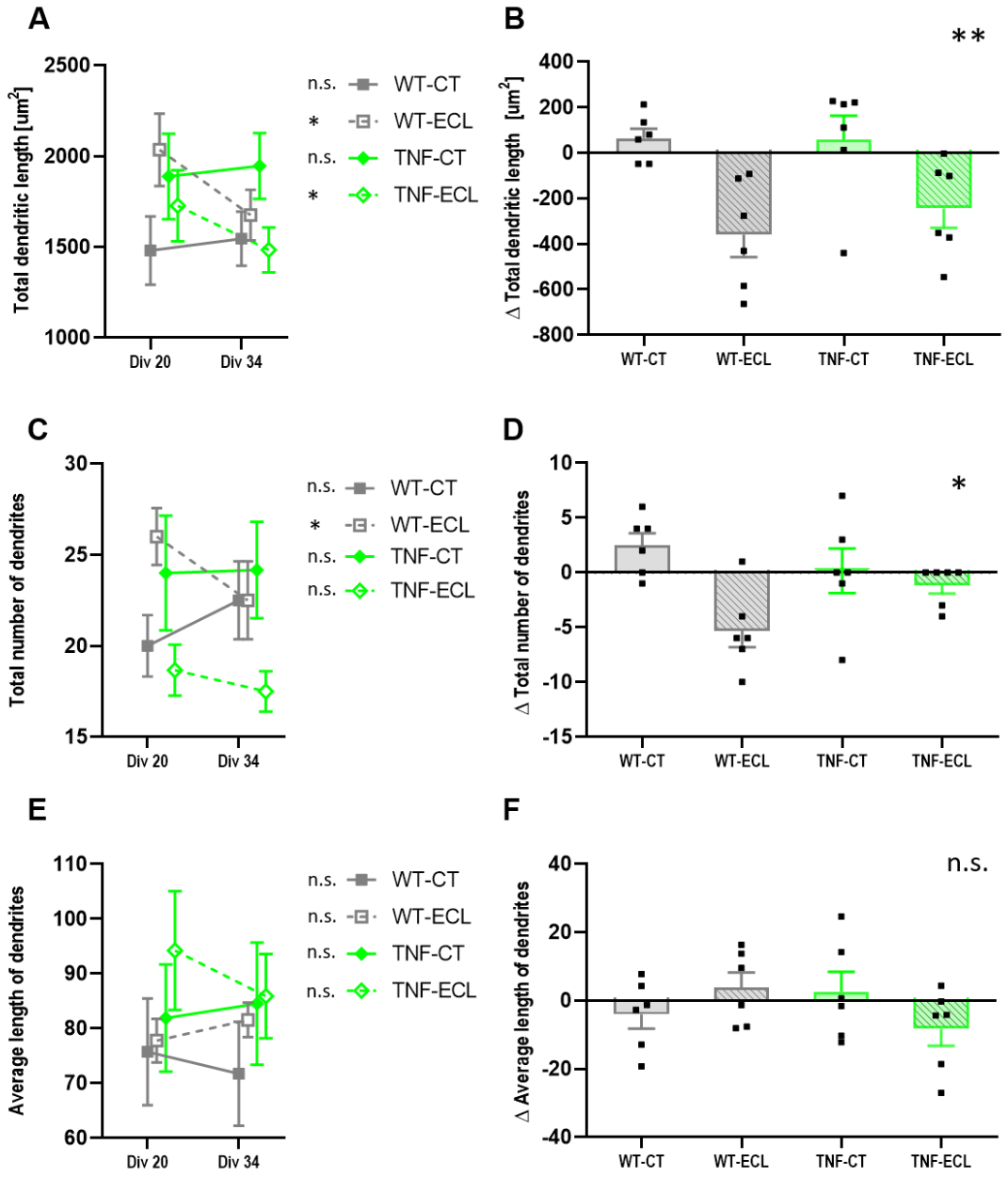

Figure 15. Analysis of dendritic parameters of Thy1-eGFP granule cells in organotypic hippocampo-entorhinal cultures. (A) Total length of dendrites remains unchanged between DIV20 and DIV34 for non-transected cultures: Thy1-eGFP (WT CT): n.s. = non significant; p = 0.1563, Thy1-eGFP-TNF-KO (KO CT) n.s. = non significant; p = 0.4375. Length of dendrites was drastically reduced between DIV20 and DIV34 for cultures that had the entorhinal cortex transected: Thy1-eGFP entorhinal cortex lesion (WT ECL), *p = 0.0313; Thy1-eGFP-TNF-KO-ECL (KO ECL), *p = 0.0313, Wilcoxon matched-pairs signed rank test. **(B)** Comparing the delta of differences between total dendritic length at DIV20 and DIV34 shows that the effects of the ECL are pronounced in both WT-ECL and TNF-KO-ECL group. **p = 0.0048, H(3) = 12.93, Kruskal-Wallis test by ranks. **(C)** The number of dendrites was

reduced in the WT ECL group (WT ECL: *p = 0.0313), but not in the KO ECL group. As expected, there was no change in both control groups. n.s. = non significant; (WT CT: p = 0.1250; KO CT: p > 0.9999; KO ECL: p = 0.5000), Wilcoxon matched-pairs signed rank test. **(D)** Comparing the delta of differences between total number of dendritic segments at DIV20 and DIV34 shows the pronounced effect on WT ECL group. *p = 0.0297, H(3) = 8.971, Kruskal-Wallis test by ranks. **(E)** Average lengths of individual dendritic segments were unchanged in all groups (WT CT: p = 0.5625; WT ECL: p = 0.4375; KO CT: p = 0.8438; KO ECL: p = 0.1563), Wilcoxon matched-pairs signed rank test. **(F)** Comparing the delta of differences between average lengths of dendritic segments at DIV20 and DIV34 showed no differences. n.s. p = 0.4380, H(3) = 2.713, Kruskal-Wallis test by ranks.

5.1.2. Sholl analysis reveals the resistance of TNF-alpha-KO cells to ECL

In order to perform the morphometric Sholl analysis, we plotted the number of intersections with circles centered on the soma of the investigated neuron at DIV20, against the distance from the cell body, in 20 µm increments, and then analyzed the same neurons at DIV34 (Fig 16A, B). This was followed by measurements of total dendritic complexity (Fig. 16C) and the change in total dendritic complexity (Fig. 16D) with analysis of the complete dendritic arbors of all investigated paired neurons. We saw significant changes in both the WT-ECL group (Fig. 156; $F(5, 95) = 5.965$; $^{***}p < 0.001$) and in the TNF-ECL group (Fig. 16D; $F(5, 95) = 9.324$; $^{**}p = 0.002$). The cultured neurons of the WT-ECL group behaved as expected, with neurons at DIV34, 14 days after lesion, having a tendency for less complex dendritic arbors at all measured increments. In the TNF-ECL group, however, we saw a strong tendency for higher complexity of dendritic arbors at 40 and 60 µm distance from soma, with subsequent distances having less complexity. Total dendritic complexity was significantly reduced by ~17% in the WT-ECL group ($^{*}p = 0.031$), while in the TNF-ECL group, the total dendritic complexity was not significantly changed (Fig. 16C). This was also reflected when comparing between these two groups, where the reduction of dendritic complexity in WT-ECL group had a tendency of larger reduction compared to the TNF-ECL group (Fig. 16F, n.s. $p = 0.119$). In this regard, cultured neurons made from mouse mutants lacking TNF respond to ECL with fewer morphological deficits and retain their dendritic complexity with a bimodal change paradigm, with lower dendritic complexities at the deafferentiated areas of the MML/OML and a reactive higher dendritic complexity at the non-deafferentiated area of the IML.

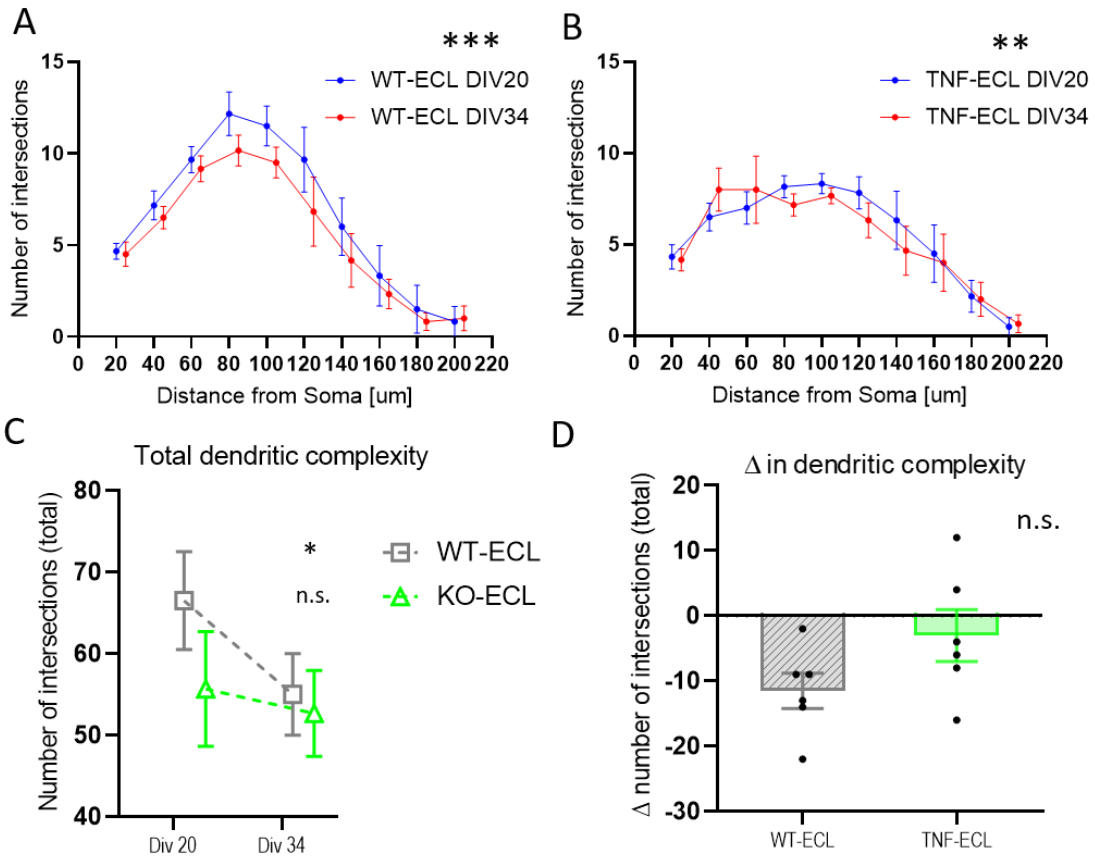

Figure 16. **Sholl analysis of granule cells after entorhinal denervation. (A)** Cultures of lesioned wildtype cultures (WT-ECL) show a significantly reduced branching pattern after 14 days *in vitro*. ***p < 0.001, Repeated measures one-way ANOVA test. n = 6. **(B)** Cultures of lesioned wildtype cultures (TNF-ECL) also show a significantly reduced branching pattern after 14 days *in vitro*. **p = 0.002, Repeated measures one-way ANOVA test. n = 6. **(C)** Total number of intersections as a measure of dendritic complexity shows significant reductions in lesioned wildtypes (WT-ECL, *p = 0.031), but not in lesioned mouse mutants (TNF-ECL, n.s. p = 0.219). Wilcoxon matched-pairs signed rank test. n = 6 in all genotypes at DIV 20 and DIV 34. **(F)** Comparing the change at DIV20 and DIV34 between lesioned groups showcase a tendency for a bigger change in the WT-ECL group. n.s. p = 0.093,Mann-Whitney ranked test. n = 6.

5.2. Results from the TNF-alpha analysis

5.2.1. Granule cell dendrites of TNF-KO mice exhibit a reduced spine density

Previous work showed that TNF is an important factor in the control of synaptic strength (7,154,155,159). Since synaptic strength and spine geometry are tightly linked (64,65,67,204), we speculated that genetic knockout of TNF *in vivo* may have a structural correlate at the level of spines. To address this question we first studied dendritic segments of Alexa-filled granule cells (Fig. 17A, B) in the outer molecular layer of the DG of TNF-deficient and age-matched C57BL/6J control mice. TNF-KO mice exhibited a significant reduction in spine density (Fig. 17C): whereas wildtype mice had 2.03 spines / µm, TNF-KO mice had 1.62 spines / µm, i.e. ~20% fewer spines. Next, we analyzed spine head area, since spine head area correlates well with synaptic strength and the density of AMPA-Rs. Average spine head area was not significantly different between genotypes (Fig. 17D), although a trend towards higher values was seen in TNF-KO segments. Finally, we calculated total spine head area per segment (Fig. 17E), which illustrates how changes in spine density and head area affect the available spine head area for neurotransmission. This parameter takes the number of spines into account and shows that the total spine head area per segment decreases in the TNF-KO mice.

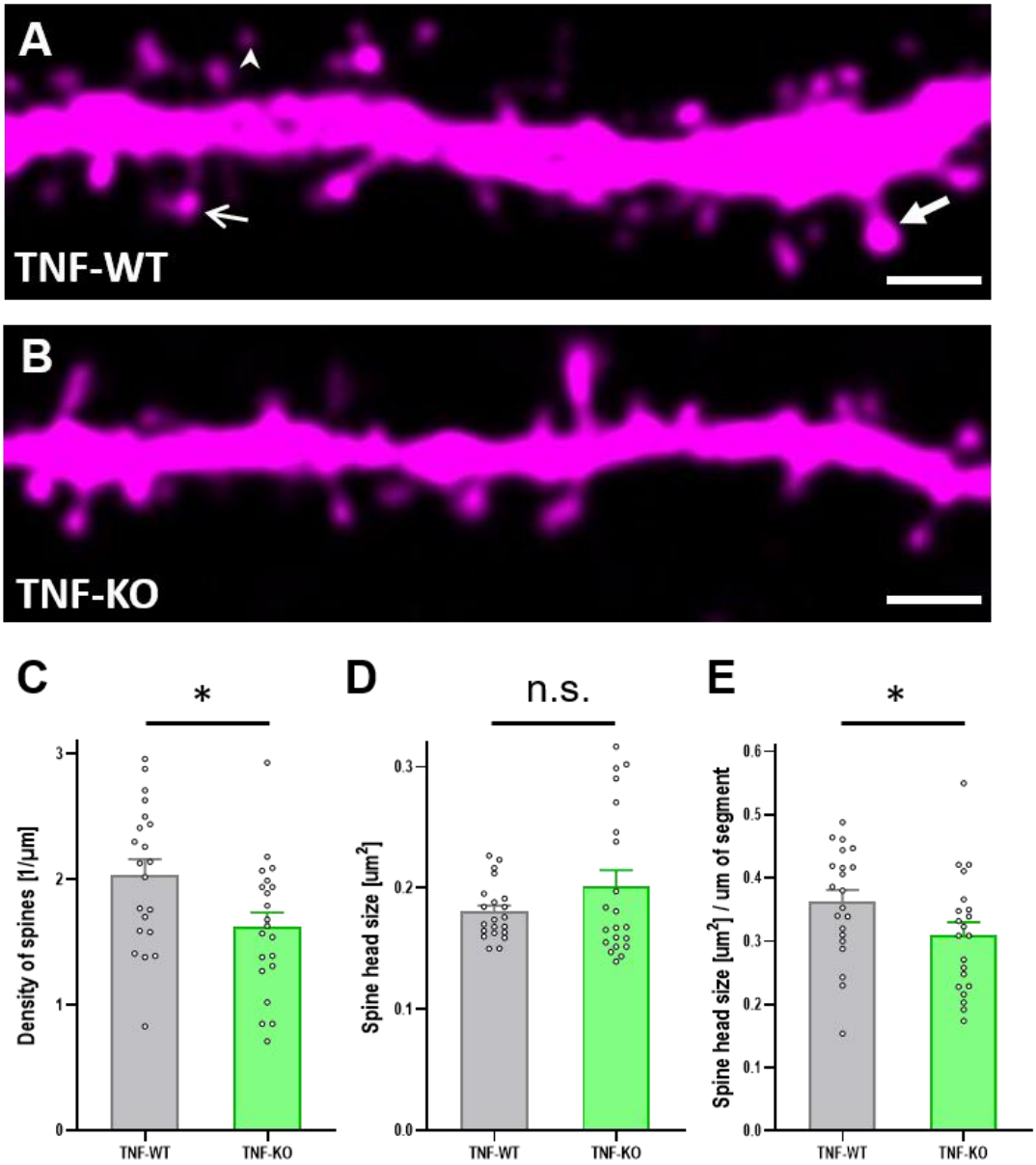

Figure 17. Granule cell dendrites of TNF-KO mice exhibit a reduced spine density. (A, B) Single confocal sections of granule cell dendrites in the OML of TNF-WT **(A)** and TNF-KO **(B)** mice. Scale bar = 2 um. Large (thick arrow), medium (thin arrow), and small (arrowhead) spines are indicated. **(C)** Density of dendritic spines on TNF-KO segments is significantly reduced (~1.62 1/µm) compared to controls (~2.03 1/µm). Analysis based on 7 WT and 7 KO mice; 1 segment per cell; 3 dendritic segments per animal (n=21 segments); 1633 TNF-WT; 1306 TNF-KO spines. *p = 0.0166, Mann-Whitney U-test. **(D)** Average spine head areas per segment of TNF-WT (~0.18 µm^2) and TNF-KO (~0.20 µm^2) mice are not significantly (n.s.) different; p = 0.999; Mann-Whitney U-test; n = 21 segments per group. **(E)** Total spine head area divided by the length of the analyzed segment shows a ~14% reduction in spine area per

µm of the segment for TNF-KO (~0.31 µm^2/µm) compared to TNF-WT (~0.36 µm^2/µm), *p = 0.044; Mann-Whitney U-test. n = 21 segments per group.

5.2.2. TNF-KO mice show an increase in the fraction and area of large spines.

After analyzing dendritic segments, we shifted our attention to the entire population of spines and compared their spine head area distributions (Fig. 18A). This revealed a highly significant difference between the two distributions, with differences most prominent at the beginning of the curve, i.e. small spine heads, and at the end of the curve, i.e. large spine heads. To investigate this further, we distinguished three categories of spines (Fig. 18B): small (<0.15 µm^2), medium (0.15 – 0.30 µm^2), and large (>0.30 µm^2) sized spines and compared average spine head area between control and TNF-KO spines. Although average spine head areas were not different for medium sized spines, large spines were ~19% bigger and small spines were ~8% smaller in TNF-deficient granule cells (Fig. 18C). These changes in spine head areas significantly shifted the fraction of spines belonging to each of the three categories (Fig. 18D): TNF-deficient granule cells mice had more small (~54% compared to ~49%) and large (~17% compared to ~13%) sized spines than controls, whereas TNF-WT granule cells had more medium sized spines (38% compared to 29%) compared to TNF-deficient cells.

.

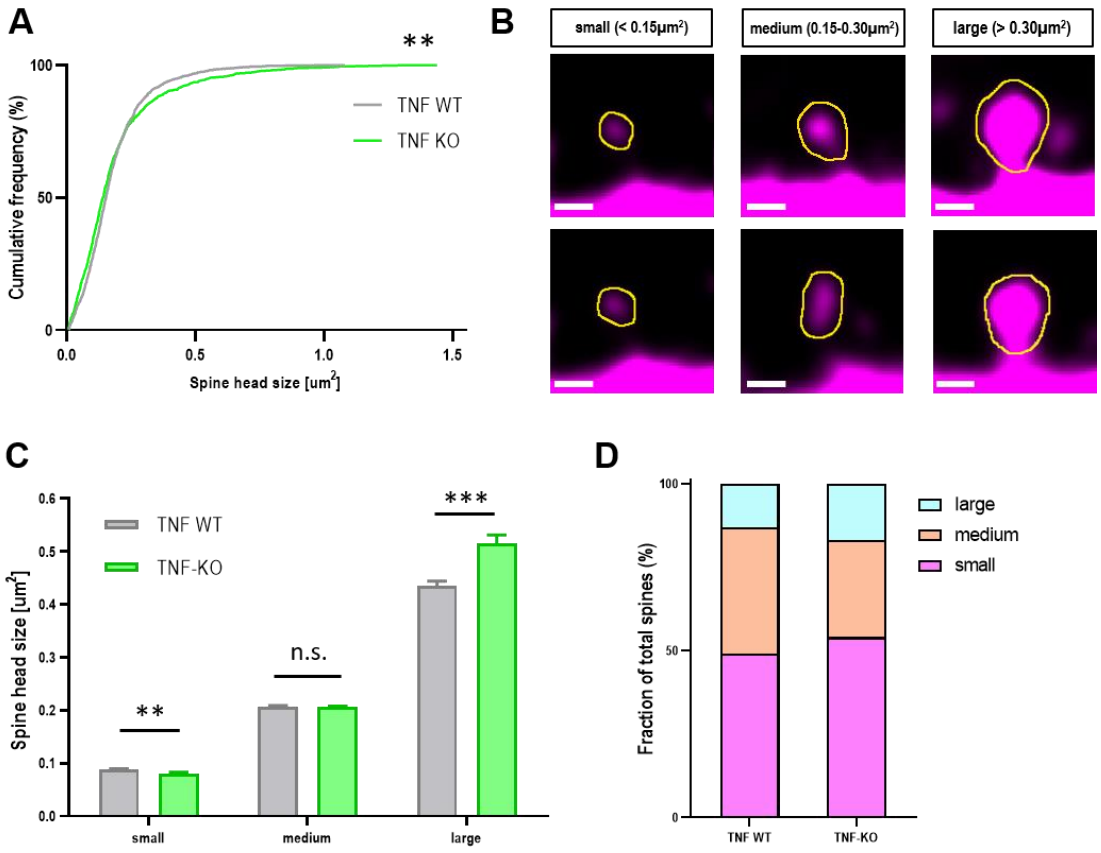

Figure 18. TNF-KO mice show an increase in the fraction and area of large spines. (A) Cumulative frequency plot of spine head areas of TNF-KO and TNF-WT mice. **p = 0.0023; Kolmogorov-Smirnov test; TNF-WT spines n = 1633; TNF-KO spines n = 1306. **(B)** Spines were divided into three classes: small (<0.15 µm^2), medium (0.15 – 0.30 µm^2), and large (>0.30 µm^2) spines. Scale bar = 0.5 µm. **(C)** Large spines were ~19% bigger in TNF-KO mice (~0.52 µm^2) compared to TNF-WT mice (~0.43 µm^2); ***p = 0.00035; while small sized TNF-KO spines (~0.0815 µm^2) were ~8% smaller compared to TNF-WT spines (~0.0885 µm^2); **p = 0.0014. Medium sized spines were not significantly (n.s.) different. p = 0.644; Mann-Whitney U-test; TNF-WT n = 800, 625, 207; TNF-KO n = 704; 386; 215 (small/medium/large). **(D)** Fraction of spine classes per genotype: TNF-KO mice had more large (~17% compared to ~13%) and small (~54% compared to ~49%) spines and fewer medium spines (~29% compared to ~38%) compared to WT.

5.2.3. Synaptopodin-positive spines are larger in TNF-KO mice compared to wildtype

Because of the conspicuous increase in the area of large spines, we wondered about the distribution of the actin-modulating and plasticity-related protein SP, which is primarily associated with this subgroup of spines (9,10,205,206). Using a double-labeling approach, Alexa-568 injected granule cells were also immunolabeled for SP. As previously described, SP clusters were abundant in the molecular layer of the DG (164,177). Using single identified granule cell segments, the presence or absence of SP within spines was noted and the maximum spine head area as well, as the maximum cross-sectional area of SP clusters were measured (Fig. 14 A, B). In both genotypes, the majority of spines were SP- (Fig. 19A; TNF-WT, 13.8% SP+; 86.2% SP-; TNF-KO, 15.3% SP+; 84.7% SP-; ***$p < 0.001$, Mann-Whitney U-test) and SP+ spines were significantly larger than SP- spines in both genotypes (Fig. 19B; TNF-WT ~0.35 μm^2 SP+; ~0.15 μm^2 SP-; TNF-KO ~0.45 μm^2 SP+, ~0.15 μm^2 SP-; ***$p < 0.001$, Mann-Whitney U-test). Testing the cumulative distributions between genotypes, there was a small but highly significant left-shift of SP- spine head areas in TNF-KO animals (Fig. 19C; ***$p < 0.001$; Kolmogorov-Smirnov test) and a pronounced and highly significant right-shift of SP+ spine head areas in TNF-KO animals (Fig. 19D; ***$p < 0.001$; Kolmogorov-Smirnov test). Since the overall density of spines is lower in TNF-deficient granule cells (Fig. 17) and the fraction of SP+ spines is constant, the absolute number of SP+ spines is, however, reduced by ~14% in the TNF-KO.

.

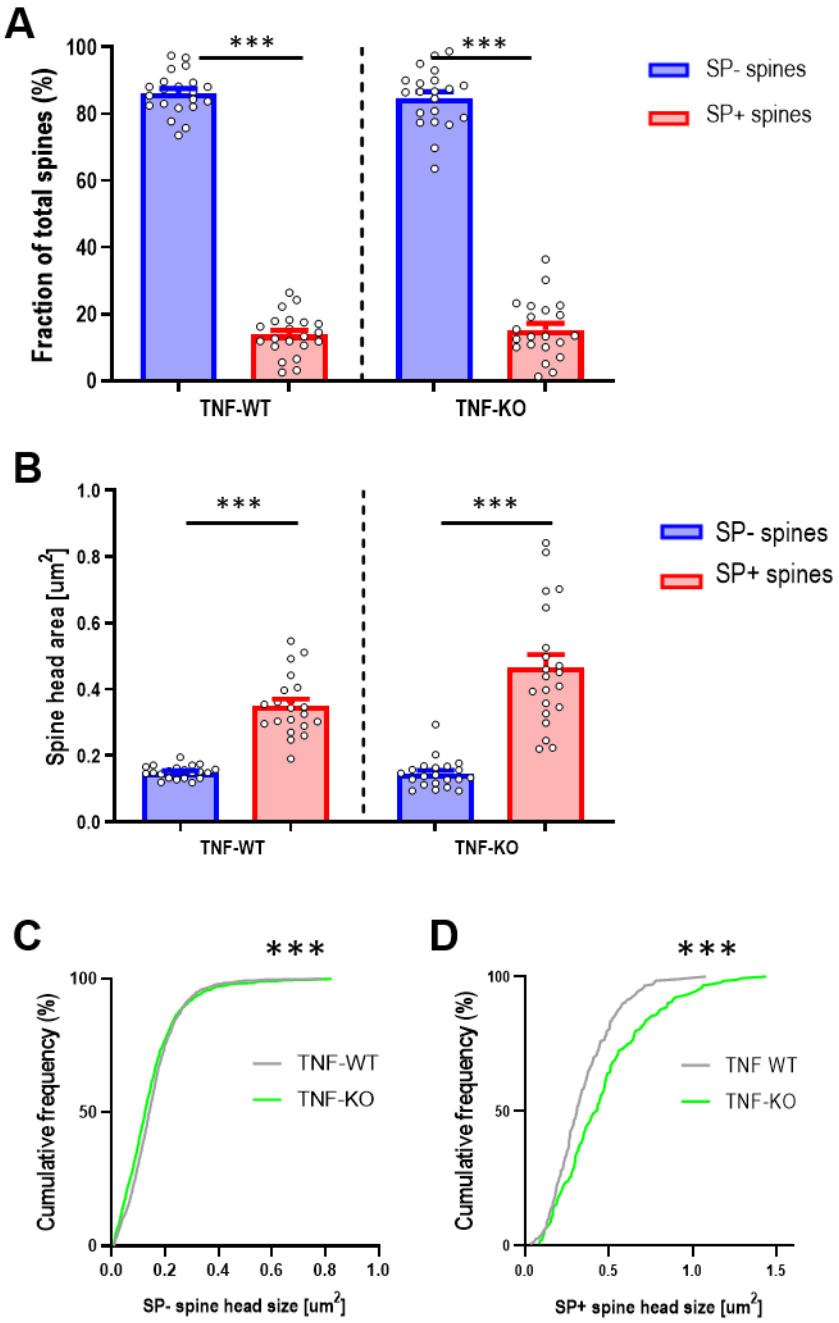

Figure 19. Synaptopodin+ spines are larger in TNF-KO mice compared to wildtype. (A) Fraction of SP- (~86.2%) and SP+ (~13.8%) spines in TNF-WT and fraction of SP- (~84.7%) and SP+ (~15.3%) spines in TNF-KO animals. ***p < 0.001, Mann-Whitney U-test. Number of segments per genotype n = 21. **(B)** Mean head area of SP+ and SP- spines (TNF-WT ~0.35 μm^2 SP+; ~0.15 μm^2 SP-; TNF-KO ~0.45 μm^2 SP+, ~0.15 μm^2 SP-). SP+ spines have larger spine head areas compared to SP- spines in both genotypes. ***p < 0.001; Mann-Whitney U-test. Number of segments per genotype n = 21. **(C)** Cumulative frequency plot of the spine head area of SP- spines. ***p = 0.0002; Kolmogorov-Smirnov test; TNF-WT n = 1423; TNF-

KO n = 1120. **(D)** Cumulative frequency plot of the spine head area of SP+ spines. ***p = 0.0002; Kolmogorov-Smirnov test; TNF-WT n = 209; TNF-KO n = 183.

5.2.4. Large SP+ spines are selectively enlarged in TNF-KO mice

We now divided SP+ and SP- spines into the three size categories (Fig. 18B). Most SP+ spines were found belonging to the large spine category (Fig. 20A, TNF-WT ~53.1%; Fig. 20B, TNF-KO ~69.4%), whereas only a few SP- spines were in this category (Fig. 20A, TNF-WT ~6.7%; Fig. 20B, TNF-KO ~7.9%). In the subgroup of large spines, SP+ spines were ~23% bigger in TNF-KO mice compared to controls (Fig. 20C3) whereas large SP- spines were not different between genotypes (Fig. 20D3). In the subgroup of small spines, SP+ spines were rare (Fig. 20A, TNF-WT ~12.0%; Fig. 20B, TNF-KO ~8.2%), whereas SP- spines were abundant (Fig. 20A, TNF-WT ~54.5%; Fig. 20B, TNF-KO ~61.4%). SP+ spines belonging to the small category did not differ significantly between TNF-deficient and TNF-WT granule cells (Fig. 20C1). In contrast, SP- spines showed a significant reduction of ~10% in spine head area in TNF-KO mice (Fig. 20D1). There was no significant difference between genotypes for spines belonging to the medium sized subgroup (Fig. 20C2). The cumulative distribution of SP+ large-sized spines was right-shifted for TNF-KO mice (Fig. 20C4) and the cumulative distribution of SP- small-sized spines was left-shifted for TNF-KO mice (Fig. 20D4). We conclude from these findings, that (i) the increase in spine head area of large spines observed in TNF-KO granule cells (Fig. 18C) is the result of an enlargement of large SP+ spines (Fig. 20C3,4), and, (ii) the reduction in spine head area of small spines (Fig. 18C) is the result of a diminution of small SP- spines (Fig. 20D1,4).

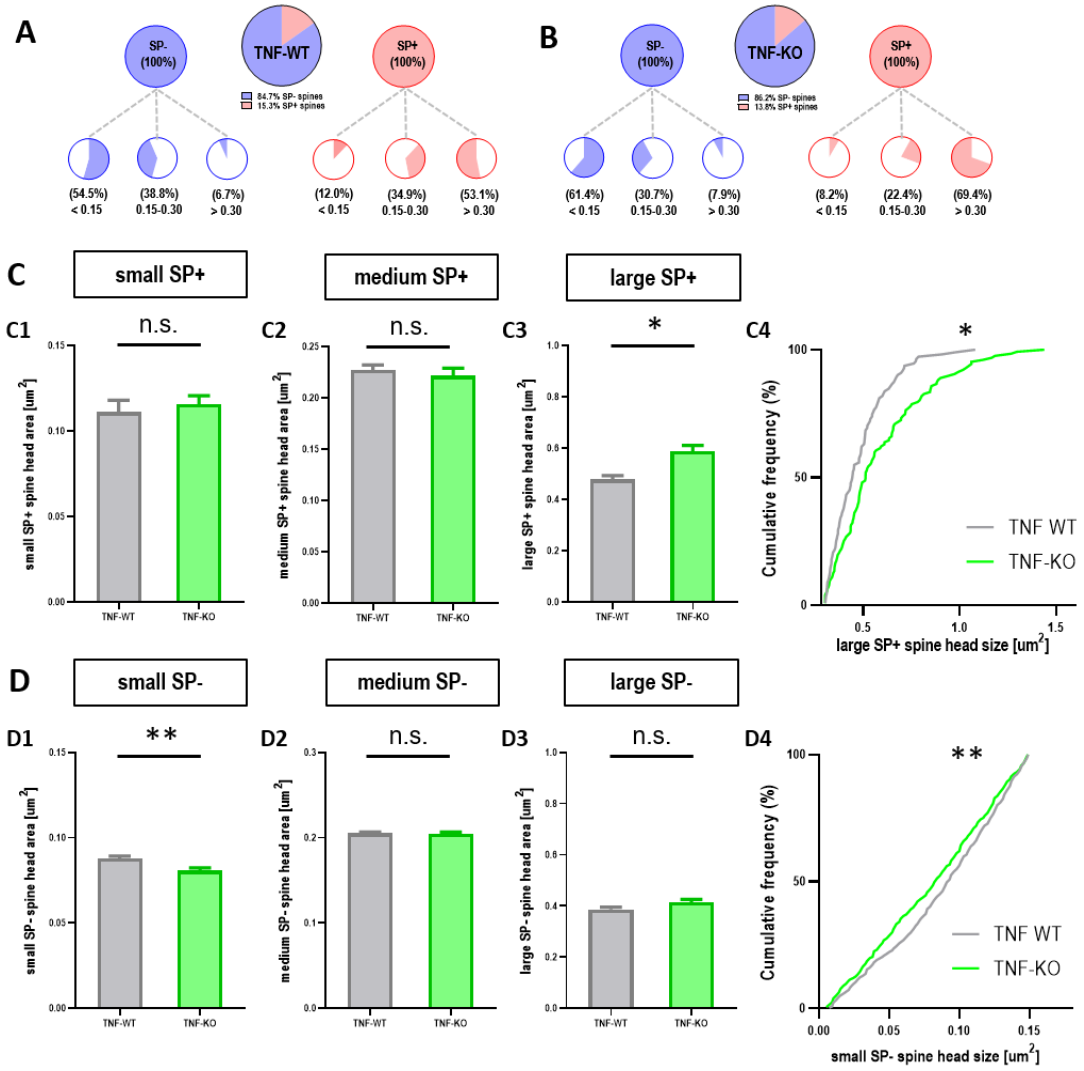

Figure 20. Large SP+ spines are selectively enlarged in TNF-KO mice. (A, B) Fractions of SP- (blue) and SP+ (red) spines for WT **(A)** and TNF-KO **(B)** mice. SP- and SP+ spines were subdivided into the three spine classes. In both genotypes, the majority of SP- spines were small spines and the majority of SP+ spines were large spines. Of note, the fraction of large SP+ spines was higher in TNF-KO mice. (TNF-WT: SP- spines n = 1423 total; n = 775/552/96 small/medium/large SP- spines; SP+ spines n = 209 total; n = 25/73/111 small/medium/large SP+ spines; TNF-KO: SP- spines n = 1120 total; 688/344/88 small/medium/large SP- spines; SP+ spines n = 183 total; n = 15/41/127 small/medium/large SP+ spines). **(C)** Comparison of SP+ spine classes between genotypes. TNF-KO mice have bigger large sized (C3) SP+ spines (~0.58 µm^2) compared to WT (~0.46 µm^2); *p = 0.010. Small (C1; n.s. p = 0.584) and medium (C2; n.s. p = 0.639) sized spines were not significantly different. Cumulative frequency plot of the spine head area of SP+ large sized spines (C4). *p = 0.01; Kolmogorov-Smirnov test; TNF-WT n = 111; TNF-KO n = 127. **(D)** Comparision of SP- spine classes between genotypes. TNF-KO mice have smaller small sized (D1) SP- spines (~0.08 µm^2) compared to WT (~0.09 µm^2);

**p = 0.002; Medium (D2; n.s. p = 0.986) and large (D3; n.s. p = 0.480) sized spines were not significantly different. Cumulative frequency plot of the spine head area of SP- spines (C4). **p = 0.002; Kolmogorov-Smirnov test; TNF-WT n = 775; TNF-KO n = 688.

5.2.5. SP cluster size is increased in spines of TNF-deficient granule cells

The fact that SP+ spines of TNF-deficient granule cells have larger heads made us wonder whether this increase is matched by a corresponding increase in SP clusters, since these two parameters are highly correlated (10,206). Indeed, average SP cluster areas were ~25% bigger in TNF-deficient granule cell segments (Fig. 21A). Similarly, the cumulative distribution of SP cluster areas was right-shifted in the mutant compared to control (Fig. 21B). SP-clusters were preferentially found in the spine head of both genotypes, with a shift towards the spine base in the mutant (Fig. 21C, D). Finally, we analyzed the relationship between SP-cluster area and spine head area. Both genotypes showed a strong positive correlation between the two parameters (Fig. 21E). However, WT clusters showed a significantly stronger correlation than clusters from the TNF-mutants.

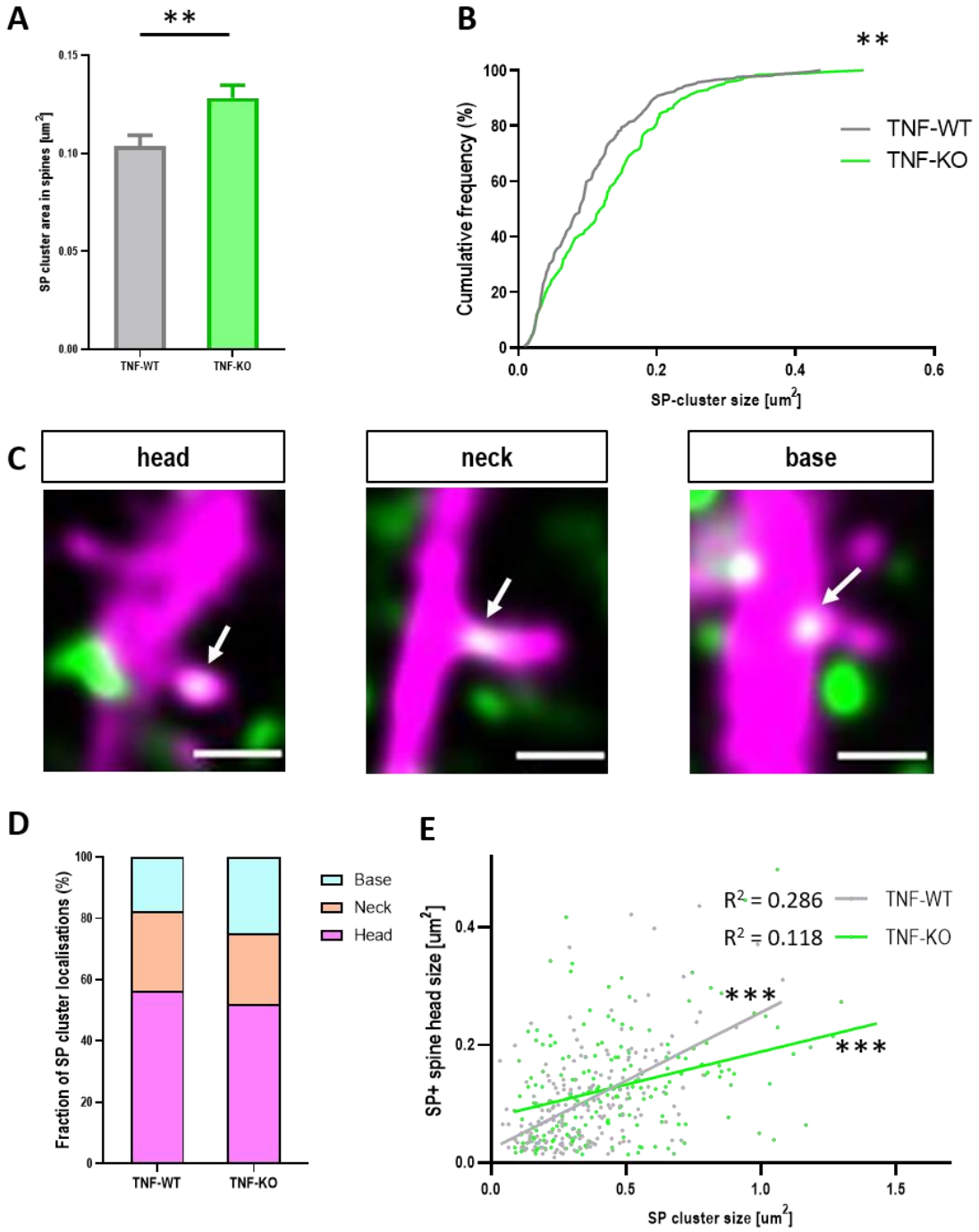

Figure 21. SP cluster size is increased in spines of TNF-deficient granule cells. (a) Area of SP clusters was compared between TNF-WT (~0.10 µm^2) and TNF-KO mice (~0.13 µm^2). TNF-KO had ~33% bigger SP clusters. **p = 0.0037; Mann-Whitney U-test. TNF-WT mice = 209; TNF-KO mice = 183 clusters. **(b)** Cumulative frequency plot of SP cluster areas for both genotypes. **p = 0.002, Kolmogorov-Smirnov test. TNF-WT mice = 209; TNF-KO mice = 183 clusters. **(c)** Higher magnifications of dendritic segments of a TNF-WT mouse immunolabeled for SP. SP clusters were found in the head, neck or base of spines (arrows). Scale bars = 1 µm. **(d)** Localization of SP clusters in TNF-WT and TNF-KO mice. TNF-WT:

56/26/18%, head/neck/base; TNF-KO: 52/23/25%, head/neck/base. TNF-WT n = 209; TNF-KO = 183 clusters. **(e)** Correlation between spine head area and SP cluster area for the two genotypes. ***p < 0.001. TNF-WT: r = 0.5344; TNF-KO: r = 0.344. TNF-WT, n = 209; TNF-KO, n = 183 clusters.

5.3. Results from the TNF-receptor knockout analysis

TNF-alpha signaling is mediated by two ligands (sTNF and mTNF) which bind to two different receptors: TNF-receptor 1 (TNF-R1) and TNF-receptor 2 (TNF-R2) (138). mTNF binds to both TNF-R1 and TNF-R2, while sTNF binds selectively to TNF-R1 (138). Due to this, we wanted to investigate how does the deletion of TNF-R1 (TNF-R1-KO), TNF-R2 (TNF-R2-KO) and the deletion of both receptors (TNF-R1+2-DKO) influence the dendritic spines of granule cells and what role synaptopodin plays in these mouse mutants (145). The summary of the analysis is shown in table 1.

Table 1. Summary of all results from TNF-KO, TNF-R1-KO, TNF-R2-KO and TNF-R1+2-DKO animals compared to their respective wildtypes. Dendritic spine density was affected only in the TNF-KO group. Average spine head size was only reduced in TNF-R1+2-DKO animals, which could be due to the similar functions of TNF-R1 and TNF-R2 and the redundancy of their function with regards to spine dynamics. Removal of any actor in the TNF system caused a pronounced decrease of small spine head sizes (and this was due to SP- spines, since SP+ spines were unchanged). It is likely that the effects of TNF-alpha on large, SP+ spines are mediated by the TNF-R1, since in both cases large spine head size, SP+ spine head size and SP+ large spine head size were increased when compared to their wildtype littermates. The reduction of small spine head sizes could be a secondary, compensatory mechanism as a response to the increase of SP+ large spines.

Compared to WT	TNF-alpha-KO	TNF-R1-KO	TNF-R2-KO	TNF-R1+2-DKO
Spine density	↓	n.s.	n.s.	n.s.
Spine head size	n.s.	n.s.	n.s.	↓
Small spine head size	↓	↓	↓	↓
Medium spine head size	n.s.	n.s.	n.s.	n.s.
Large spine head size	↑	↑	n.s.	n.s.
SP+ spine head size	↑	↑	n.s.	n.s.
SP- spine head size	n.s.	n.s.	n.s.	↓
SP+ small spine head size	n.s.	n.s.	n.s.	n.s.
SP+ medium spine head size	n.s.	n.s.	n.s.	n.s.
SP+ large spine head size	↑	↑	n.s.	n.s.
SP- small spine head size	↓	↓	↓	↓
SP- medium spine head size	n.s.	n.s.	n.s.	n.s.
SP- large spine head size	n.s.	n.s.	n.s.	n.s.
SP clusters size	↑	n.s.	n.s.	n.s.

5.3.1. The presence of either TNF receptor is enough for normal spine density and size.

Throughout the last 20 years, it has been shown that the beneficial effects of TNF-α are mediated by both TNF-R1 and TNF-R2 and that there seems to be considerable overlap in the function of those receptors concerning AMPA receptor clustering and synaptic strength (145,152,158). Therefore, we next analyzed the density of dendritic spines located in the OML of TNF-R1-KO, TNF-R2-KO mice and their respective wildtypes (Fig. 22A, B; Fig. 23A, B). The analysis has shown that neither the removal of TNF-R1 (Fig. 22C), nor the removal of TNF-R2 (Fig. 23C) change the density of spines in granule cells of the hippocampus. Large changes to spines were not expected in the removal of a single receptor, since the other receptor could partially compensate for the loss of function. This holds true for spine head sizes as well, since there weren't any changes in TNF-R1-KO (Fig. 22D) and TNF-R2-KO (Fig. 23D) mice compared to their wildtype littermates. Due to both of these results, there was no global reduction of total spine area per length of dendritic segment (Fig. 22E, 23E). While there was no difference in the cumulative distribution of spine head sizes of TNF-R2-KO animals compared to controls (Fig. 23F), the distribution of spine head sizes of TNF-R1-KO animals was significantly different (Fig. 22F) and we saw the same pattern as was seen in TNF-KO group (Fig. 18A). Wanting to confirm our suspicions, we then focused on the general analysis of mouse mutants lacking both TNF-R1 and TNF-R2 (TNF-R1+2-DKO), to see if the changes mimic those seen in TNF-KO animals.

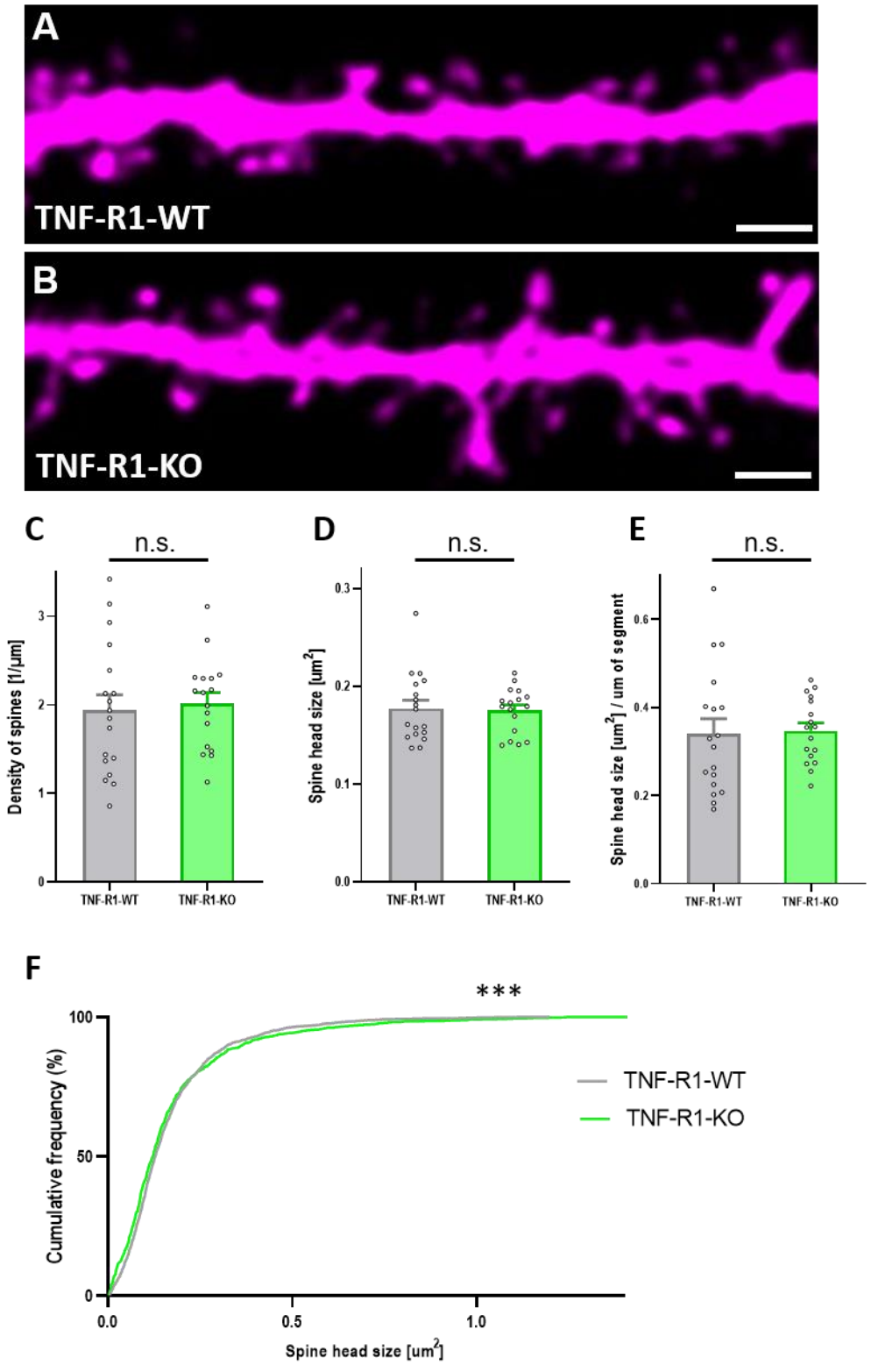

Figure 22. TNF-R1-KO animals show no deficits in spine density and average spine head size. Single slices of dendritic segments of a TNF-R1-WT **(A)** and TNF-R1-KO **(B)** granule cell in the OML shown at higher magnification. Scale bar = 2 um. **(C)** The density of dendritic

spines is not significantly (n.s.) different between TNF-R1-WT (~1.94 1/µm) and TNF-R1-KO (~2.01 1/µm) mice. p = 0.4282, Mann-Whitney U-test. Number of TNF-R1-WT and TNF-R1-KO mice = 6; n = 18 segments analyzed in TNF-R1-WT (1391 spines); n = 17 segments analyzed in TNF-R1-KO (1330 spines). **(D)** Average spine head sizes of TNF-R1-WT (~0.18 μm^2) and TNF-R1-KO (~0.18 μm^2) mice are not significantly (n.s.) different, p = 0.9351; Mann-Whitney U-test. n = 18 TNF-R1-WT segments; n = 17 TNF-R1-KO segments. **(E)** Total spine head size divided by the length of the analyzed segment in TNF-R1-WT (~0.34 $\mu m^2/\mu m$) and TNF-R1-KO (~0.35 $\mu m^2/\mu m$) mice are not significantly (n.s.) different, p = 0.4626; Mann-Whitney U-test. n = 18 TNF-R1-WT segments; n = 17 TNF-R1-KO segments. **(F)** Cumulative frequency plot of individual head sizes for TNF-R1-WT and TNF-R1-KO mice. ***p < 0.0001. Kolmogorov-Smirnov test. TNF-R1-WT spines = 1391 spines; TNF-R1-KO spines = 1330.

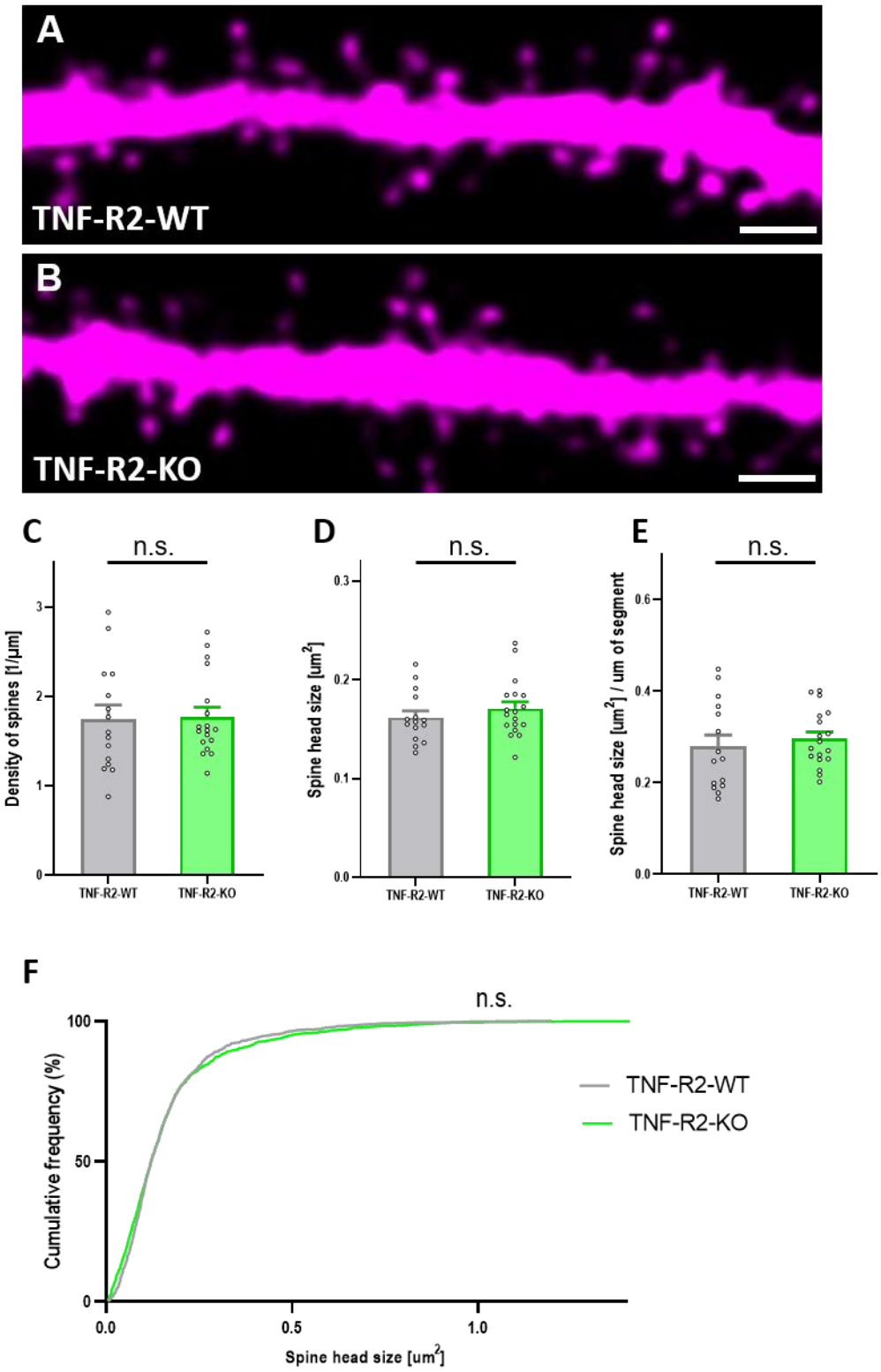

Figure 23. TNF-R2-KO animals show no deficits in spine density and average spine head size. Single slices of dendritic segments of a TNF-R2-WT **(A)** and TNF-R2-KO **(B)** granule cell in the OML shown at higher magnification. Scale bar = 2 um. **(C)** The density of dendritic spines is not significantly (n.s.) different between TNF-R2-WT (~1.75 1/µm) and TNF-R2-KO

(~1.77 1/µm) mice. p = 0.7013, Mann-Whitney U-test. Number of TNF-R2-WT mice = 5; Number of TNF-R2-KO mice = 6; n = 15 segments analyzed in TNF-R2-WT (1021 spines); n = 18 segments analyzed in TNF-R2-KO (1186 spines). **(D)** Average spine head sizes of TNF-R2-WT (~0.16 μm^2) and TNF-R2-KO (~0.17 μm^2) mice are not significantly (n.s.) different, p = 0.3428; Mann-Whitney U-test. n = 15 TNF-R2-WT segments; n = 18 TNF-R2-KO segments. **(E)** Total spine head size divided by the length of the analyzed segment in TNF-R1-WT (~0.28 $\mu m^2/\mu m$) and TNF-R1-KO (~0.30 $\mu m^2/\mu m$) mice are not significantly (n.s.) different, p = 0.3293; Mann-Whitney U-test. n = 15 TNF-R2-WT segments; n = 18 TNF-R2-KO segments. . **(F)** Cumulative frequency plot of individual head sizes for TNF-R2-WT and TNF-R2-KO mice. n.s. p = 0.219. Kolmogorov-Smirnov test. TNF-R2-WT spines = 1021 spines; TNF-R2-KO spines = 1186.

5.3.2. Knockout of both TNF receptors leads to a drastic reduction in spine head size in granule cells of the DG.

We hypothesized that the removal of both TNF-R1 and TNF-R2 would result in similar results as we have reported for TNF-KO mice (Fig. 17). To this end, we generated a TNF-R1+2-DKO mouse by cross-breeding our TNF-R1-KO and TNF-R2-KO animals. In order to investigate the morphology of its dendritic spines, we once again intracellularly filled granule cells and imaged segments in the OML of the hippocampus (Fig. 24A, B). To our surprise, analysis of dendritic spine density showed no differences between the double-knockout animal and wildtypes (Fig. 24C). However, further investigation revealed a drastic reduction of ~28% in spine head size in the mutant mice (Fig. 24D). This disparity of results (i.e. the reduction of dendritic spine density in TNF-KO animals and the reduction of average spine head size in TNF-R1+2-DKO animals) could be explained by the activation of astrocitic P2Y1 receptors via TNF-α in TNF-R1+2-DKO animals (159), or by the constitutive activity of TNF-β which can activate both TNF-R1 and TNF-R2 in TNF-KO animals (207–209). Due to the reduction in spine head size and the consistency of spine densities, we can speculate a significant reduction in synaptic transmission strength. The morphological correlate of this functional deficit; total spine area per micrometer of dendritic length, was also reduced in TNF-R1-2-DKO animals (Fig. 24E), similarly to TNF-KO animals (Fig. 17E). The important distinction between these genotypes is better seen when viewing the entire population of spines. Spine head size distribution in TNF-R1+2-DKO mice was significantly shifted to the left for all

spines, irregardless of spine head size classes (Fig. 24F), while this was true only for small spines in TNF-KO animals, as large spine sizes were shifted to the right (Fig. 18A).

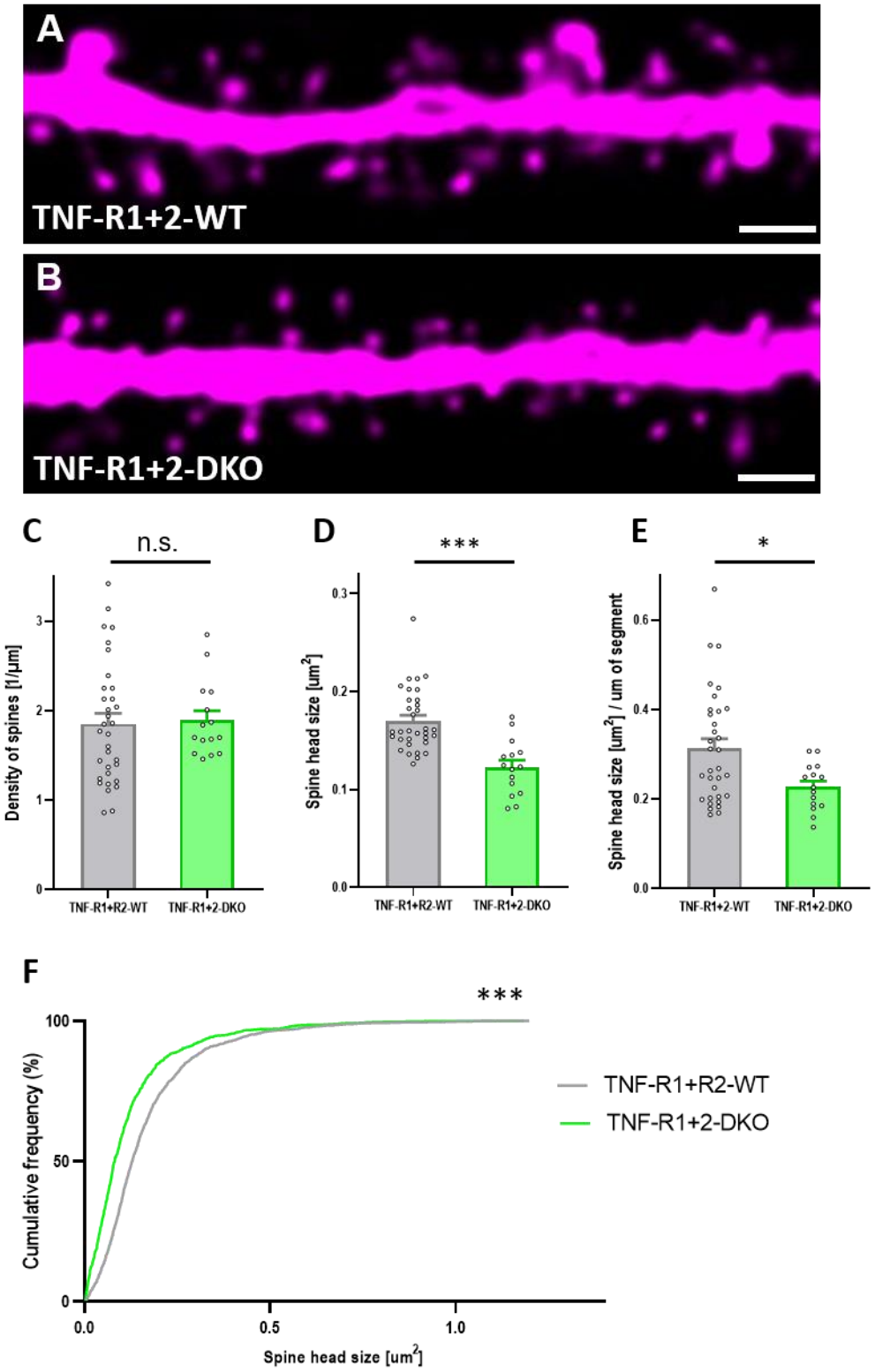

Figure 24. TNF-R1+2-DKO mice show large deficits in spine head size. Single slices of dendritic segments of a TNF-R1+2-WT **(A)** and TNF-R1+2-DKO **(B)** granule cell in the OML

shown at higher magnification. Scale bar = 2 um. **(C)** The density of dendritic spines is not significantly (n.s.) different between TNF-R1+2-WT (~1.85 1/µm) and TNF-R1+2-DKO (~1.89 1/µm) mice. p = 0.5859, Mann-Whitney U-test. Number of TNF-R1+2-WT mice = 11; Number of TNF-R1+2-DKO mice = 5; n = 33 segments analyzed in TNF-R1+2-WT (2412 spines); n = 155 segments analyzed in TNF-R1+2-DKO (1039 spines). **(D)** Average spine head size is significantly and drastically reduced in TNF-R1+2-DKO (~0.12 μm^2) mice compared to TNF-R1+2-WT (~0.17 μm^2) , ***p < 0.0001; Mann-Whitney U-test. n = 33 TNF-R1+2-WT segments; n = 15 TNF-R1+2-DKO segments. **(E)** Total spine head size divided by the length of the analyzed segment shows significant differences between TNF-R1+2-WT (~0.31 $\mu m^2/\mu m$) and TNF-R1+2-DKO (~0.23 $\mu m^2/\mu m$) segments, which is due to smaller spine sizes, *p = 0.0285; Mann-Whitney U-test. n = 33 TNF-R1+2-WT segments; n = 15 TNF-R1+2-DKO segments. **(F)** Cumulative frequency plot of individual head sizes for TNF-R1+2-WT and TNF-R1+2-DKO mice, note the left-shift of spine sizes of the knockout mice. ***p < 0.0001. Kolmogorov-Smirnov test. TNF-R1+2-WT spines = 2412 spines; TNF-R1+2-DKO spines = 1039.

5.3.3. Morphological changes in TNF-R1-KO mice closely follow the changes seen in TNF-KO mice.

Since previous work reported a decreased surface expression of AMPAR and frequency of miniature excitatory postsynaptic current in TNF-R1-KO animals but not in TNF-R2-KO animals (152), we focused on a more detailed analysis of individual dendritic spine sizes in this mouse mutant. Deeper analysis of dendritic spines in TNF-R1-KO animals and their respective wildtypes revealed a number of similarities to TNF-KO animals. After we divided spine head sizes into the three aforementioned categories (Fig. 18B): small (<0.15 μm^2), medium 0.15 – 0.30 μm^2), and large (>0.30 μm^2) sized spines; we investigated differences in those categories between all spines, SP+ spines and SP- spines. The results seemed to mimic the results of TNF-KO animals, with no difference in average spine head sizes for medium sized spines, while large spines were ~14% bigger and small spines were ~7% smaller (Fig. 25A). Furthermore, SP+ spines were larger by a factor of >3 in both genotypes compared to SP- spines (Fig. 25B). A notable right shift of SP+ spines was also seen in the cumulative distribution of all SP+ spines (Fig. 25C), while a small but significant left shift of SP- spines was seen in the

cumulative distribution compared to wildtypes (Fig. 25D). To confirm our suspicions, we next focused on the different spine classes of SP+ and SP- spines in TNF-KO animals.

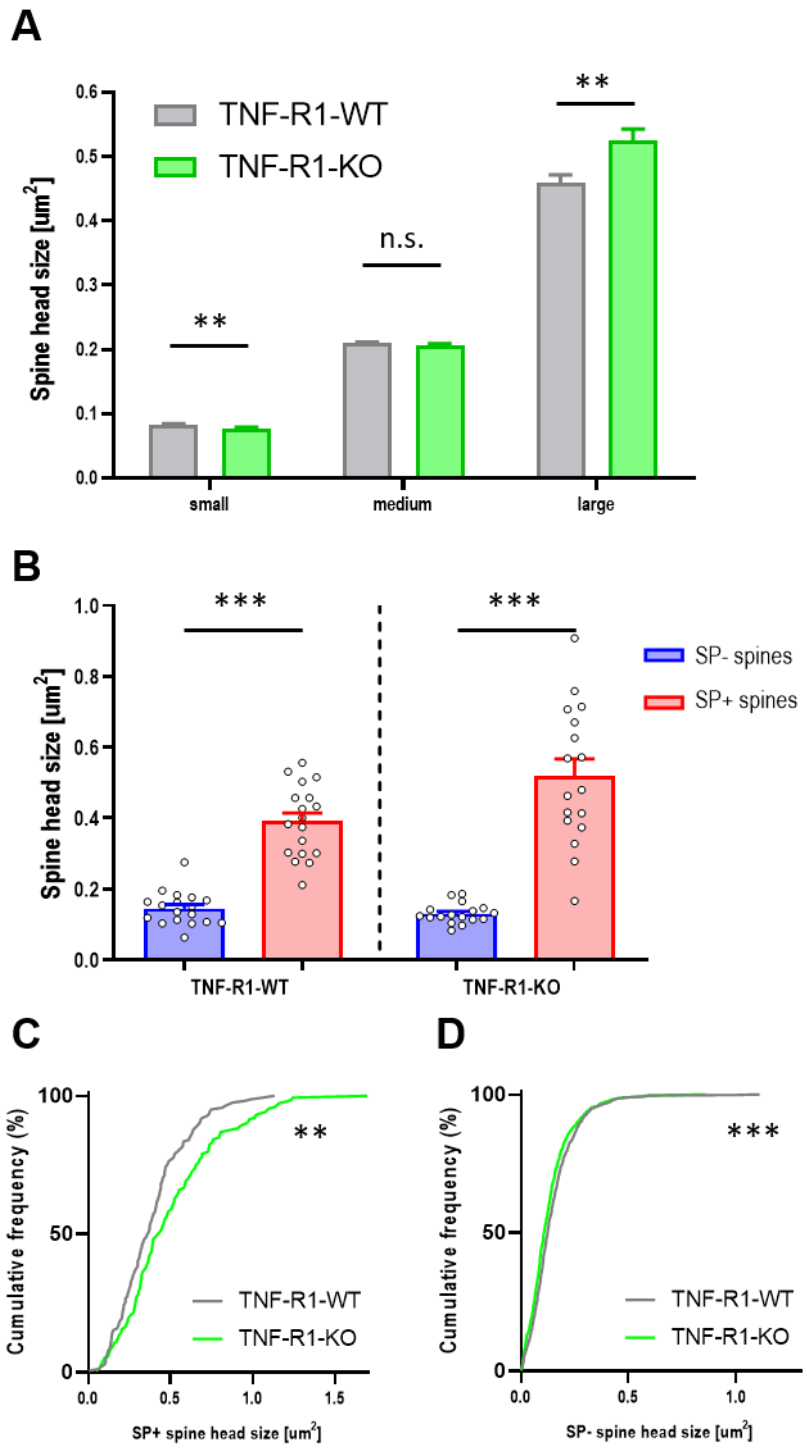

Figure 25. SP+ spines are enlarged due to the absence of TNF-R1. (A) Large-sized spines are ~14% bigger in TNF-R1-KO mice (~0.52 µm^2) compared to TNF-R1-WT mice (~0.46 µm^2) *p = 0.0265; while small-sized TNF-R1-KO spines (~0.0779 µm^2) were ~7% smaller compared to TNF-R1-WT spines (~0.0835 µm^2). **p = 0.0040. Medium sized spines were not

significantly (n.s.) different. p = 0.5920. Mann-Whitney U-test. Number of small TNF-R1-WT spines n = 771; small TNF-R1-KO spines n = 818; medium TNF-R1-WT spines n = 423; medium TNF-R1-KO spines n = 321; large TNF-R1-WT spines n = 197; large TNF-R1-KO spines n = 191. **(B)** Mean head size of SP+ and SP- spines (TNF-R1-WT ~0.39 μm^2 SP+; ~0.14 μm^2 SP-; TNF-R1-KO ~0.52 μm^2 SP+, ~0.13 μm^2 SP-). SP+ spines have larger spine head sizes compared to SP- spines in both genotypes. ***p < 0.001, Mann-Whitney U-test. Compared to wildtype controls, TNF-R1-KO mice had ~33% bigger SP+ spine head sizes. *p = 0.034, while SP- spine head sizes were not (n.s.) significantly different. p = 0.488 Mann-Whitney U-test. n = 18 TNF-R1-WT segments; n = 17 TNF-R1-KO segments. **(C)** Cumulative frequency plot of individual SP+ head sizes in these genotypes. **p = 0.0073, Kolmogorov-Smirnov test. SP+ spines and clusters in TNF-R1-WT n = 164; TNF-R1-KO n = 153. **(D)** Cumulative frequency plot of individual SP- head sizes in these genotypes. ***p < 0.001, Kolmogorov-Smirnov test. SP- spines and clusters in TNF-R1-WT n = 1227; TNF-R1-KO n = 1177.

5.3.4. Large SP+ spines are enlarged, while small SP- spines are reduced in TNF-R1-KO mice

In TNF-R1-KO animals, when comparing to TNF-R1-WT animals, we see an increase in the ratio of small sized SP- spines of ~7.4% and an increase in the ratio of large sized SP+ spines of ~9.7% (Fig. 26A, B). It is important to note that these results are very similar to TNF-KO animals, where SP+ large spines were also larger and SP- small spines were smaller in size compared to their wildtypes (Fig. 20A, B). When looking at SP+ and SP- spine classes, TNF-R1-KO mice had an increase of ~21% in large, SP+ spine head sizes (Fig. 26C_3) and a ~6% reduction in small, SP- spine head sizes (Fig. 26D_1), which once again closely followed the changes seen in TNF-KO mice (Fig. 20C, D). This was further confirmed with cumulative distributions, where we saw a significant right shift of large SP+ spines in TNF-R1-KO mice (Fig. 26C_4) and a slight, but significant left shift of small SP- spines compared to wildtype controls (Fig. 26D_4). The changes that were seen in large, SP+ spines in these genotypes could not be replicated in TNF-R2-KO mice (see later), therefore it is highly likely that the lack of TNF-R1 drives changes in spine morphology that are closely tied to synaptopodin.

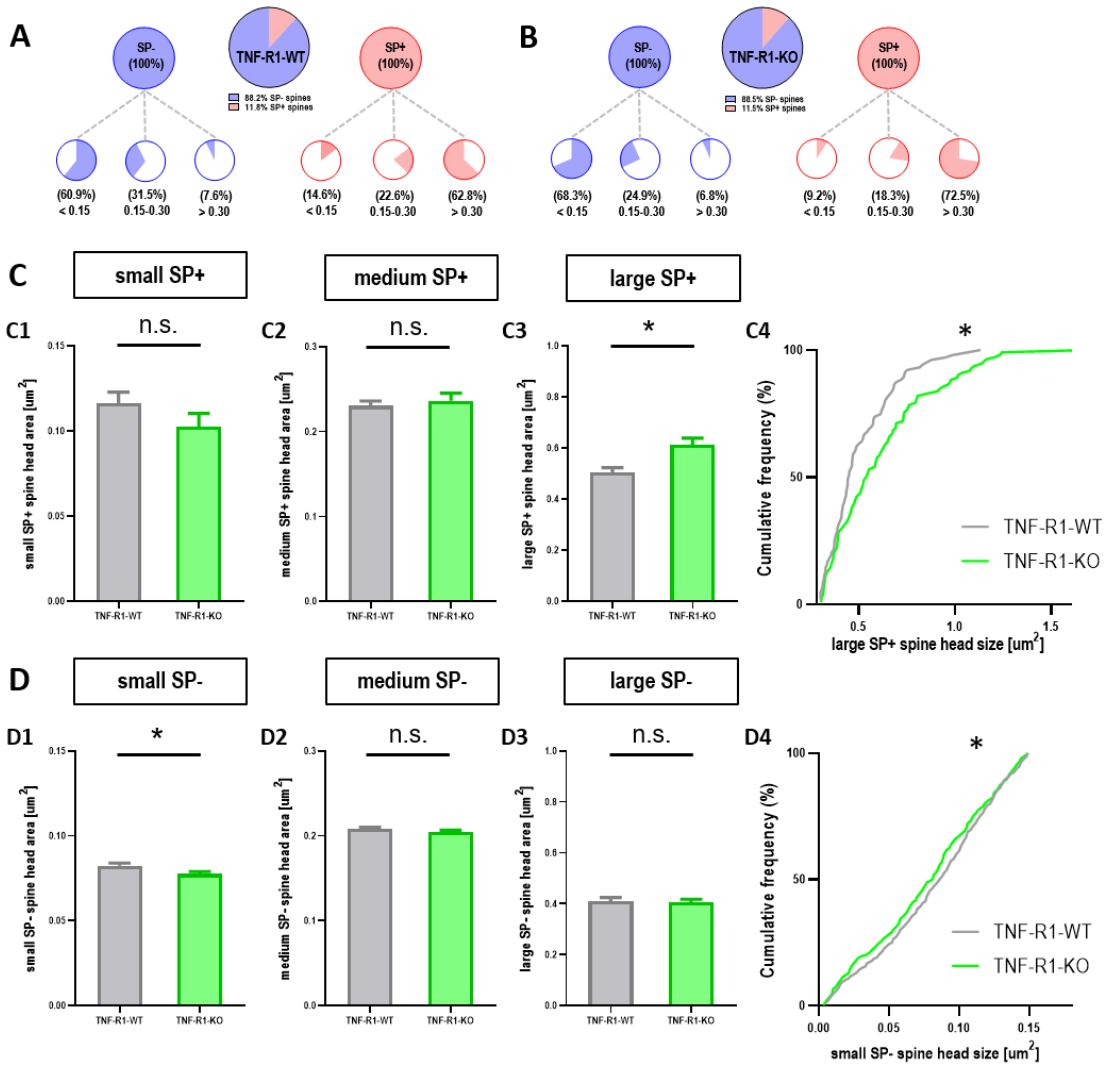

Figure 26. Large SP+ spines are similarly enlarged in TNF-R1-KO mice (A, B) Fractions of SP- (blue) and SP+ (red) spines for WT **(A)** and TNF-R1-KO **(B)** mice. As was the case with TNF-KO mice; SP- and SP+ spines were subdivided into the three spine classes. In both genotypes, the majority of SP- spines were small spines and the majority of SP+ spines were large spines. Of note, the fraction of large SP+ spines was higher in TNF-KO mice. (TNF-R1-WT: SP- spines n = 1227 total; n = 747/386/94 small/medium/large SP- spines; SP+ spines n = 164 total; n = 24/37/103 small/medium/large SP+ spines; TNF-R1-KO: SP- spines n = 1177 total; 804/293/80 small/medium/large SP- spines; SP+ spines n = 153 total; n = 14/28/111 small/medium/large SP+ spines). **(C)** Comparison of SP+ spine classes between genotypes. TNF-R1-KO mice had an ~22% enlargement of large sized SP+ spines (~0.61 μm^2) compared to TNF-R1-WT (~0.50 μm^2), C3; *p = 0.02; while small (C1; n.s. p = 0.11) and medium sized spines (C2; n.s. p = 0.28) were not significantly different between genotypes. Cumulative frequency plot of the spine head area of SP+ large sized spines shows significant differences in these spine populations (C4; *p = 0.02); Kolmogorov-Smirnov test. **(D)** Comparision of SP-

spine classes between genotypes. We found a ~6% reduction in TNF-R1-KO small sized SP- spines (~0.077µm^2) compared to TNF-R1-WT (~0.082µm^2) D1; *p = 0.0139; while medium (D2; n.s. p = 0.55) and large (D3; n.s. p = 0.91) sized spines were not significantly different between genotypes. Cumulative frequency plot of the spine head area of SP- spines shows significant differences in the small spine populations (D4; **p = 0.002); Kolmogorov-Smirnov test.

5.3.5. TNF-receptor knockout mice show a reduction of the medium spine population in favour of small or large spines depending on the genotype.

Since dendritic spine head sizes follow a log-normal size distribution (64,210), it is not surprising that the small spines made up the largest ratio of spine classes in all investigated genotypes. TNF-R1-KO mice had more small and large sized spines with a smaller fraction of medium spines (Fig. 26A), again in line with research in TNF-KO mice (Fig. 18D). TNF-R2-KO mice had minuscule changes compared with their respective wildtypes (Fig. 27B). TNF-R1+2-DKO animals had a large expansion of the ratio of small sized spines compared to their wildtypes, an increase of ~17%, which was the highest for any class of spines in all genotypes (Fig. 27C).

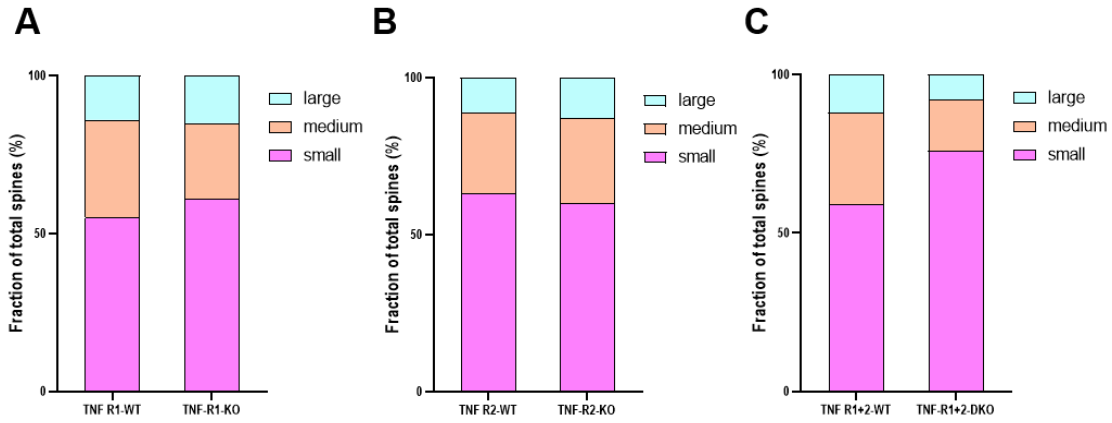

Figure 27. Fractions of subclasses of spines in different genotypes compared to their respective wildtypes. (A) Spine head sizes classes ratios per genotype: TNF-R1-KO mice had more small (~61% compared to ~55%) and large (~15% compared to ~14%) sized spines, while TNF-R1-WT mice had more medium sized spines (~31% compared to ~24%). **(B)** TNF-R2-KO mice had more medium (~27% compared to ~26%) and large (~13% compared to ~11%) sized spines, while TNF-R2-WT mice had more small sized spines (~63% compared to ~60%).

(C) Spine head sizes classes ratios per genotype: TNF-R1+2-DKO mice had more small (~76% compared to ~59%) sized spines, while TNF-R1+2-WT mice had more medium (~29% compared to ~16%) and large sized spines (~12% compared to ~8%).

5.3.6. TNF-R2 knockout mice have mild dendritic spine changes that are independent of synaptopodin presence in dendritic spines.

As we did with TNF-KO and TNF-R1-KO animals, we wanted to investigate the connection of the changes in TNF-R2-KO animals to synaptopodin. We hypothesized that either TNF-R1 or TNF-R2, not both, would be responsible for the beneficial compensatory changes in SP+ spines that we saw in TNF-KO animals. We therefore investigated changes in spine sizes between small, medium and large sized SP- or SP+ spines and compared them to spines analyzed in TNF-R2-WT mice. The only change that was noticed was in small sized spines (Fig. 28D_1). In contrast to TNF-R1-KO animals (Fig. 25A; Fig. 26 C_3), there was no significant difference between large sized spine heads (Fig. 28A). This was also confirmed in the cumulative distribution of SP+ spines (Fig. 28C) and SP- spines (Fig. 28D), as there was no difference between the mutant mice and its wildtype.

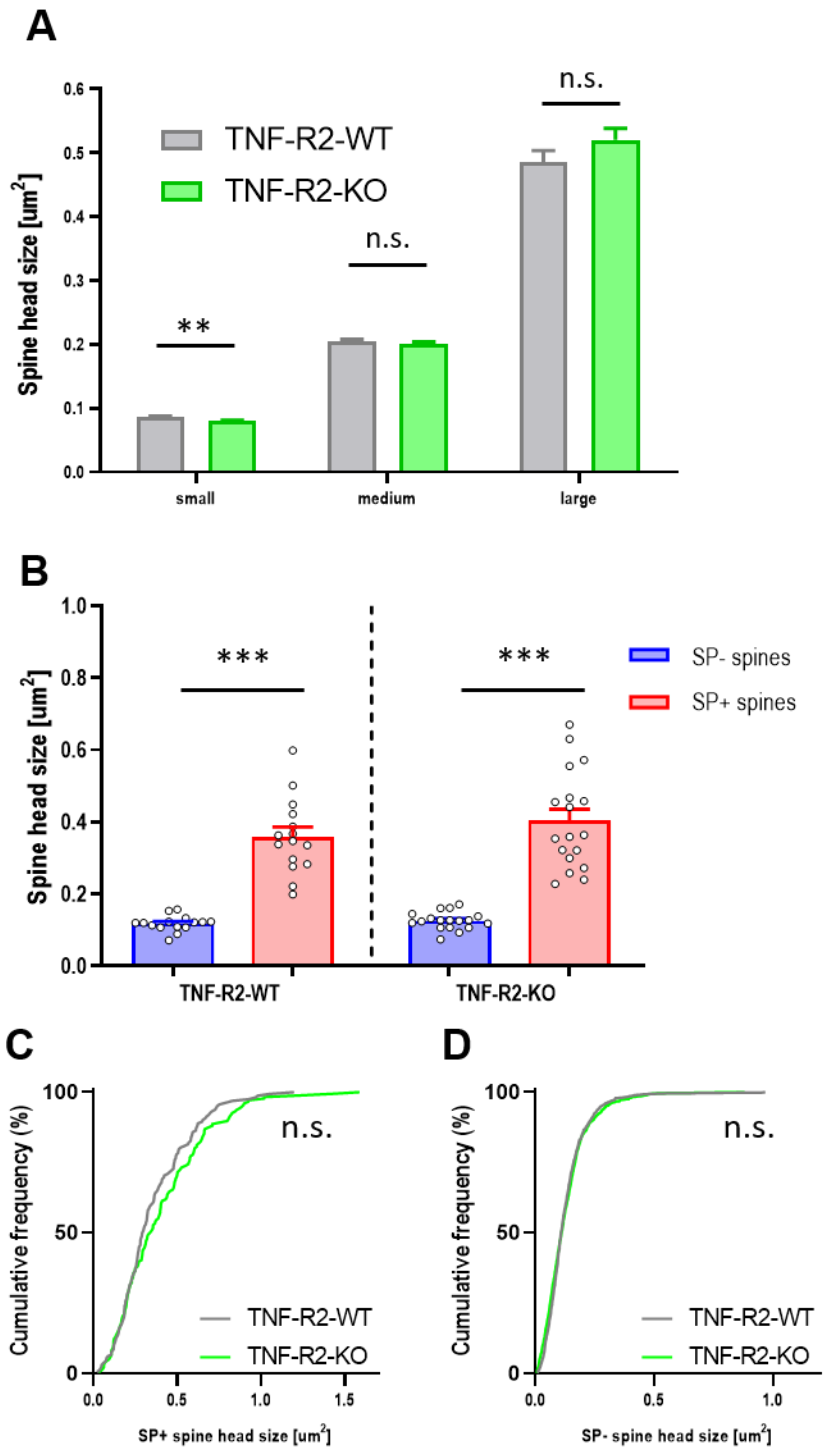

Figure 28. TNF-R2-KO mice show a reduction of small spines (A) Small-sized TNF-R2-KO spines (~0.0797 µm^2) were ~8% smaller compared to TNF-R2-WT spines (~0.0862 µm^2). **p = 0.0061. Medium sized spines were not significantly (n.s.) different. p = 0.3613; Likewise, large sized spines were also not significantly (n.s.) different. p = 0.4354. Mann-Whitney U-test. Number of small TNF-R2-WT spines n = 645; small TNF-R2-KO spines n = 714; medium TNF-R2-WT spines n = 268; medium TNF-R2-KO spines n = 324; large TNF-R2-WT spines

n = 108; large TNF-R2-KO spines n = 148. **(B)** Mean head size of SP+ and SP- spines (TNF-R2-WT ~0.36 μm^2 SP+; ~0.12 μm^2 SP-; TNF-R2-KO ~0.40 μm^2 SP+, ~0.13 μm^2 SP-). SP+ spines have larger spine head sizes compared to SP- spines in both genotypes. ***$p < 0.001$, Mann-Whitney U-test. SP+ ($p = 0.442$) and SP- ($p = 0.270$) spine head sizes were not (n.s.) significantly different between genotypes. Mann-Whitney U-test. n = 15 TNF-R2-WT segments; n = 18 TNF-R2-KO segments. **(C)** Cumulative frequency plot of individual SP+ head sizes in these genotypes. n.s. $p = 0.2653$, Kolmogorov-Smirnov test. SP+ spines and clusters in TNF-R2-WT n = 162; TNF-R2-KO n = 176. **(D)** Cumulative frequency plot of individual SP- head sizes in these genotypes. n.s. $p = 0.1857$, Kolmogorov-Smirnov test. SP- spines and clusters in TNF-R2-WT n = 859; TNF-R2-KO n = 1010.

We then focused our attention on SP+ and SP- spines in TNF-R2-KO animals. In TNF-R2-KO animals, we see an interesting albeit small shift towards a higher ratio of medium (~2.3%) and large SP- spines (~0.9%), and a higher ratio of large SP+ spines (~4.1%) (Fig. 29A, B). However, these changes were too small to warrant significant morphological changes. All subclasses of SP+ spines were unchanged between TNF-R2-KO mice and TNF-R2-WT mice (Fig. 29C). The only change that was noticed was in small sized spines (Fig. $28D_1$), which was replicated only in the group of SP-, and not SP+, small sized spines (Fig. $29D_{1,4}$). Since the changes in SP- small sized spines were seen in both TNF-R1-KO animals and TNF-R2-KO animals, we hypothesized that the removal of both receptors should have a larger effect on this spine population.

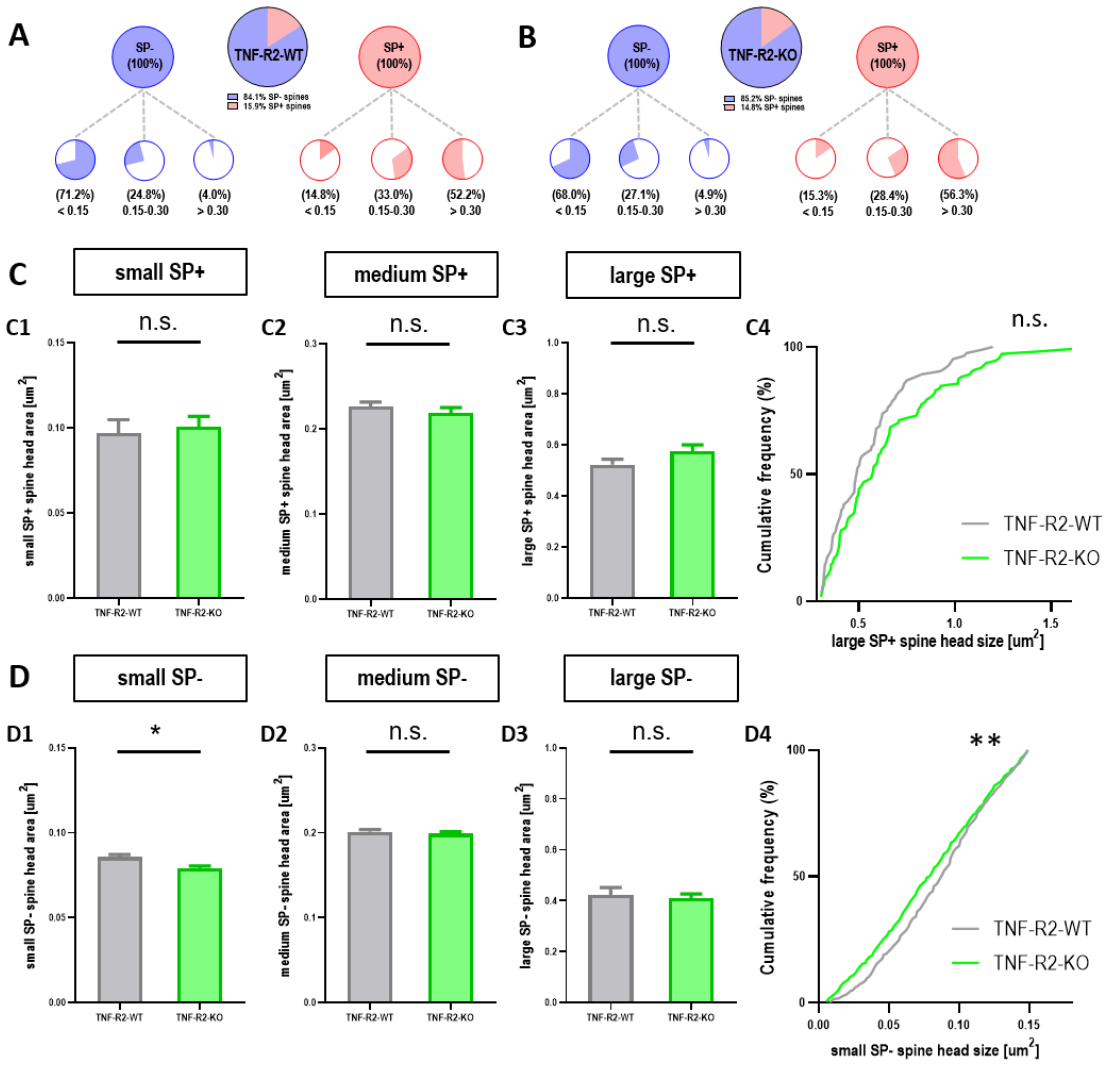

Figure 29. The removal of TNF-R2 does not affect SP+ spines, while reducing small SP- spines. (A) Fraction of SP- (~84.1%) and SP+ spines (~15.9%) in TNF-R2-WT mice. Number of TNF-R2-WT SP- spines = 859: small spines = 612, medium spines = 213, large spines = 34; Number of TNF-R2-WT SP+ spines = 162: small spines = 24, medium spines = 58, large spines = 80. **(B)** Fraction of SP- (~85.2%) and SP+ spines (14.8%) in TNF-R2-KO mice. Number of TNF-R2-KO SP- spines =1010: small spines = 687, medium spines = 274, large spines = 49; Number of TNF-R2-KO SP+ spines = 176: small spines = 27, medium spines = 50, large spines = 99. **(C)** Comparison of SP+ spine classes between genotypes shows no significant differences in small (C1; n.s. p = 0.967), medium (C2; n.s. p = 0.503) and large (C3; n.s. p = 0.581) sized spines. Cumulative frequency plot of the spine head area of SP+ large sized spines confirms that there were no differences in these spine populations (C4; n.s. p = 0.581); Kolmogorov-Smirnov test. **(D)** Comparision of SP- spine classes between genotypes shows no significant differences in medium (D2; n.s. p = 0.541) and large (D3; n.s. p = 0.649) sized spines, however, the size of small SP- spines was significantly reduced compared to wildtypes

(D1; *p = 0.034). Cumulative frequency plot of the spine head area of SP- spines shows significant differences in the small spine populations (D4; **p = 0.008); Kolmogorov-Smirnov test.

5.3.7. The mechanism of spine head reduction in TNF-R1+2-DKO mice is independent of synaptopodin expression.

TNF-R1+2-DKO animals had a ~28.1% reduction in spine head size of all spines (Fig. 24D). To that end, we wanted to see if there was a global reduction of spines or if this was due to a specific subset of spines. We now showed that TNF-R1+2-DKO animals have a significant ~23% reduction in size of only small sized spines (Fig. 30A). When looking at SP+ and SP- spines, the same ~trifold increase in average spine head sizes was seen in SP+ spines (Fig. 30B). Cumulative distribution showed no differences between the genotypes for SP+ spines (Fig. 30C), however, we can see a prominent and highly significant left-shift in the cumulative distribution of SP- spines compared to wildtype controls (Fig. 30D).

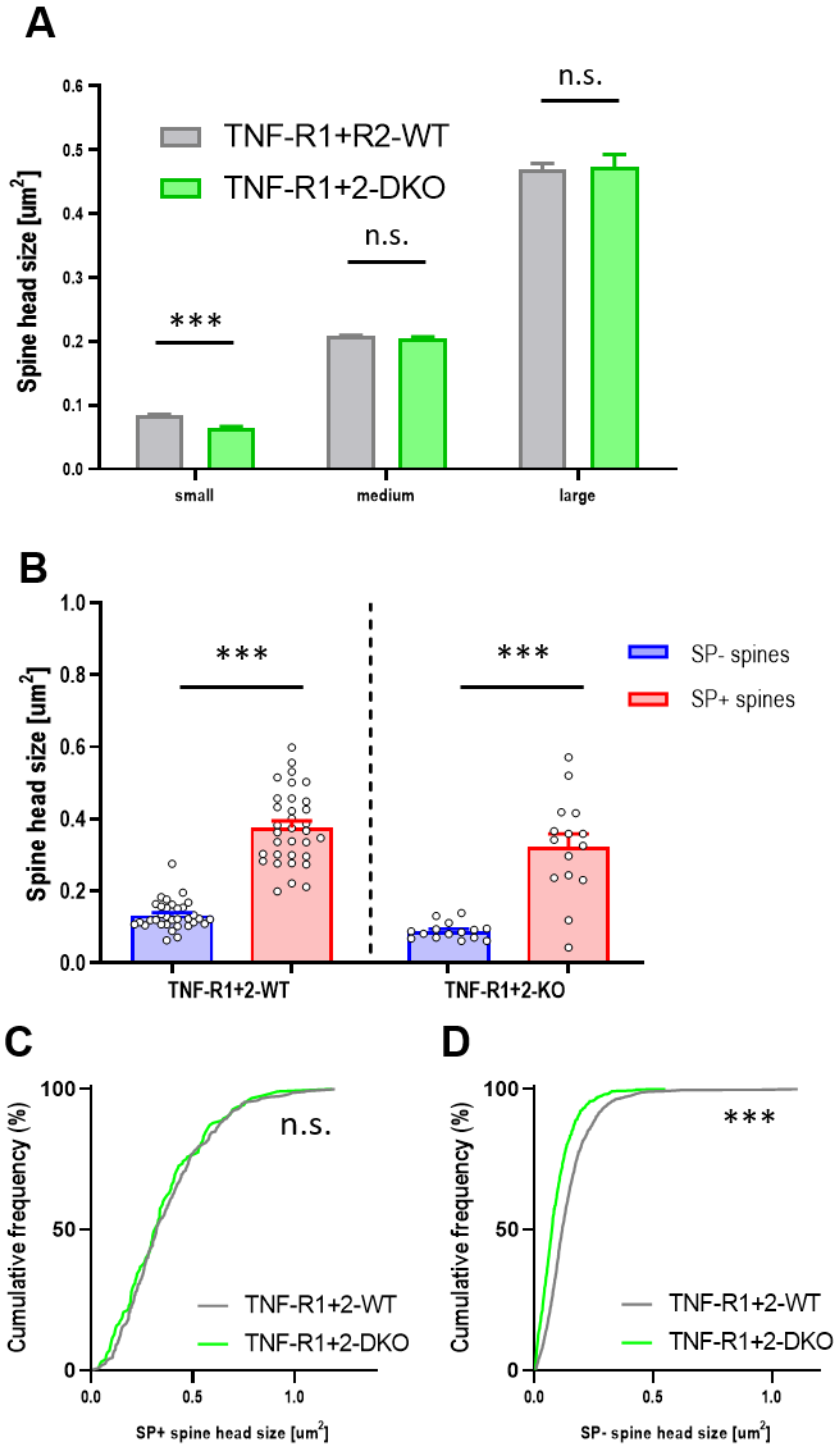

Figure 30. TNF-R1+2-DKO mice reduction of spine head sizes is due to SP- spines. (A) Small-sized TNF-R1+2-DKO spines (~0.06547 µm^2) were ~23% smaller compared to TNF-R1+2-WT spines (~0.08474 µm^2). **p < 0.0001. Medium sized spines were not significantly (n.s.) different. p = 0.3328; Likewise, large sized spines were also not significantly (n.s.) different. p = 0.6387. Mann-Whitney U-test. Number of small TNF-R1+2-WT spines n = 1416; small TNF-R1+2-DKO spines n = 786; medium TNF-R1+2-WT spines n = 691; medium

TNF-R1+2-DKO spines n = 169; large TNF-R1+2-WT spines n = 305; large TNF-R1+2-DKO spines n = 84. **(B)** Mean head size of SP+ and SP- spines (TNF-R1+2-WT ~0.38 μm^2 SP+; ~0.13 μm^2 SP-; TNF-R1+2-DKO ~0.42 μm^2 SP+, ~0.09 μm^2 SP-). SP+ spines have larger spine head sizes compared to SP- spines in both genotypes. ***$p < 0.001$, Mann-Whitney U-test. SP+ ($p = 0.222$) spine head sizes were not (n.s.) significantly different between genotypes, while SP- ($p < 0.0001$) spines were drastically reduced in size. Mann-Whitney U-test. n = 33 TNF-R1+2-WT segments; n = 15 TNF-R1+2-DKO segments. **(C)** Cumulative frequency plot of individual SP+ head sizes in these genotypes shows no significant differences. $p = 0.762$, Kolmogorov-Smirnov test. **(D)** Cumulative frequency plot of individual SP- head sizes in these genotypes, we can notice the same left shift as with all spines. $p < 0.0001$, Kolmogorov-Smirnov test.

The sharp increase in the ratio of small spines population in TNF-R1+2-DKO animals (compared to wildtypes, Fig. 27C) is due to SP- spines, since they increased by ~18.4%, while the ratio of SP+ small spines only increased by ~3.7% (Fig. 31A, B): There was also a minute decrease in the ratio of large SP+ spine population by ~2.6%. All subclasses of SP+ spines were unchanged between TNF-R1+2-DKO mice and TNF-R1+2-WT mice (Fig. 31C). Even though SP- medium and large sized spines had a tendency to be smaller in size, they were not significantly different between the genotypes. Small SP- spines were ~23% smaller, the biggest difference between mice mutants and their respective genotypes in all investigated groups (Fig. 20D; 26D; 29D; 31D). It would seem that both TNF-R1 and TNF-R2 play an important role in spine morphology of small sized spines.

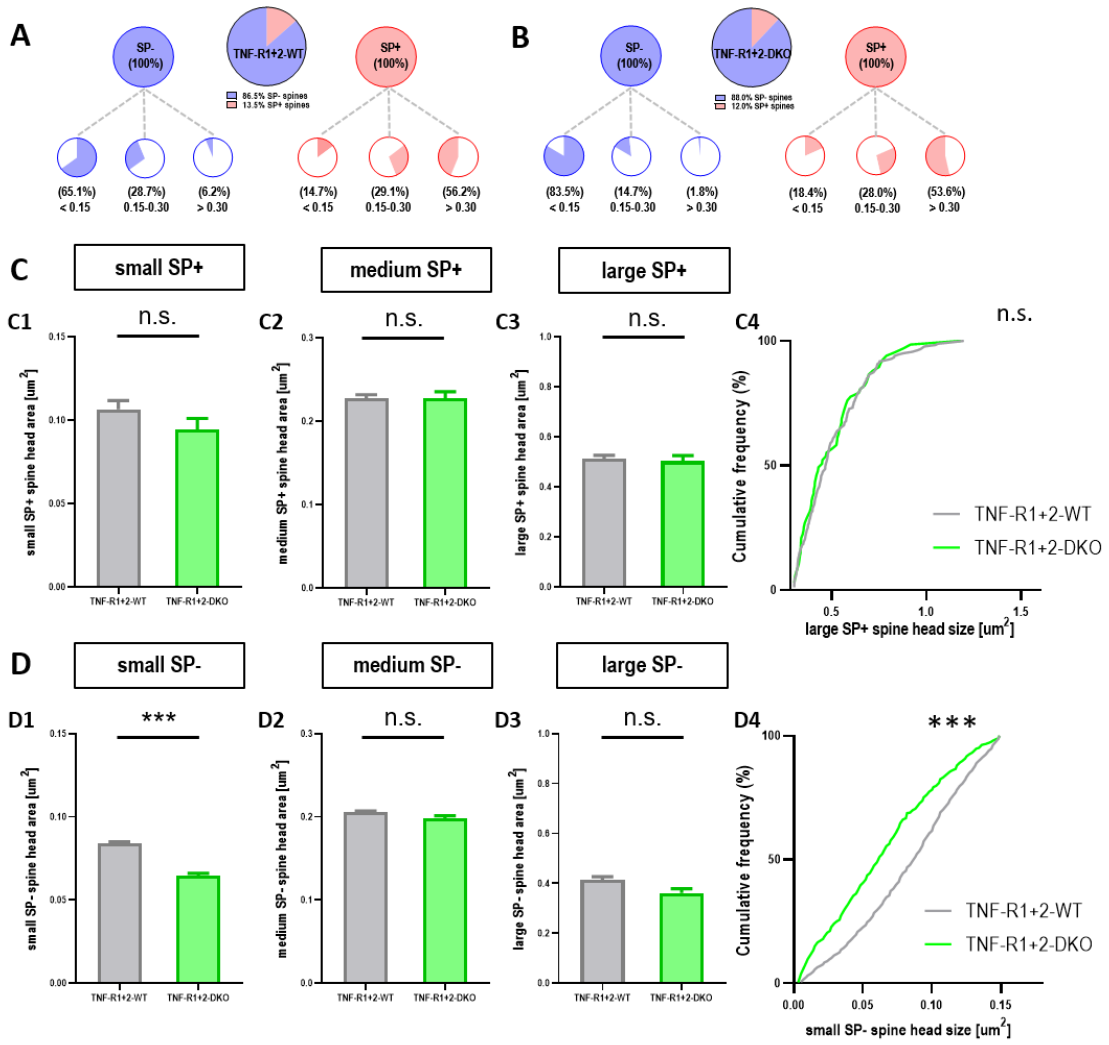

Fig. 31 Small SP- spines are the dominant contributor to the reduction of spine head sizes in TNF-R1+2-DKO mice. (A) Fraction of SP- (~86.5%) and SP+ spines (~13.5%) in TNF-R1+2-WT mice. Number of TNF-R1+2-WT SP- spines = 2086: small spines = 1359, medium spines = 599, large spines = 128; Number of TNF-R1+2-WT SP+ spines = 326: small spines = 48, medium spines = 95, large spines = 183. **(B)** Fraction of SP- (~88.0%) and SP+ spines (12.0%) in TNF-R1+2-DKO mice. The removal of both receptors caused a large increase in the population of small SP- spines (~83.5%) compared to TNF-R1+2-WT mice (~65.1%). Number of TNF-R1+2-DKO SP- spines = 914: small spines = 763, medium spines = 134, large spines = 17; Number of TNF-R1+2-DKO SP+ spines = 125: small spines = 23, medium spines = 35, large spines = 67. **(C)** Comparison of SP+ spine classes between genotypes shows no significant differences in small (C1; n.s. p = 0.088), medium (C2; n.s. p = 0.724) and large (C3; n.s. p = 0.790) sized spines. Cumulative frequency plot of the spine head area of SP+ large sized spines confirms that there were no differences in these spine populations (C4; n.s. p =

0.891); Kolmogorov-Smirnov test. **(D)** Comparision of SP- spine classes between genotypes shows no significant differences in medium (D2; n.s. p = 0.724) and large (D3; n.s. p = 0.891) sized spines, however, the size of small SP- spines was significantly reduced compared to wildtypes (D1; ***p < 0.001). Cumulative frequency plot of the spine head area of SP- spines shows significant differences in the small spine populations (D4; ***p < 0.001); Kolmogorov-Smirnov test.

5.3.8. Synaptopodin clusters are predominantly located in the base of spine heads.

Previous work reported that synaptopodin clusters are most often located at the base of the spine head, where it forms an essential part of the SA (9,164,168,177). This was the case for all investigated genotypes (Fig. 32A-C), however, in TNF-KO animals, we saw a shift towards more clusters located at the base of the spine, very close to the dendritic shaft (Fig. 21D). When comparing differences between mouse mutants and their respective wildtypes, we saw an increase of ~6% in the localization of SP clusters in spine heads, with spine neck and base localization being reduced in TNF-R1-KO mice (Fig. 31A). In TNF-R2-KO mice, there was a negligent increase of ~1% in spine head localization and of ~2% in spine base localization, in line with previously shown analysis of this receptor's non-association with synapopodin clusters (Fig. 31B). TNF-R1+2-DKO mice had a shift towards more SP clusters in spine necks, ~9% more than wildtypes on account of fewer SP clusters in spine heads (Fig. 31C).

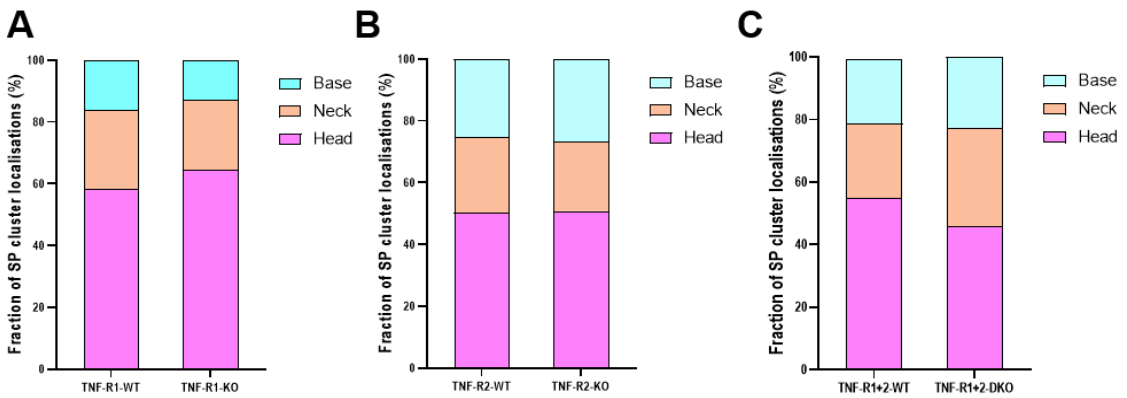

Figure 32. Localization of synaptopodin clusters in different TNF receptor genotypes compared to their respective wildtypes. (A) The fraction of SP cluster localizations in TNF-R1 mice. Most SP clusters were found to be colocalized inside spine heads (TNF-R1-WT ~58%; TNF-R1-KO ~64%), followed by spine necks (TNF-R1-WT ~26%; TNF-R1-KO

~23%) and lastly inside the base of the (TNF-R1-WT ~16%; TNF-R1-KO ~13%). Number of SP clusters in TNF-R1-WT = 164: spine head = 96, spine neck = 42, spine base = 26; Number of SP clusters in TNF-R1-KO = 153: spine head = 99, spine neck = 35, spine base = 19. **(B)** The fraction of SP cluster localizations in TNF-R2 mice. Colocalization was most often inside spine heads (TNF-R2-WT ~50%; TNF-R2-KO ~51%), followed by spine necks (TNF-R2-WT ~25%; TNF-R2-KO ~22%) and lastly inside the base of the (TNF-R2-WT ~25%; TNF-R2-KO ~27%). Number of SP clusters in TNF-R2-WT = 162: spine head = 81, spine neck = 41, spine base = 40; Number of SP clusters in TNF-R2-KO = 176: spine head = 89, spine neck = 39, spine base = 48. **(C)** The fraction of SP cluster localizations in TNF-R1+2 mice. SP clusters were again found to be most often colocalized inside spine heads (TNF-R1+2-WT ~55%; TNF-R1+2-DKO ~46%), followed by spine necks (TNF-R1+2-WT ~24%; TNF-R1+2-DKO ~33%) and lastly inside the base of the (TNF-R1+2-WT ~21%; TNF-R1+2-DKO ~23%). Number of SP clusters in TNF-R1+2-WT = 326: spine head = 179, spine neck = 78, spine base = 69; Number of SP clusters in TNF-R1+2-DKO = 125: spine head = 57, spine neck = 40, spine base = 28.

5.3.9. Spine head size correlates with SP cluster size in all analyzed groups.

As we showed before (Fig. 21E), in TNF-KO and TNF-WT mice, there was a pronounced positive correlation between SP-cluster size and spine head size. Since the correlation was shown to be stronger in wildtype mice, we wanted to see if we can replicate this finding in receptor knockout mice. Correlation analysis showed a significant correlation in all genotypes (Fig. 33A-C). TNF-R1-KO and TNF-R2-KO mice followed the same pattern as with TNF-KO mice, where we saw a higher correlation (denoted by a higher value of the Spearman r and R^2) in their respective wildtypes (Fig. 33A, B). In the case of TNF-R1+2-DKO mice, we saw the opposite effect. When compared to their wildtype mice, TNF-R1+2-DKO mice had more than double linear regression analysis values, and these values were the highest in all analyzed genotypes (Fig. 33C).

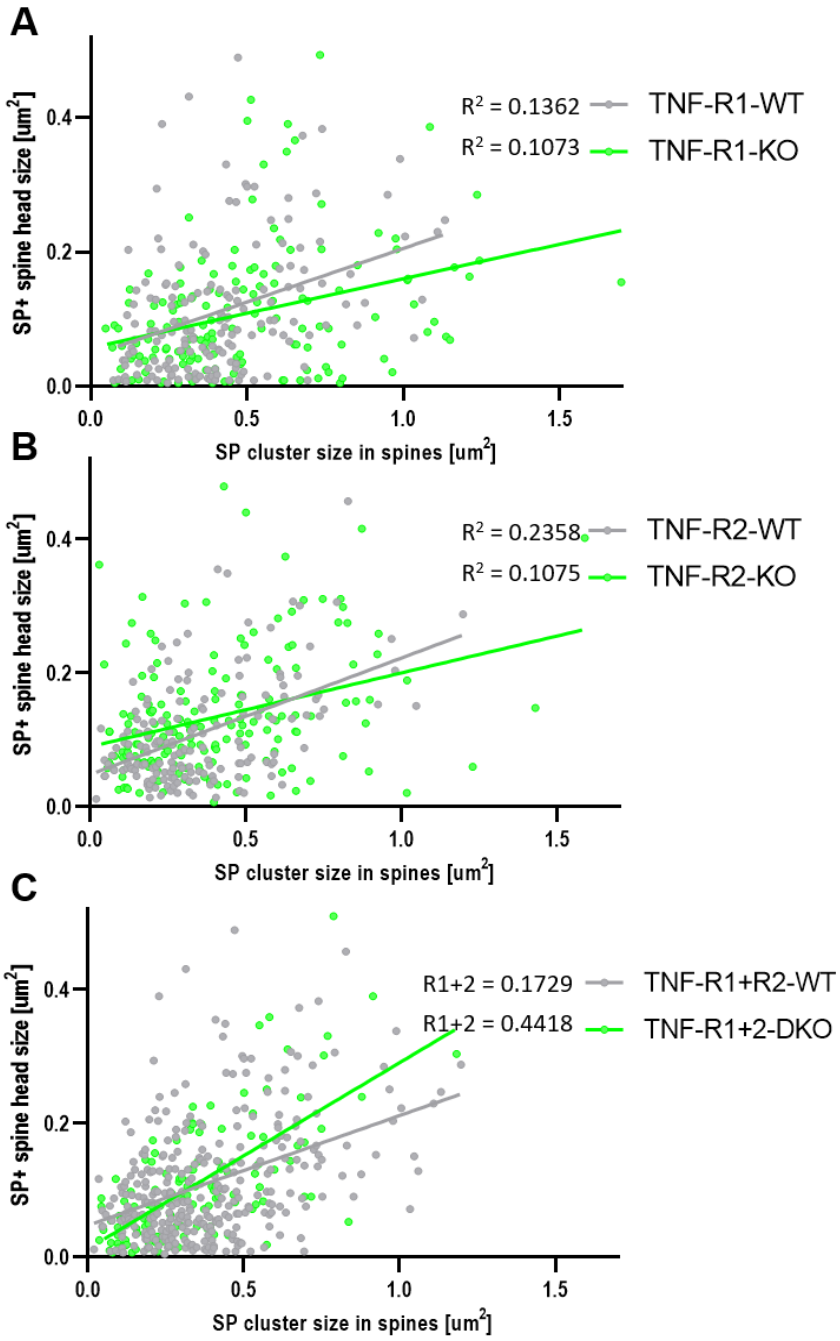

Figure 33. Correlation of SP+ spine head size and SP cluster size in different TNF receptor knockouts and their respective wildtypes. (A) Correlation analysis between spine head size and SP cluster size for all TNF-R1 genotypes. ***p < 0.001. TNF-R1-WT: Spearman r = 0.369, Linear regression analysis: R^2 = 0.136; TNF-R1-KO: Spearman r = 0.327, Linear regression analysis: R^2 = 0.107. Number of TNF-R1-WT SP+ spines and clusters = 164; Number of TNF-R1-KO SP+ spines and clusters = 153. **(B)** Correlation analysis between spine head size and SP cluster size for all TNF-R2 genotypes. ***p < 0.001. TNF-R2-WT: Spearman r = 0.4856, Linear regression analysis: R^2 = 0.2358; TNF-R2-KO: Spearman r = 0.3278, Linear

regression analysis: R^2 = 0.1075. Number of TNF-R2-WT SP+ spines and clusters = 162; Number of TNF-R2-KO SP+ spines and clusters = 176. **(C)** Correlation analysis between spine head size and SP cluster size for all TNF-R1+2 genotypes. ***p < 0.001. TNF-R1+2-WT: Spearman r = 0.4158, Linear regression analysis: R1+2 = 0.1729; TNF-R1+2-DKO: Spearman r = 0.6646, Linear regression analysis: R1+2 = 0.4418. Number of TNF-R1+2-WT SP+ spines and clusters = 326; Number of TNF-R1+2-DKO SP+ spines and clusters = 125.

6. DISCUSSION

The morphology of dendrites and dendritic spines has long been studied. To quote Shepherd (47): „the spine creates a microcompartment with a range of properties that enable it to operate as a multifunctional integrative unit“. In that light, many of the functions of spines have been elucidated: depending on their shape, they can serve for learning or memory retention (211), cognition (210), synaptic tagging and capture (212) and synaptic strength regulation (53,68,79). Studying the size of spine heads allows us to gain insights into post-synaptic densities and their influence on long term potentiation (213). AMPA receptor density, which is taken as a substitute for synaptic strength, is closely correlated with the size of the dendritic spines, allowing us to infer physiological changes in neuronal activity through the analysis of spine sizes (66,69,214,215). In this regard, ample molecules have been found to influence the morphology of spines, and this is done by interactions with the highly shifting actin filaments located within (91).

This doctoral work focused on two such important molecules that have structural and plasticity-related functions, i.e. TNF-α and SP. The seminal work of Beattie et al. has shown the importance of TNF-α in synaptic plasticity (7). It binds to TNF-R1, TNF-R2 and glial P2Y1 receptors, exerting different, but slightly overlapping effects (89,138). Constitutive TNF-α activity promotes the surface expression of AMPA receptors and the endocytosis of $GABA_A$ receptors, thereby changing the excitation/inhibition balance in favor of excitation (154,155). It has concentration-dependent effects on synaptic plasticity, with slightly elevated levels easing LTP generation, while highly elevated levels had opposing effects, impairing synaptic plasticity (8). It is also a critical instructive signal for the initiation of synaptic scaling (108) and plays an important role in gliotransmission through the binding with purinergic P2Y1 receptors (90). Although many of its molecular and electrophysiological effects are known, the role of TNF-α in the morphological landscape of dendrites and dendritic spines is still an unanswered question.

The actin-modulating molecule synaptopodin has been linked with the formation of the spine apparatus organelle that serves as an internal calcium store of dendritic spines (9,162,164,165). It is a part of the downstream machinery changing synaptic strength (185) and promoting AMPA receptor accumulation at the post-synaptic density of excitatory synapses (169,171). It has an important role in regulating Hebbian (180,181), homeostatic (205) and metaplastic (8)

forms of synaptic plasticity. These molecules, TNF-α and SP, have recently been linked, for TNF-α relies on intracellular calcium stores, as regulated by SP, to exert its effects on synaptic plasticity. This doctorate work hoped to shed more light on this connection in the context of *ex vivo* morphological investigations.

The main findings can be summarized as follows: (a) Deafferentiated granule cells of TNF-deficient mice grown *in-vitro* exhibit fewer deficits in dendritic tree arborization and complexity compared to wildtype controls. (b) Granule cells of TNF-deficient mice have ~20% fewer spines than wildtype controls *ex vivo*. (c) TNF-deficient mice have larger SP+ spines and SP-clusters. (d) Dendritic spines of mice lacking TNF-R1 mimic the changes seen in TNF-deficient mice. (e) Genetic knockout of both TNF receptors causes a ~28% reduction in average spine sizes compared to wildtype controls. (f) Genetic removal of TNF-α, or any of its receptors, has the effect of reducing the size of small SP- spines compared to controls.

6.1. Morphological deficits in the dendritic tree in mice lacking TNF-alpha are milder compared to wildtype controls

Entorhinal denervation has long been studied as an experimental deafferentiation model since the majority of excitatory inputs to hippocampal granule cells come from the entorhinal cortex via the perforant pathway (32,198). Granule cells usually respond to the lesion with a reduction of dendritic arbor sizes and dendritic complexity (37,202,203). In this doctoral work, we focused on *in-vitro* grown granule cells of TNF-deficient mice to see if they respond differently to the lesion when compared to controls. Our investigations showed that both genotypes have a pronounced reduction in dendritic length in comparison with non-lesioned cultures. While the average length of individual dendrites was not significantly altered, we logically expected a similar reduction in the total number of dendrites in the lesioned cultures. This was the case for wildtypes, however, granule cells of TNF-deficient cultures did not have a significantly reduced number of dendrites.

In order to elucidate this discrepancy, we employed a Sholl analysis of dendritic trees in the deafferentiated groups. Both genotypes had significantly different dendritic trees 14 days after the lesion, with a tendency for lower dendritic complexity at all measured distances from the cell body. However, in the case of TNF-deficient mice, there was a tendency for higher dendritic complexity closer to the cell body and reduced complexity at distant intersections.

We consider this bimodality in response to deafferentation to be a direct result of the lack of constitutive TNF in these cells, which by itself causes lesion-like changes in the dendritic arbor so that these cells have a comparatively smaller reduction in dendritic complexity due to the lesion. Following this, total dendritic complexity was only changed in wildtype mice. We concluded that these effects cannot be explained only in the context of dendrites themselves and that we needed to see how dendritic spines, the main effectors of the afferent part of the neuron, behave in TNF-deficient mice.

6.2. Structural alterations of spines in TNF-deficient mice follow closely the changes seen in entorhinal denervation

After intracellularly filling granule cells of TNF-deficient mice *ex vivo* we found a reduced density of dendritic spines, which indicates reduced entorhinal innervation. We consider it likely that alterations in the balance of network excitation/inhibition due to the constitutive absence of TNF could have caused this defect as a secondary change. Due to the fact that the majority of spines in the adult are innervated (216), and that excitatory input on adult spiny neurons terminates nearly always on dendritic spines (217), this finding could be viewed as a structural indicator of a reduced glutamatergic innervation of granule cells in the dentate gyrus of TNF-deficient mice. Detailed analysis showed that these neurons have a significant increase in the size of large spines. These spines are characterized by large PSDs (213), high density of AMPA receptors (69,71,75,204,215), and (10) by large SP clusters. In this context large spines are physiologically strong, bringing forth the largest amount of excitation to the neuron. This shifted our focus towards SP+ spines, as we hypothesized that these changes are inherently connected to synaptopodin presence in spines.

6.3. SP positive spines are highly affected by the removal of TNF-α

SP, as an F-actin interacting protein (173), is located primarily in dendritic spines and is essential for the formation and function of the spine apparatus organelle (9,162,163,168). This doctoral work showed that in all investigated mouse mutants and wildtypes, SP is predominantly found in the base of the spine head, confirming its relative position inside spines. Previous work has shown a positive correlation between the presence of an SP cluster inside

spines and spine head size, be it in dissociated hippocampal neurons (183), acute hippocampal brain slices (181) or organotypic tissue cultures (10).

In our investigations, we have confirmed this connection in *ex vivo* preparations, and furthermore, we have shown that the size of an SP cluster and the size of the dendritic spine in which it is located are almost linearly positively correlated. Spines that contain SP are few in number, averaging around 15% of total spines, however, they are trifold larger compared to SP- spines. As we discussed before, spine head size (69,71,75), and the presence of SP clusters in dendritic spines (169) are positively correlated with AMPA receptor density, the increase in spine head size of SP+ spines is a *bona fide* structural indicator of increased synaptic strength of these dendritic spines. It would seem that TNF-deficient granule cells compensate for a reduction in spine density by homeostatically increasing the size and SP content of their remaining spines. The results of investigations done on dendritic spines of TNF-deficient granule cells showcase that these neurons already have similar changes to what is usually observed under experimental denervation conditions. It is therefore not surprising that the full extent of these changes was not seen in the context of dendritic tree alterations in the previously reported denervation experiments, since these neurons were already adapted as if they had reduced glutamatergic innervation.

6.4. Dendritic spines of mice lacking TNF-R1 undergo comparable changes to those seen in mice lacking TNF-α

TNF-α primarily binds to two receptors, TNF-R1 and TNF-R2 (125,138). One of the main physiological effects of TNF-α, the increase in the excitation/inhibition ratio of a neuron, is mediated by the promotion of AMPA receptor surface expression on excitatory synapses (7). This effect is achieved through the activation of TNF-R1, due to the fact that genetic deletion of TNF-R1, but not TNF-R2, decreases AMPA receptor expression (152). Likewise, the effects of TNF-α on P2Y1 glial receptors provide an external source of glutamate to the dendritic spine (89), and this mechanism seems to be inherently connected to the activity of TNF-R1 (90).

Our morphological investigations on granule cells of TNF-R1-deficient mice show that these neurons, similarly to TNF-deficient mice, have an increase in the size of large spines, and a concomitant reduction in the size of small spines. Furthermore, again following closely the results in TNF-deficient mice, the increase in large spine sizes is due to SP+ spine population,

while small spine sizes of only SP- spines are reduced. Shifting our focus to TNF-R2-deficient mice, we noticed that only the reduction in small SP- spine head sizes was maintained. It would seem that the effect TNF-α has on small spines is significantly mediated by both TNF-R1 and TNF-R2. On the other hand, the control TNF-α exerts on SP and its association with large spines is achieved through the activation of TNF-R1. There appears to be some redundancy in the function of both receptors since there was no reduction of dendritic spine density in TNF-R1-deficient mice. These results affirm that TNF-R1 is the dominant effector for plasticity related changes that TNF-α influences.

6.5. Dendritic spines of mice lacking both TNF receptors have a severe reduction in average size

While we expected similar results in the TNF-KO and TNF-R1+2-DKO groups, we were surprised to see a number of disparities. Firstly, instead of having a reduced density of spines, TNF-R1+2-DKO mice had a large decrease in the average size of all dendritic spines. As we extended our analysis we noticed that this decrease was only replicated in small sized spines. This deficit was not due to synaptopodin presence in spines, since there were no differences between all investigated SP+ spine size classes. As we compared SP- spines, we saw only small-sized spines to be smaller compared to wildtypes. In this regard, the important difference between TNF-KO and TNF-R1+2-DKO animals is that in the double-knockout mice TNF-α is still able to bind to purinergic P2Y1 glial receptors. This connection warrants further investigation in order to elucidate the driving mechanism for this reduction.

6.6. All investigated genotypes exhibit a reduction in the size of small SP- spines compared to controls

Investigations in the ratio of spine size classes showed that small SP- spines are the largest group of all SP- spines, with more than half spines belonging to this spine size class. In all analyzed genotypes, we saw a reduction in small SP- spine sizes compared to their respective wildtypes. A large number of small spines lack AMPA receptors and are highly likely „silent spines“ (218). In this regard these spines are physiologically weak, contributing little to the excitatory drive of the neuron. Since this reduction was not associated with SP presence inside spines, we have turned to explore different mechanisms to explain this change. We plan on

expanding our experiments on these mice mutants, applying an entorhinal cortex lesion *in vivo* to study how these, already changed dendritic spines react to deafferentiation.

6.7. Importance of obtained data and future research directions

One of the major findings of this doctoral thesis was a strong reduction in dendritic spine density in TNF-KO mouse mutants. It is established that afferent projections towards the target neuron are essential for normal development and subsequent preservation of dendrites and dendritic spines. Denervation, which occurs in multiple human diseases such as stroke, trauma, and Parkinson's disease, will have an effect on the denervated neurons, with changes ranging from dendritic spine loss and atrophy of dendrites to cell death (219–221). While much is known concerning the remodeling of dendritic spines in development, the mechanisms which are responsible for dendrite and dendritic spine degeneration in adult animals are still largely unknown. The current hypothesis is that reduced signaling in both NMDA receptors and mGlu receptors is required for the loss of spines (222,223). Downstream, the calcium-dependent activation of calcineurin, mediated by cofilin is in part responsible for this loss (83). However, since these studies relied on broad synaptic stimulation, it was not possible to connect these mechanisms to input-specific alterations such as denervation in neurons. There is also the function of astrocytes to consider since these glial cells mediate synapse elimination in adults (224). Dendritic destabilization has been associated with the reduced activity of calcium-calmodulin-dependent protein kinase II, which is activated by elevated levels of intracellular calcium (225). In this regard, it is important to note that synaptopodin has been identified as a regulator of the homeostatic changes that occur in dendritic spines after denervation (205). We have now shown that TNF-α is a candidate molecule for the regulation of dendritic and spine reorganization following denervation since its absence has similar effects on these structures. Our next step is to perform *in vivo* ECL experiments in TNF-KO mice, so as to fully determine the role TNF-α has in denervation-induced morphological changes in dendritic spines. The functional properties of neurons are tightly entwined to their morphology. A wealth of literature exists connecting the firing properties, plasticity changes, and signal propagation to detectable changes in the architecture of dendrites and dendritic spines. Therefore, after the period of development, it is critical to keep neuronal morphology in optimal conditions in adult animals. Using different mouse mutants, we can now directly study the causal relationship between potential candidate molecules and their role in dendrite and dendritic spine reorganization following denervation. The potential of this research is in the development of possible future

therapeutical approaches for multiple human diseases affected by the deafferentation of neurons. Possible outcomes of intervention after stroke, central nervous system injury, or neurodegenerative diseases include the reduction or complete prevention of dendritic and spine degeneration in the affected areas.

7. CONCLUSION

Our results highlight the importance of TNF-α and SP in dendritic and spine morphology *in vivo* in adult animals. The absence of TNF-α or its receptors was followed by substatial alterations in dendritic arborisation, dendritic spine density and size in affected animals, which was homeostatically compensated through synaptopodin-mediated mechanisms. Due to the fact that multiple brain pathologies such as stroke, injury, neurodegenerative diseases exhibit similar morphological deficits in neurons, it is our goal to further elucidate the role of TNF-α in these contexts. This could in turn reveal important mechanisms in the pathophysiology of these disorders, allowing us to target specific molecular targets as a possible therapeutical approach.

A. Major findings:

1. Dendrites of granule cells in TNF-deficient mice are partially resistant to denervation.
2. Granule cells of TNF-deficient mice have a 20% reduction in dendritic spine density.
3. TNF-deficiency causes an increase in size of large spines and is tightly connected to the enlargement of synaptopodin-positive spines and synaptopodin clusters.
4. The removal of TNF-R1 has a similar effect to TNF-deficiency with regards to dendritic spines.
5. The removal of both TNF-R1 and TNF-R2 causes a 28% reduction in spine head sizes.
6. The removal of TNF-α, or any of its receptors, reduces the size of small dendritic spines that do not contain synaptopodin.

8. ABSTRACT IN ENGLISH

Changes in the morphology of dendrites and dendritic spines are tightly correlated to the functional properties of neurons. The underlying mechanisms are under strict control by multiple effectors. One of such proteins, the tumor necrosis factor α (TNF-α) has been shown to influence synaptic transmission and plasticity and is tightly connected to the actin-modulating protein synaptopodin (SP). We performed a detailed analysis of dendritic arbors and dendritic spines of dentate granule cells in mice mutants lacking TNF-α or its receptors. Fixed hippocampal sections were double-stained for SP, a molecular marker for strong and stable spines. We have shown that granule cells of TNF-deficient mice have fewer deficits in dendritic tree arborization after denervation. Dendritic spine density was reduced by 20% in these mice, and a compensatory increase in the size of large, SP+ spines was seen. A strikingly similar pattern of changes was seen in mice lacking TNF-R1, but not in mice lacking TNF-R2, showcasing that TNF-R1 is the dominant effector for this mechanism. Genetic removal of both receptors caused a large, 28% reduction in average spine sizes, and the compensatory, homeostatic increase of large spine sizes and SP content was absent.

9. ABSTRACT IN CROATIAN

Morfološka analiza dendritičkog stabla te izražaj i lokalizacija aktin-modulirajućeg proteina synaptopodina u hipokampalnim zrnatim stanicama TNF-α-KO miševa.

Promjene u morfologiji dendrita i dendritičkih trnova usko su povezane s funkcionalnim svojstvima neurona. Osnovni mehanizmi tih promjena su pod strogom kontrolom mnogih molekula. Pokazalo se da jedan od takvih proteina, faktor tumorske nekroze α (TNF-α) utječe na sinaptički prijenos i plastičnost te je usko povezan s aktin-modulirajućim proteinom synaptopodinom (SP). U ovom radu smo detaljno analizirali dendritičko stablo i dendritičke trnove zrnatih stanica girusa dentatusa u miševa mutanata kojima nedostaje gen za TNF-α ili njegovi receptori. Fiksirane hipokampalne kriške su bile imunohistokemijski obojene za SP, molekularni marker stabilnih i snažnih dendritičkih trnova. Pokazali smo da zrnate stanice miševa kojima nedostaje gen za TNF-α imaju manje promjena u grananju dendritičkog stabla nakon denervacije. Gustoća dendritičkih trnova je smanjena za 20% kod tih miševa, a uočen je nadomjesni porast veličine velikih SP+ dendritičkih trnova. Zapanjujuće, sličan obrazac promjena viđen je kod miševa kojima nedostaje gen za TNF-R1, ali ne i kod miševa kojima nedostaje gen za TNF-R2, ukazujući na to da je TNF-R1 odlučujući čimbenik u nastanku ovih promjena. Genetsko uklanjanje oba receptora prouzročilo je veliko, 28% smanjenje prosječnih veličina dendritičkih trnova, te je u tim miševima izostao kompenzacijski, homeostatski porast velikih dendritičkih trnova, kao i sadržaja SP.

10. BIBLIOGRAPHY

1. Ramón y Cajal S. Histologie du système nerveux de l'homme & des vertébrés. Paris: Maloine; 1909.
2. Yuste R, Denk W. Dendritic spines as basic functional units of neuronal integration. Nature. 1995;375(6533):682–4.
3. Amaral DG, Scharfman HE, Lavenex P. The dentate gyrus: fundamental neuroanatomical organization (dentate gyrus for dummies). Prog Brain Res. 2007;163:3-22.
4. Diekmann S, Ohm TG, Nitsch R. Long-lasting transneuronal changes in rat dentate granule cell dendrites after entorhinal cortex lesion. A combined intracellular injection and electron microscopy study. Brain Pathol. 1996;6(3):205-14.
5. Urbanska M, Blazejczyk M, Jaworski J. Molecular basis of dendritic arborization. Acta Neurobiol Exp. 2008;68(2):264–88.
6. Alvarez VA, Sabatini BL. Anatomical and physiological plasticity of dendritic spines. Annu Rev Neurosci. 2007;30:79–97.
7. Beattie EC, Stellwagen D, Morishita W, Bresnahan JC, Ha BK, Zastrow M von, et al. Control of synaptic strength by glial TNFalpha. Science. 2002;295(5563):2282–5.
8. Maggio N, Vlachos A. Tumor necrosis factor (TNF) modulates synaptic plasticity in a concentration-dependent manner through intracellular calcium stores. J Mol Med. 2018;96(10):1039–47.
9. Deller T, Korte M, Chabanis S, Drakew A, Schwegler H, Stefani GG, et al. Synaptopodin-deficient mice lack a spine apparatus and show deficits in synaptic plasticity. Proc Natl Acad Sci U S A. 2003;100(18):10494–9.
10. Yap K, Drakew A, Smilovic D, Rietsche M, Paul MH, Vuksic M, et al. The actin-modulating protein synaptopodin mediates long-term survival of dendritic spines. Elife. 2020;9:e62944.
11. Braak H, Braak E. On areas of transition between entorhinal allocortex and temporal isocortex in the human brain. Normal morphology and lamina-specific pathology in Alzheimer's disease. Acta Neuropathol. 1985;68(4):325–32.
12. Witter MP, Doan TP, Jacobsen B, Nilssen ES, Ohara S. Architecture of the Entorhinal Cortex: A Review of Entorhinal Anatomy in Rodents with Some Comparative Notes. Front Syst Neurosci 2017;11:46.

13. Shepherd MD, Grillner M. Handbook of Brain Microcircuits. Oxford: Oxford University Press; 2010.
14. Cameron HA, McKay RD. Adult neurogenesis produces a large pool of new granule cells in the dentate gyrus. J Comp Neurol. 2001;435(4):406–17.
15. Ding S-L. Comparative anatomy of the prosubiculum, subiculum, presubiculum, postsubiculum, and parasubiculum in human, monkey, and rodent. J Comp Neurol. 2013;521(18):4145–62.
16. The Croonian lecture. — La fine structure des centres nerveux. Proc R Soc Lond. 1894;55(331-335):444–68.
17. Dalley R, Ng L, Guillozet-Bongaarts A. Dentate Gyrus. Nat Prec. 2008;34:100-16.
18. Paxinos G. The rat nervous system. 3rd. ed. San Diego CA: Academic Press; 2004.
19. Andersen P, Morris R, Amaral D, Bliss T, O'Keefe J. The hippocampus book. Oxford: Oxford University Press; 2007.
20. Paxinos G, Watson C. The rat brain in stereotaxic coordinates. 6th. ed. Cambridge MA: Academic Press; 2006.
21. Neves G, Cooke SF, Bliss TVP. Synaptic plasticity, memory and the hippocampus: a neural network approach to causality. Nat Rev Neurosci. 2008;9(1):65–75.
22. Scharfman H, Witter MP. The Dentate Gyrus: A Comprehensive Guide to Structure, Function, and Clinical Implications. Cambridge MA: Academic Press; 2007.
23. Hjorth-Simonsen A, Jeune B. Origin and termination of the hippocampal perforant path in the rat studied by silver impregnation. J Comp Neurol. 1972;144(2):215–32.
24. Shapiro LA, Korn MJ, Shan Z, Ribak CE. GFAP-expressing radial glia-like cell bodies are involved in a one-to-one relationship with doublecortin-immunolabeled newborn neurons in the adult dentate gyrus. Brain Res. 2005;1040(1-2):81–91.
25. Lübbers K, Frotscher M. Fine structure and synaptic connections of identified neurons in the rat fascia dentata. Anat Embryol. 1987;177(1):1–14.
26. Seress L, Ribak CE. Direct commissural connections to the basket cells of the hippocampal dentate gyrus: anatomical evidence for feed-forward inhibition. J Neurocytol. 1984;13(2):215–25.
27. Wenzel HJ, Buckmaster PS, Anderson NL, Wenzel ME, Schwartzkroin PA. Ultrastructural localization of neurotransmitter immunoreactivity in mossy cell axons and their synaptic targets in the rat dentate gyrus. Hippocampus. 1997;7(5):559–70.
28. Milner TA, Bacon CE. Ultrastructural localization of somatostatin-like immunoreactivity in the rat dentate gyrus. J Comp Neurol. 1989;290(4):544–60.

29. Soriano E, Frotscher M. A GABAergic axo-axonic cell in the fascia dentata controls the main excitatory hippocampal pathway. Brain Res. 1989;503(1):170–4.
30. Scharfman HE, Myers CE. Hilar mossy cells of the dentate gyrus: a historical perspective. Front Neural Circuits. 2013;6:106.
31. Laatsch RH, Cowan WM. Electron microscopic studies of the dentate gyrus of the rat. I. Normal structure with special reference to synaptic organization. J Comp Neurol. 1966;128(3):359–95.
32. Nafstad PH. An electron microscope study on the termination of the perforant path fibres in the hippocampus and the fascia dentata. Z Zellforsch Mikrosk Anat. 1967;76(4):532–42.
33. Soriano E, Frotscher M. Mossy cells of the rat fascia dentata are glutamate-immunoreactive. Hippocampus. 1994;4(1):65–9.
34. Ribak CE, Shapiro LA. Ultrastructure and synaptic connectivity of cell types in the adult rat dentate gyrus. Prog Brain Res. 2007;163:155–66.
35. Desmond NL, Levy WB. Granule cell dendritic spine density in the rat hippocampus varies with spine shape and location. Neurosci Lett. 1985;54(2-3):219–24.
36. Perederiy JV, Westbrook GL. Structural plasticity in the dentate gyrus- revisiting a classic injury model. Front Neural Circuits. 2013;7:17.
37. Vuksic M, Del Turco D, Vlachos A, Schuldt G, Müller CM, Schneider G, et al. Unilateral entorhinal denervation leads to long-lasting dendritic alterations of mouse hippocampal granule cells. Exp Neurol. 2011;230(2):176–85.
38. Phinney AL, Calhoun ME, Woods AG, Deller T, Jucker M. Stereological analysis of the reorganization of the dentate gyrus following entorhinal cortex lesion in mice. Eur J Neurosci. 2004;19(7):1731–40.
39. Ramirez JJ, McQuilkin M, Carrigan T, MacDonald K, Kelley MS. Progressive entorhinal cortex lesions accelerate hippocampal sprouting and spare spatial memory in rats. Proc Natl Acad Sci U S A. 1996;93(26):15512–7.
40. Steward O. Lesion-induced synapse reorganization in the hippocampus of cats: sprouting of entorhinal, commissural/associational, and mossy fiber projections after unilateral entorhinal cortex lesions, with comments on the normal organization of these pathways. Hippocampus. 1992;2(3):247–68.
41. Del Turco D, Paul MH, Beeg Moreno VJ, Hildebrandt-Einfeldt L, Deller T. Re-innervation of the Denervated Dentate Gyrus by Sprouting Associational and

Commissural Mossy Cell Axons in Organotypic Tissue Cultures of Entorhinal Cortex and Hippocampus. Front Mol Neurosci. 2019;12:270.

42. Lenz M, Galanis C, Kleidonas D, Fellenz M, Deller T, Vlachos A. Denervated mouse dentate granule cells adjust their excitatory but not inhibitory synapses following in vitro entorhinal cortex lesion. Exp Neurol. 2019;312:1–9.
43. Alkadhi KA. Cellular and Molecular Differences Between Area CA1 and the Dentate Gyrus of the Hippocampus. Mol Neurobiol. 2019;56(9):6566–80.
44. Beining M, Jungenitz T, Radic T, Deller T, Cuntz H, Jedlicka P, et al. Adult-born dentate granule cells show a critical period of dendritic reorganization and are distinct from developmentally born cells. Brain Struct Funct. 2017;222(3):1427–46.
45. Aimone JB, Wiles J, Gage FH. Computational influence of adult neurogenesis on memory encoding. Neuron. 2009;61(2):187–202.
46. Tavosanis G. Dendritic structural plasticity. Dev Neurobiol. 2012;72(1):73–86.
47. Shepherd GM. The dendritic spine: a multifunctional integrative unit. J Neurophysiol. 1996;75(6):2197–210.
48. Bourne JN, Harris KM. Balancing structure and function at hippocampal dendritic spines. Annu Rev Neurosci. 2008;31:47–67.
49. Sorra KE, Harris KM. Overview on the structure, composition, function, development, and plasticity of hippocampal dendritic spines. Hippocampus. 2000;10(5):501–11.
50. Arellano JI, Benavides-Piccione R, Defelipe J, Yuste R. Ultrastructure of dendritic spines: correlation between synaptic and spine morphologies. Front Neurosci. 2007;1(1):131–43.
51. Spacek J, Harris KM. Three-Dimensional Organization of Smooth Endoplasmic Reticulum in Hippocampal CA1 Dendrites and Dendritic Spines of the Immature and Mature Rat. J Neurosci. 1997;17(1):190–203.
52. Nimchinsky EA, Sabatini BL, Svoboda K. Structure and Function of Dendritic Spines. Annu Rev Physiol. 2002;64(1):313–53.
53. Koleske AJ. Molecular mechanisms of dendrite stability. Nat Rev Neurosci. 2013;14(8):536–50.
54. Dailey ME, Smith SJ. The Dynamics of Dendritic Structure in Developing Hippocampal Slices. J Neurosci. 1996;16(9):2983–94.
55. Cline H, Haas K. The regulation of dendritic arbor development and plasticity by glutamatergic synaptic input: a review of the synaptotrophic hypothesis. J Physiol. 2008;586(6):1509–17.

56. Lefebvre JL, Sanes JR, Kay JN. Development of dendritic form and function. Annu Rev Cell Dev Biol. 2015;31:741–77.
57. Scheibel A, Conrad T, Perdue S, Tomiyasu U, Wechsler A. A quantitative study of dendrite complexity in selected areas of the human cerebral cortex. Brain Cogn 1990;12(1):85–101.
58. Tsaneva-Atanasova K, Burgo A, Galli T, Holcman D. Quantifying neurite growth mediated by interactions among secretory vesicles, microtubules, and actin networks. Biophys J. 2009;96(3):840–57.
59. Konietzny A, Bär J, Mikhaylova M. Dendritic Actin Cytoskeleton: Structure, Functions, and Regulations. Front Cell Neurosci. 2017;11:147.
60. Keck T, Mrsic-Flogel TD, Vaz Afonso M, Eysel UT, Bonhoeffer T, Hübener M. Massive restructuring of neuronal circuits during functional reorganization of adult visual cortex. Nat Neurosci. 2008;11(10):1162–7.
61. Trachtenberg JT, Chen BE, Knott GW, Feng G, Sanes JR, Welker E, et al. Long-term in vivo imaging of experience-dependent synaptic plasticity in adult cortex. Nature. 2002;420(6917):788–94.
62. Conde C, Cáceres A. Microtubule assembly, organization and dynamics in axons and dendrites. Nat Rev Neurosci. 2009;10(5):319–32.
63. Burton PR. Dendrites of mitral cell neurons contain microtubules of opposite polarity. Brain Res. 1988;473(1):107–15.
64. Kasai H, Matsuzaki M, Noguchi J, Yasumatsu N, Nakahara H. Structure–stability–function relationships of dendritic spines. Trends Neurosci. 2003;26(7):360–8.
65. Bonhoeffer T, Yuste R. Spine Motility. Neuron. 2002;35(6):1019–27.
66. Asrican B, Lisman J, Otmakhov N. Synaptic strength of individual spines correlates with bound Ca2+-calmodulin-dependent kinase II. J Neurosci. 2007;27(51):14007–11.
67. Fifková E, van Harreveld A. Long-lasting morphological changes in dendritic spines of dentate granular cells following stimulation of the entorhinal area. J Neurocytol. 1977;6(2):211–30.
68. Segal M. Dendritic spines: Morphological building blocks of memory. Neurobiol Learn Mem. 2017;138:3–9.
69. Noguchi J, Nagaoka A, Watanabe S, Ellis-Davies GCR, Kitamura K, Kano M, et al. In vivo two-photon uncaging of glutamate revealing the structure-function relationships of dendritic spines in the neocortex of adult mice. J Physiol. 2011;589(Pt 10):2447–57.

70. Yang G, Pan F, Gan W-B. Stably maintained dendritic spines are associated with lifelong memories. Nature. 2009;462(7275):920–4.
71. Zito K, Scheuss V, Knott G, Hill T, Svoboda K. Rapid functional maturation of nascent dendritic spines. Neuron. 2009;61(2):247–58.
72. Hotulainen P, Hoogenraad CC. Actin in dendritic spines: connecting dynamics to function. J Cell Biol. 2010;189(4):619–29.
73. Matus A. Actin-based plasticity in dendritic spines. Science. 2000;290(5492):754–8.
74. Rosenmund C, Stern-Bach Y, Stevens CF. The tetrameric structure of a glutamate receptor channel. Science. 1998;280(5369):1596–9.
75. Matsuzaki M, Ellis-Davies GC, Nemoto T, Miyashita Y, Iino M, Kasai H. Dendritic spine geometry is critical for AMPA receptor expression in hippocampal CA1 pyramidal neurons. Nat Neurosci. 2001;4(11):1086–92.
76. McKinney RA, Capogna M, Dürr R, Gähwiler BH, Thompson SM. Miniature synaptic events maintain dendritic spines via AMPA receptor activation. Nat Neurosci. 1999;2(1):44–9.
77. Paoletti P, Neyton J. NMDA receptor subunits: function and pharmacology. Curr Opin Pharmacol. 2007;7(1):39–47.
78. Brünig I, Kaech S, Brinkhaus H, Oertner TG, Matus A. Influx of extracellular calcium regulates actin-dependent morphological plasticity in dendritic spines. Neuropharmacology. 2004;47(5):669–76.
79. McKinney RA. Excitatory amino acid involvement in dendritic spine formation, maintenance and remodelling. J Physiol. 2010;588(1):107–16.
80. Malenka RC, Bear MF. LTP and LTD: an embarrassment of riches. Neuron. 2004;44(1):5–21.
81. Yang Y, Wang X, Frerking M, Zhou Q. Spine expansion and stabilization associated with long-term potentiation. J Neurosci. 2008;28(22):5740–51.
82. Maren S, Tocco G, Standley S, Baudry M, Thompson RF. Postsynaptic factors in the expression of long-term potentiation (LTP): increased glutamate receptor binding following LTP induction in vivo. Proc Natl Acad Sci U S A. 1993;90(20):9654–8.
83. Zhou Q, Homma KJ, Poo M. Shrinkage of dendritic spines associated with long-term depression of hippocampal synapses. Neuron. 2004;44(5):749–57.
84. Beattie EC, Carroll RC, Yu X, Morishita W, Yasuda H, Zastrow M von, et al. Regulation of AMPA receptor endocytosis by a signaling mechanism shared with LTD. Nat Neurosci. 2000;3(12):1291–300.

85. Araque A, Parpura V, Sanzgiri RP, Haydon PG. Tripartite synapses: glia, the unacknowledged partner. Trends Neurosci. 1999;22(5):208–15.
86. Perea G, Araque A. Glial calcium signaling and neuron-glia communication. Cell Calcium. 2005;38(3-4):375–82.
87. Newman EA. New roles for astrocytes: Regulation of synaptic transmission. Trends Neurosci. 2003;26(10):536–42.
88. Perea G, Araque A. Properties of synaptically evoked astrocyte calcium signal reveal synaptic information processing by astrocytes. J Neurosci. 2005;25(9):2192–203.
89. Jourdain P, Bergersen LH, Bhaukaurally K, Bezzi P, Santello M, Domercq M, et al. Glutamate exocytosis from astrocytes controls synaptic strength. Nat Neurosci. 2007;10(3):331–9.
90. Domercq M, Brambilla L, Pilati E, Marchaland J, Volterra A, Bezzi P. P2Y1 receptor-evoked glutamate exocytosis from astrocytes: control by tumor necrosis factor-alpha and prostaglandins. J Biol Chem. 2006;281(41):30684–96.
91. Calabrese B, Wilson MS, Halpain S. Development and regulation of dendritic spine synapses. Physiology (Bethesda). 2006;21:38–47.
92. Hebb DO. The organization of behavior: a neuropsychological theory: Hoboken NJ: Wiley; 1949.
93. Surmeier DJ, Foehring R. A mechanism for homeostatic plasticity. Nat Neurosci. 2004;7(7):691–2.
94. Dubes S, Favereaux A, Thoumine O, Letellier M. miRNA-Dependent Control of Homeostatic Plasticity in Neurons. Front Cell Neurosci. 2019;13:536.
95. Turrigiano G. Homeostatic synaptic plasticity: local and global mechanisms for stabilizing neuronal function. Cold Spring Harb Perspect Biol. 2012;4(1):a005736.
96. Zhang W, Linden DJ. The other side of the engram: experience-driven changes in neuronal intrinsic excitability. Nat Rev Neurosci. 2003;4(11):885–900.
97. Davis GW. Homeostatic control of neural activity: from phenomenology to molecular design. Annu Rev Neurosci. 2006;29:307–23.
98. Gonzalez-Islas C, Wenner P. Spontaneous network activity in the embryonic spinal cord regulates AMPAergic and GABAergic synaptic strength. Neuron. 2006;49(4):563–75.
99. Marder E, Goaillard JM. Variability, compensation and homeostasis in neuron and network function. Nat Rev Neurosci. 2006;7(7):563–74.

100. Turrigiano GG. The self-tuning neuron: synaptic scaling of excitatory synapses. Cell. 2008;135(3):422–35.
101. Barnes SJ, Franzoni E, Jacobsen RI, Erdelyi F, Szabo G, Clopath C, et al. Deprivation-Induced Homeostatic Spine Scaling In Vivo Is Localized to Dendritic Branches that Have Undergone Recent Spine Loss. Neuron. 2017;96(4):871-82.
102. Gainey MA, Hurvitz-Wolff JR, Lambo ME, Turrigiano GG. Synaptic scaling requires the GluR2 subunit of the AMPA receptor. J Neurosci. 2009;29(20):6479–89.
103. Rutherford LC, Nelson SB, Turrigiano GG. BDNF Has Opposite Effects on the Quantal Amplitude of Pyramidal Neuron and Interneuron Excitatory Synapses. Neuron. 1998;21(3):521–30.
104. Shepherd JD, Rumbaugh G, Wu J, Chowdhury S, Plath N, Kuhl D, et al. Arc/Arg3.1 mediates homeostatic synaptic scaling of AMPA receptors. Neuron. 2006;52(3):475–84.
105. Goddard CA, Butts DA, Shatz CJ. Regulation of CNS synapses by neuronal MHC class I. Proc Natl Acad Sci U S A. 2007;104(16):6828–33.
106. Sun Q, Turrigiano GG. PSD-95 and PSD-93 play critical but distinct roles in synaptic scaling up and down. J Neurosci. 2011;31(18):6800–8.
107. Stellwagen D, Malenka RC. Synaptic scaling mediated by glial TNF-alpha. Nature. 2006;440(7087):1054–9.
108. Steinmetz CC, Turrigiano GG. Tumor necrosis factor-α signaling maintains the ability of cortical synapses to express synaptic scaling. J Neurosci. 2010;30(44):14685–90.
109. Flood DG. Region-specific stability of dendritic extent in normal human aging and regression in Alzheimer's disease. II. Subiculum. Brain Res. 1991;540(1-2):83–95.
110. Falke E, Nissanov J, Mitchell TW, Bennett DA, Trojanowski JQ, Arnold SE. Subicular Dendritic Arborization in Alzheimer's Disease Correlates with Neurofibrillary Tangle Density. Am J Pathol. 2003;163(4):1615–21.
111. Terry RD, Masliah E, Salmon DP, Butters N, DeTeresa R, Hill R, et al. Physical basis of cognitive alterations in Alzheimer's disease: synapse loss is the major correlate of cognitive impairment. Ann Neurol. 1991;30(4):572–80.
112. Becker L, Mito T, Takashima S, Onodera K. Growth and development of the brain in Down syndrome. Prog Clin Biol Res. 1991;373:133–52.
113. Vukšić M, Petanjek Z, Rašin MR, Kostović I. Perinatal growth of prefrontal layer III pyramids in down syndrome. Pediatr Neurol. 2002;27(1):36–8.

114. Drevets WC. Functional anatomical abnormalities in limbic and prefrontal cortical structures in major depression. Prog Brain Res. 2000;126:413–31.
115. Cotter D, Mackay D, Chana G, Beasley C, Landau S, Everall IP. Reduced neuronal size and glial cell density in area 9 of the dorsolateral prefrontal cortex in subjects with major depressive disorder. Cereb Cortex. 2002;12(4):386–94.
116. Kang HJ, Voleti B, Hajszan T, Rajkowska G, Stockmeier CA, Licznerski P, et al. Decreased expression of synapse-related genes and loss of synapses in major depressive disorder. Nat Med. 2012;18(9):1413–7.
117. Schumann CM, Hamstra J, Goodlin-Jones BL, Lotspeich LJ, Kwon H, Buonocore MH, et al. The amygdala is enlarged in children but not adolescents with autism; the hippocampus is enlarged at all ages. J Neurosci. 2004;24(28):6392–401.
118. Hutsler JJ, Zhang H. Increased dendritic spine densities on cortical projection neurons in autism spectrum disorders. Brain Res. 2010;1309:83–94.
119. Bagni C, Zukin RS. A Synaptic Perspective of Fragile X Syndrome and Autism Spectrum Disorders. Neuron. 2019;101(6):1070–88.
120. Martínez-Cerdeño V. Dendrite and spine modifications in autism and related neurodevelopmental disorders in patients and animal models. Dev Neurobiol. 2017;77(4):393–404.
121. Goldman-Rakic PS, Selemon LD. Functional and anatomical aspects of prefrontal pathology in schizophrenia. Schizophr Bull. 1997;23(3):437–58.
122. Broadbelt K. Evidence for a decrease in basilar dendrites of pyramidal cells in schizophrenic medial prefrontal cortex. Schizophr Res. 2002;58(1):75–81.
123. Tata DA, Anderson BJ. The effects of chronic glucocorticoid exposure on dendritic length, synapse numbers and glial volume in animal models: implications for hippocampal volume reductions in depression. Physiol Behav. 2010;99(2):186–93.
124. Brown CE, Boyd JD, Murphy TH. Longitudinal in vivo imaging reveals balanced and branch-specific remodeling of mature cortical pyramidal dendritic arbors after stroke. J Cereb Blood Flow Metab. 2010;30(4):783–91.
125. Locksley RM, Killeen N, Lenardo MJ. The TNF and TNF Receptor Superfamilies. Cell. 2001;104(4):487–501.
126. Montgomery SL, Bowers WJ. Tumor necrosis factor-alpha and the roles it plays in homeostatic and degenerative processes within the central nervous system. J Neuroimmune Pharmacol. 2012;7(1):42–59.

127. Shohami E, Bass R, Wallach D, Yamin A, Gallily R. Inhibition of tumor necrosis factor alpha (TNFalpha) activity in rat brain is associated with cerebroprotection after closed head injury. J Cereb Blood Flow Metab. 1996;16(3):378–84.
128. Taupin V, Renno T, Bourbonnière L, Peterson AC, Rodriguez M, Owens T. Increased severity of experimental autoimmune encephalomyelitis, chronic macrophage/microglial reactivity, and demyelination in transgenic mice producing tumor necrosis factor-alpha in the central nervous system. Eur J Immunol. 1997;27(4):905–13.
129. Sriram K, Matheson JM, Benkovic SA, Miller DB, Luster MI, O'Callaghan JP. Mice deficient in TNF receptors are protected against dopaminergic neurotoxicity: implications for Parkinson's disease. FASEB J. 2002;16(11):1474–6.
130. He P, Zhong Z, Lindholm K, Berning L, Lee W, Lemere C, et al. Deletion of tumor necrosis factor death receptor inhibits amyloid beta generation and prevents learning and memory deficits in Alzheimer's mice. J Cell Biol. 2007;178(5):829–41.
131. Hofman FM, Hinton DR, Johnson K, Merrill JE. Tumor necrosis factor identified in multiple sclerosis brain. J Exp Med 1989;170(2):607–12.
132. Grimaldi LM, Martino GV, Franciotta DM, Brustia R, Castagna A, Pristerà R, et al. Elevated alpha-tumor necrosis factor levels in spinal fluid from HIV-1-infected patients with central nervous system involvement. Ann Neurol. 1991;29(1):21–5.
133. Vivas M, Force E, El Haj C, Tubau F, Ariza J, Cabellos C. Experimental study of cerebrospinal fluid tumor necrosis factor-alpha release in penicillin- and cephalosporin-resistant pneumococcal meningitis treated with different antibiotic schedules. J Microbiol Immunol Infect. 2017;50(4):435–9.
134. Liu T, Clark RK, McDonnell PC, Young PR, White RF, Barone FC, et al. Tumor necrosis factor-alpha expression in ischemic neurons. Stroke. 1994;25(7):1481–8.
135. Ross SA, Halliday MI, Campbell GC, Byrnes DP, Rowlands BJ. The presence of tumour necrosis factor in CSF and plasma after severe head injury. Br J Neurosurg. 1994;8(4):419–25.
136. Santello M, Volterra A. TNFα in synaptic function: switching gears. Trends Neurosci. 2012;35(10):638–47.
137. Peschon JJ, Torrance DS, Stocking KL, Glaccum MB, Otten C, Willis CR, et al. TNF receptor-deficient mice reveal divergent roles for p55 and p75 in several models of inflammation. J Immunol. 1998;160(2):943–52.

138. Grell M, Douni E, Wajant H, Löhden M, Clauss M, Maxeiner B, et al. The transmembrane form of tumor necrosis factor is the prime activating ligand of the 80 kDa tumor necrosis factor receptor. Cell. 1995;83(5):793–802.
139. Wallach D, Varfolomeev EE, Malinin NL, Goltsev YV, Kovalenko AV, Boldin MP. Tumor necrosis factor receptor and Fas signaling mechanisms. Annu Rev Immunol. 1999;17:331–67.
140. Micheau O, Tschopp J. Induction of TNF Receptor I-Mediated Apoptosis via Two Sequential Signaling Complexes. Cell. 2003;114(2):181–90.
141. Vanden Berghe T, Linkermann A, Jouan-Lanhouet S, Walczak H, Vandenabeele P. Regulated necrosis: the expanding network of non-apoptotic cell death pathways. Nat Rev Mol Cell Biol. 2014;15(2):135–47.
142. Olszewski MB, Groot AJ, Dastych J, Knol EF. TNF trafficking to human mast cell granules: mature chain-dependent endocytosis. J Immunol. 2007;178(9):5701–9.
143. Medvedev AE, Sundan A, Espevik T. Involvement of the tumor necrosis factor receptor p75 in mediating cytotoxicity and gene regulating activities. Eur J Immunol. 1994;24(11):2842–9.
144. Eissner G, Kirchner S, Lindner H, Kolch W, Janosch P, Grell M, et al. Reverse signaling through transmembrane TNF confers resistance to lipopolysaccharide in human monocytes and macrophages. J Immunol. 2000;164(12):6193–8.
145. Probert L. TNF and its receptors in the CNS: The essential, the desirable and the deleterious effects. Neuroscience. 2015;302:2–22.
146. Breder CD, Tsujimoto M, Terano Y, Scott DW, Saper CB. Distribution and characterization of tumor necrosis factor-alpha-like immunoreactivity in the murine central nervous system. J Comp Neurol. 1993;337(4):543–67.
147. Sawada M, Kondo N, Suzumura A, Marunouchi T. Production of tumor necrosis factor-alpha by microglia and astrocytes in culture. Brain Res. 1989;491(2):394–7.
148. Lieberman AP, Pitha PM, Shin HS, Shin ML. Production of tumor necrosis factor and other cytokines by astrocytes stimulated with lipopolysaccharide or a neurotropic virus. Proc Natl Acad Sci U S A. 1989;86(16):6348–52.
149. Balosso S, Ravizza T, Pierucci M, Calcagno E, Invernizzi R, Di Giovanni G, et al. Molecular and functional interactions between tumor necrosis factor-alpha receptors and the glutamatergic system in the mouse hippocampus: implications for seizure susceptibility. Neuroscience. 2009;161(1):293–300.

150. Eugster H-P, Frei K, Bachmann R, Bluethmann H, Lassmann H, Fontana A. Severity of symptoms and demyelination in MOG-induced EAE depends on TNFR1. Eur J Immunol. 1999;29(2):626–32.
151. Yang L, Lindholm K, Konishi Y, Li R, Shen Y. Target Depletion of Distinct Tumor Necrosis Factor Receptor Subtypes Reveals Hippocampal Neuron Death and Survival through Different Signal Transduction Pathways. J Neurosci. 2002;22(8):3025–32.
152. He P, Liu Q, Wu J, Shen Y. Genetic deletion of TNF receptor suppresses excitatory synaptic transmission via reducing AMPA receptor synaptic localization in cortical neurons. FASEB J. 2012;26(1):334–45.
153. Leonoudakis D, Zhao P, Beattie EC. Rapid tumor necrosis factor alpha-induced exocytosis of glutamate receptor 2-lacking AMPA receptors to extrasynaptic plasma membrane potentiates excitotoxicity. J Neurosci. 2008;28(9):2119–30.
154. Stellwagen D, Beattie EC, Seo JY, Malenka RC. Differential regulation of AMPA receptor and GABA receptor trafficking by tumor necrosis factor-alpha. J Neurosci. 2005;25(12):3219–28.
155. Stück ED, Christensen RN, Huie JR, Tovar CA, Miller BA, Nout YS, et al. Tumor necrosis factor alpha mediates GABA(A) receptor trafficking to the plasma membrane of spinal cord neurons in vivo. Neural Plast. 2012;2012:261345.
156. Turrigiano GG, Leslie KR, Desai NS, Rutherford LC, Nelson SB. Activity-dependent scaling of quantal amplitude in neocortical neurons. Nature. 1998;391(6670):892–6.
157. Becker D, Zahn N, Deller T, Vlachos A. Tumor necrosis factor alpha maintains denervation-induced homeostatic synaptic plasticity of mouse dentate granule cells. Front Cell Neurosci. 2013;7:257.
158. Becker D, Deller T, Vlachos A. Tumor necrosis factor (TNF)-receptor 1 and 2 mediate homeostatic synaptic plasticity of denervated mouse dentate granule cells. Sci Rep. 2015;5:12726.
159. Santello M, Bezzi P, Volterra A. TNFα controls glutamatergic gliotransmission in the hippocampal dentate gyrus. Neuron. 2011;69(5):988–1001.
160. Baune BT, Wiede F, Braun A, Golledge J, Arolt V, Koerner H. Cognitive dysfunction in mice deficient for TNF- and its receptors. Am J Med Genet B Neuropsychiatr Genet. 2008;147(7):1056–64.
161. Mundel P, Heid HW, Mundel TM, Krüger M, Reiser J, Kriz W. Synaptopodin: an actin-associated protein in telencephalic dendrites and renal podocytes. J Cell Biol. 1997;139(1):193–204.

162. Gray EG. Axo-somatic and axo-dendritic synapses of the cerebral cortex: an electron microscope study. J Anat. 1959;93:420–33.
163. Spacek J. Three-dimensional analysis of dendritic spines. II. Spine apparatus and other cytoplasmic components. Anat Embryol (Berl). 1985;171(2):235–43.
164. Deller T, Merten T, Roth SU, Mundel P, Frotscher M. Actin-associated protein synaptopodin in the rat hippocampal formation: localization in the spine neck and close association with the spine apparatus of principal neurons. J Comp Neurol. 2000;418(2):164–81.
165. Korkotian E, Segal M. Synaptopodin regulates release of calcium from stores in dendritic spines of cultured hippocampal neurons. J Physiol. 2011;589(24):5987–95.
166. Cugno A, Bartol TM, Sejnowski TJ, Iyengar R, Rangamani P. Geometric principles of second messenger dynamics in dendritic spines. Sci Rep. 2019;9:11676.
167. Kremerskothen J, Plaas C, Kindler S, Frotscher M, Barnekow A. Synaptopodin, a molecule involved in the formation of the dendritic spine apparatus, is a dual actin/alpha-actinin binding protein. J Neurochem. 2005;92(3):597–606.
168. Deller T, Mundel P, Frotscher M. Potential role of synaptopodin in spine motility by coupling actin to the spine apparatus. Hippocampus. 2000;10(5):569–81.
169. Vlachos A, Korkotian E, Schonfeld E, Copanaki E, Deller T, Segal M. Synaptopodin regulates plasticity of dendritic spines in hippocampal neurons. J Neurosci. 2009;29(4):1017–33.
170. Konietzny A, González-Gallego J, Bär J, Perez-Alvarez A, Drakew A, Demmers JAA, et al. Myosin V regulates synaptopodin clustering and localization in the dendrites of hippocampal neurons. J Cell Sci. 2019;132(16).
171. Korkotian E, Frotscher M, Segal M. Synaptopodin regulates spine plasticity: mediation by calcium stores. J Neurosci. 2014;34(35):11641–51.
172. Mundel P, Gilbert P, Kriz W. Podocytes in glomerulus of rat kidney express a characteristic 44 KD protein. J Histochem Cytochem. 1991;39(8):1047–56.
173. Asanuma K, Kim K, Oh J, Giardino L, Chabanis S, Faul C, et al. Synaptopodin regulates the actin-bundling activity of alpha-actinin in an isoform-specific manner. J Clin Invest. 2005;115(5):1188–98.
174. Asanuma K, Yanagida-Asanuma E, Faul C, Tomino Y, Kim K, Mundel P. Synaptopodin orchestrates actin organization and cell motility via regulation of RhoA signalling. Nat Cell Biol. 2006;8(5):485–91.

175. Faul C, Asanuma K, Yanagida-Asanuma E, Kim K, Mundel P. Actin up: regulation of podocyte structure and function by components of the actin cytoskeleton. Trends Cell Biol. 2007;17(9):428–37.
176. Czarnecki K, Haas CA, Bas Orth C, Deller T, Frotscher M. Postnatal development of synaptopodin expression in the rodent hippocampus. J Comp Neurol. 2005;490(2):133–44.
177. Bas Orth C, Vlachos A, Del Turco D, Burbach GJ, Haas CA, Mundel P, et al. Lamina-specific distribution of Synaptopodin, an actin-associated molecule essential for the spine apparatus, in identified principal cell dendrites of the mouse hippocampus. J Comp Neurol. 2005;487(3):227–39.
178. Huber TB, Kwoh C, Wu H, Asanuma K, Gödel M, Hartleben B, et al. Bigenic mouse models of focal segmental glomerulosclerosis involving pairwise interaction of CD2AP, Fyn, and synaptopodin. J Clin Invest. 2006;116(5):1337–45.
179. van Petegem F. Ryanodine receptors: structure and function. J Biol Chem. 2012;287(38):31624–32.
180. Grigoryan G, Segal M. Ryanodine-mediated conversion of STP to LTP is lacking in synaptopodin-deficient mice. Brain Struct Funct. 2016;221(4):2393–7.
181. Zhang X, Pöschel B, Faul C, Upreti C, Stanton PK, Mundel P. Essential role for synaptopodin in dendritic spine plasticity of the developing hippocampus. J Neurosci. 2013;33(30):12510–8.
182. Jedlicka P, Schwarzacher SW, Winkels R, Kienzler F, Frotscher M, Bramham CR, et al. Impairment of in vivo theta-burst long-term potentiation and network excitability in the dentate gyrus of synaptopodin-deficient mice lacking the spine apparatus and the cisternal organelle. Hippocampus. 2009;19(2):130–40.
183. Okubo-Suzuki R, Okada D, Sekiguchi M, Inokuchi K. Synaptopodin maintains the neural activity-dependent enlargement of dendritic spines in hippocampal neurons. Mol Cell Neurosci. 2008;38(2):266–76.
184. Deller T, Bas Orth C, Vlachos A, Merten T, Del Turco D, Dehn D, et al. Plasticity of synaptopodin and the spine apparatus organelle in the rat fascia dentata following entorhinal cortex lesion. J Comp Neurol. 2006;499(3):471–84.
185. Jedlicka P, Deller T. Understanding the role of synaptopodin and the spine apparatus in Hebbian synaptic plasticity - New perspectives and the need for computational modeling. Neurobiol Learn Mem. 2017;138:21–30.

186. Schindelin J, Arganda-Carreras I, Frise E, Kaynig V, Longair M, Pietzsch T, et al. Fiji: an open-source platform for biological-image analysis. Nat Methods. 2012;9(7):676–82.
187. Pasparakis M, Alexopoulou L, Episkopou V, Kollias G. Immune and inflammatory responses in TNF alpha-deficient mice: a critical requirement for TNF alpha in the formation of primary B cell follicles, follicular dendritic cell networks and germinal centers, and in the maturation of the humoral immune response. J Exp Med. 1996;184(4):1397–411.
188. Fester L, Prange-Kiel J, Zhou L, Blittersdorf BV, Böhm J, Jarry H, et al. Estrogen-regulated synaptogenesis in the hippocampus: sexual dimorphism in vivo but not in vitro. J Steroid Biochem Mol Biol. 2012;131(1-2):24–9.
189. Gage GJ, Kipke DR, Shain W. Whole animal perfusion fixation for rodents. J Vis Exp. 2012(65):3564.
190. Del Turco D, Deller T. Organotypic entorhino-hippocampal slice cultures--a tool to study the molecular and cellular regulation of axonal regeneration and collateral sprouting in vitro. Methods Mol Biol. 2007;399:55–66.
191. Arends JJ, Jacquin MF. Lucifer yellow staining in fixed brain slices: Optimal methods and compatibility with somatotopic markers in neonatal brain. J Neurosci Methods. 1993;50(3):321–39.
192. Hick M, Herrmann U, Weyer SW, Mallm J-P, Tschäpe J-A, Borgers M, et al. Acute function of secreted amyloid precursor protein fragment APPsα in synaptic plasticity. Acta Neuropathol. 2015;129(1):21–37.
193. Longair MH, Baker DA, Armstrong JD. Simple Neurite Tracer: open source software for reconstruction, visualization and analysis of neuronal processes. Bioinformatics. 2011;27(17):2453–4.
194. Sholl DA. Dendritic organization in the neurons of the visual and motor cortices of the cat. J Anat. 1953;87(4):387–406.
195. Holtmaat A, Bonhoeffer T, Chow DK, Chuckowree J, Paola V de, Hofer SB, et al. Long-term, high-resolution imaging in the mouse neocortex through a chronic cranial window. Nat Protoc. 2009;4(8):1128–44.
196. Vlachos A, Müller-Dahlhaus F, Rosskopp J, Lenz M, Ziemann U, Deller T. Repetitive magnetic stimulation induces functional and structural plasticity of excitatory postsynapses in mouse organotypic hippocampal slice cultures. J Neurosci. 2012;32(48):17514–23.

197. Loewenstein Y, Kuras A, Rumpel S. Multiplicative dynamics underlie the emergence of the log-normal distribution of spine sizes in the neocortex in vivo. J Neurosci. 2011;31(26):9481–8.
198. Witter MP. The perforant path: projections from the entorhinal cortex to the dentate gyrus. Prog Brain Res.2007;163:43–61.
199. van Groen T, Miettinen P, Kadish I. The entorhinal cortex of the mouse: organization of the projection to the hippocampal formation. Hippocampus. 2003;13(1):133–49.
200. Leranth C, Hajszan T. Extrinsic afferent systems to the dentate gyrus. Prog Brain Res. 2007;163:63–799.
201. Kovac AD, Kwidzinski E, Heimrich B, Bittigau P, Deller T, Nitsch R, et al. Entorhinal cortex lesion in the mouse induces transsynaptic death of perforant path target neurons. Brain Pathol. 2004;14(3):249–57.
202. Steward O. Reinnervation of dentate gyrus by homologous afferents following entorhinal cortical lesions in adult rats. Science. 1976;194(4263):426–8.
203. Matthews DA, Cotman C, Lynch G. An electron microscopic study of lesion-induced synaptogenesis in the dentate gyrus of the adult rat. I. Magnitude and time course of degeneration. Brain Res. 1976;115(1):1–21.
204. Matsuzaki M, Honkura N, Ellis-Davies GCR, Kasai H. Structural basis of long-term potentiation in single dendritic spines. Nature. 2004;429(6993):761–6.
205. Vlachos A, Ikenberg B, Lenz M, Becker D, Reifenberg K, Bas-Orth C, et al. Synaptopodin regulates denervation-induced homeostatic synaptic plasticity. Proc Natl Acad Sci U S A. 2013;110(20):8242–7.
206. Lenz M, Kruse P, Eichler A, Muellerleile J, Straehle J, Jedlicka P, et al. All-Trans Retinoic Acid induces synaptic plasticity in human cortical neurons. Elife. 2021;10:e63026.
207. Chaturvedi MM, LaPushin R., Aggarwal B.B. Tumor necrosis factor and lymphotoxin. Qualitative and quantitative differences in the mediation of early and late cellular response. J Biol Chem. 1994;269(20):14575–83.
208. Pennica D, Lam VT, Mize NK, Weber RF, Lewis M, Fendly BM, et al. Biochemical properties of the 75-kDa tumor necrosis factor receptor. Characterization of ligand binding, internalization, and receptor phosphorylation. J Biol Chem. 1992;267(29):21172–8.
209. Xiao X, Putatunda R, Zhang Y, Soni PV, Li F, Zhang T, et al. Lymphotoxin β receptor-mediated NFκB signaling promotes glial lineage differentiation and inhibits neuronal

lineage differentiation in mouse brain neural stem/progenitor cells. J Neuroinflam. 2018;15(1):49.

210. Kasai H, Fukuda M, Watanabe S, Hayashi-Takagi A, Noguchi J. Structural dynamics of dendritic spines in memory and cognition. Trends Neurosci. 2010;33(3):121–9.

211. Bourne J, Harris KM. Do thin spines learn to be mushroom spines that remember? Curr Opin Neurobiol. 2007;17(3):381–6.

212. Rogerson T, Cai DJ, Frank A, Sano Y, Shobe J, Lopez-Aranda MF, et al. Synaptic tagging during memory allocation. Nat Rev Neurosci. 2014;15(3):157–69.

213. Harris KM, Jensen FE, Tsao B. Three-dimensional structure of dendritic spines and synapses in rat hippocampus (CA1) at postnatal day 15 and adult ages: implications for the maturation of synaptic physiology and long-term potentiation. J Neurosci. 1992;12(7):2685–705.

214. Fischer M, Kaech S, Wagner U, Brinkhaus H, Matus A. Glutamate receptors regulate actin-based plasticity in dendritic spines. Nat Neurosci. 2000;3(9):887–94.

215. Béïque J-C, Lin D-T, Kang M-G, Aizawa H, Takamiya K, Huganir RL. Synapse-specific regulation of AMPA receptor function by PSD-95. Proc Natl Acad Sci U S A. 2006;103(51):19535–40.

216. Knott GW, Holtmaat A, Wilbrecht L, Welker E, Svoboda K. Spine growth precedes synapse formation in the adult neocortex in vivo. Nat Neurosci. 2006;9(9):1117–24.

217. Mates SL, Lund JS. Developmental changes in the relationship between type 2 synapses and spiny neurons in the monkey visual cortex. J Comp Neurol. 1983;221(1):98–105.

218. Kerchner GA, Nicoll RA. Silent synapses and the emergence of a postsynaptic mechanism for LTP. Nat Rev Neurosci. 2008;9(11):813–25.

219. Brown CE, Wong C, Murphy TH. Rapid morphologic plasticity of peri-infarct dendritic spines after focal ischemic stroke. Stroke. 2008;39(4):1286–91.

220. Villalba RM, Smith Y. Loss and remodeling of striatal dendritic spines in Parkinson's disease: from homeostasis to maladaptive plasticity? J Neural Transm (Vienna). 2018;125(3):431–47.

221. Xiong Y, Mahmood A, Chopp M. Remodeling dendritic spines for treatment of traumatic brain injury. Neural Regen Res. 2019;14(9):1477–80.

222. Oh WC, Hill TC, Zito K. Synapse-specific and size-dependent mechanisms of spine structural plasticity accompanying synaptic weakening. Proc Natl Acad Sci U S A. 2013;110(4):E305-12.

223. Brigman JL, Wright T, Talani G, Prasad-Mulcare S, Jinde S, Seabold GK, et al. Loss of GluN2B-containing NMDA receptors in CA1 hippocampus and cortex impairs long-term depression, reduces dendritic spine density, and disrupts learning. J Neurosci. 2010;30(13):4590–600.

224. Chung W-S, Clarke LE, Wang GX, Stafford BK, Sher A, Chakraborty C, et al. Astrocytes mediate synapse elimination through MEGF10 and MERTK pathways. Nature. 2013;504(7480):394–400.

225. Wu GY, Cline HT. Stabilization of dendritic arbor structure in vivo by CaMKII. Science. 1998;279(5348):222–6.

11. BIOGRAPHY

Dinko Smilović was born on 17th March 1992 in Zagreb. He graduated in 2016 at the University of Zagreb, School of Medicine. After an internship in the University Hospital Centre Zagreb, he started working at the Department of Neuroscience, University of Zagreb, School of Medicine as a research and teaching assistant in 2017. He continued his work in the Institute for Clinical Neuroanatomy, Goethe University, Frankfurt am Main at the NeuroScience Center in 2019 and 2020, after which he returned to the University of Zagreb. He teaches the Basics of neuroscience and has taught Anatomy in Germany. His scientific work started during his graduate studies with a focus on the diagnosis of Alzheimer's disease, and has now shifted to the study of neuromorphology and synaptic plasticity. He started his PhD studies in 2017 at the Croatian Institute for Brain Research with Mario Vukšić, MD, PhD and Thomas Deller, MD as his mentors for the doctoral work.

He was awarded the Europass Mobility grant in 2018, Network of european bioimage analysts (NEUBIAS) COST grant in 2020 and was part of billateral Croatian-German project (Ministry of Science and Education of the Republic of Croatia and Deutsche Akademische Austauschdiesnst (MZOŠ-DAAD) project. As a student he was the chair of the Student Society for Neuroscience and an editor of the journal Gyrus.

He is a member of the Croatian Society for Neuroscience. He is fluent in Croatian, German and English. He has published 2 scientific papers in *Web of Scienec* Core Collection and 5 abstracts at international meetings.